DEVELOPMENT

OF A

SILICA SCALING TEST RIG

A thesis submitted in partial fulfilment

of the requirements for the

Degree of Master of Engineering in Mechanical Engineering

at the University of Canterbury

Luke A. Sinclair

University of Canterbury

January 2012

Abstract

One of the most significant problems faced in the geothermal power industry is that of scaling due to amorphous silica. The silica can deposit out of super-saturated brine in monomeric form and as colloidal particles. Deposition can occur at problematic rates on pipe surfaces and in the rocks of the re-injection wells. Currently there are a number of methods for controlling deposition but the fundamental mechanisms that govern the transport and attachment of silica are not well understood.

Many field experiments on silica scaling have been conducted but, due to differences in brine chemistry and operational conditions, the results are hard to compare. Many laboratory experiments have also been performed but these are difficult to correlate with the field experiments. Previous research has found that hydrodynamics are important for the deposition of colloidal particles and inertial impaction was proposed to be the dominant transport mechanism.

These results were analysed and, in contradiction, the dominant transport mechanism of the particles was theoretically expected to be that of diffusion. A series of experiments were planned that could test the effect of hydrodynamics on colloidal silica deposition in cylindrical pipe flow. Three parameters were to be varied in the experiment: particle size (10nm and 100nm), Reynolds number (750 - 23,600) and viscous boundary layer thickness (0.06 - 0.38mm).

To perform this experimentation, a Silica Scaling Test Rig was designed, built and commissioned. A method for producing synthetic brine was developed which can provide sols that are stable for at least one month and have a particle size of 10-20nm. Silica deposition has successfully been obtained in three preliminary experiments using the rig.

Without the exclusion of air from the rig significant corrosion occurs in the mild steel test piece. Protrusions that were likely to be silica deposits were found to be co-located with the corrosion, suggesting that one process promotes the other. Neither deposition nor corrosion was found on the pipe's weld seam and heat affected zone.

Corrosion was prevented using an oxygen exclusion system and two amorphous silica deposition structures were observed: a flat plate-like structure and a globular structure that consisted of 1-5µm diameter globules that built up on each other. Other field and laboratory experiments have produced globular structures similar to those found in this research.

To perform the planned experimentation, future work is required: the silica deposition rate must be increased, colloidal silica sol stability must be improved, and some modifications must be made to the rig.

Acknowledgments

Firstly, I gladly thank God the Father, maker of the world and everything in it; the Mechanic of hydrodynamics and the Sustainer of colloidal chemistry. He has given us life, breath and everything; most important of which is his son, Jesus Christ, without whom I have no hope.

Dr. Mark Jermy has been an invaluable supervisor; I have learnt much and laughed more. Dr Kevin Brown has brought Chemistry and insight to one who had precious little – I am greatly indebted. I thank you both for your guidance on this project and thesis.

Mighty River Power has been most generous in providing this fascinating project and by funding both it and myself. Especial thanks to Joe Gamman and Michael Rock.

My co-workers also deserve many thanks: Dr. Mathieu Sellier and Siti Masuri, working on the numerical model; George Starling, the Chemist; and Pavlo Kokhanenko, the one taking on the heavy and challenging mantle that is this project.

A multi-disciplinary project requires multi-disciplinary assistance and there are too many at the University of Canterbury to thank by name for their advice given and equipment lent. To mention a few: Mechanical Engineering - Jim McLean, Julian Phillips, Scott Amies, Graeme Harris; Civil Engineering - Ian Sheppard, Stuart Toase; Chemistry - Rob Stainthorpe; and the Chemical and Process Engineering technical staff.

My family have supported, housed and fed me over this degree, for which I am very grateful.

And, finally, Agnetha – your contribution has been incalculable. For who can quantify the number of long hours at work that were persevered merely for the prospect of, later, being with you?

Table of Contents

Chapter 1. Introduction

1.1. Geothermal Energy and Electricity Production

Geothermal energy is thermal energy obtained on or near the earth's surface that has originated from deeper down in the subsurface. The temperature gradient between the subsurface and the surface drives a heat flow via several processes acting in combination. These include heat conduction through the earth's crust and the convection of fluids, such as magma, oil or water. Close to tectonic plate boundaries, volcanic episodes may occur and magma may intrude up into the crust heating the nearby rock. If this rock is porous and fractured, meteoric water may seep deep into them and also heat up, forming geothermal reservoirs. Fluid from the reservoirs may naturally rise to the earth's surface and form hot pools and geysers.

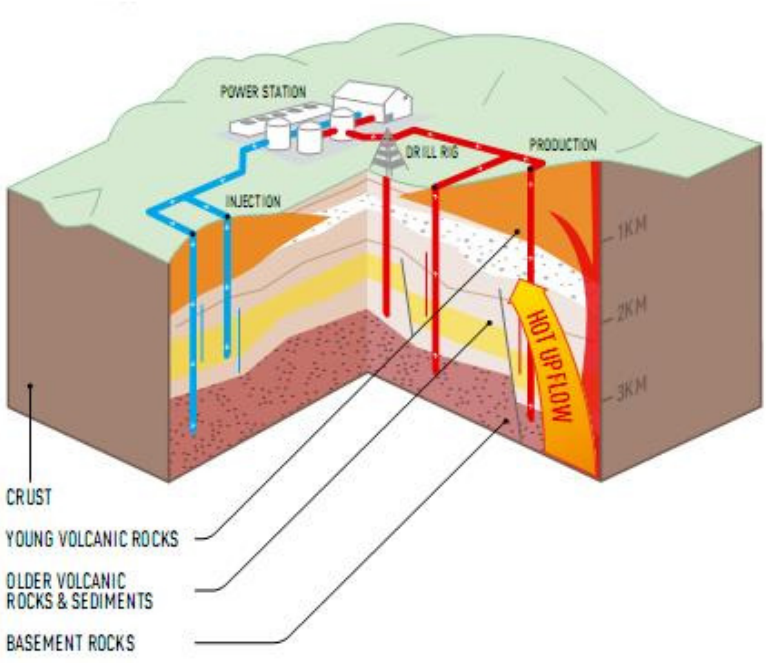

Figure 1.1: Geothermal Power Plant Schematic. Source: [1]

All of the geothermal energy power stations in New Zealand operate by extracting heat from such geothermal reservoirs and converting it to electricity. Wells are drilled into the reservoir and the geothermal fluid is brought to the surface, at which it usually becomes a two-phase fluid. Depending on the type of power station, the fluid may be separated once or multiple times and the vapour passed through a multi-stage steam turbine, producing electricity. The remaining geothermal fluid (or in some cases, all of the geothermal fluid) may be passed through a heat exchanger to heat up a binary fluid which, in turn, is passed through a binary turbine to produce electricity. In most geothermal power stations, all of the geothermal fluid gets re-injected back into the geothermal reservoir. A schematic of a typical geothermal power station is shown above in Figure 1.1. Electricity produced from geothermal energy provides about 13% of New Zealand's total power generation [2].

1.2. Silica Scaling

One of the most significant challenges to the geothermal power industry is that of silica scaling. The permeable rocks of the geothermal reservoir typically contain large quantities of quartz (SiO_2). This quartz dissolves into the geothermal fluid until it reaches an equilibrium concentration. As the geothermal fluid is brought to the surface, the temperature and pressure of the fluid decreases and it initially becomes two-phase. At the surface, the fluid is separated to provide steam for the turbine while leaving behind the liquid phase, which is often called brine. With the decrease in temperature and pressure, combined with the effect of the mass loss of water through steam separation, the quartz may become super-saturated in the brine.

At lower temperatures, super-saturated SiO_2 forms colloidal particles of amorphous silica rather than crystalline quartz. The colloidal particles, as well as the monomeric amorphous silica, may attach to the mild steel pipe walls. The formation and deposition of colloidal particles is described in more detail in Chapter 2.

As large quantities of the brine are passed through a power station each day, the growth rates of the silica scale can be quite significant, potentially blocking up entire pipelines. Scaling is particularly a problem in heat exchangers, re-injection pipelines, well casings and re-injection formation rocks. As the scale build-up increases, greater pumping pressure is required to re-inject the geothermal fluid and there can be a large cost to clean or replace the pipework. The most significant cost occurs when a new re-injection well has to be drilled, which can cost up to $8m [1].

1.3. Current Geothermal Silica Scaling Control Methods

Silica scaling occurs in numerous geothermal systems in New Zealand and around the world. Geothermal power station developers have been investigating methods for controlling scaling for decades. Gallup and Hirtz [3] have described the most common methods used:

1. Processing the brine at temperatures that prevent silica saturation.
2. Diluting the brine with fresh water to prevent silica saturation.
3. Reducing the pH of the brine to slow the polymerisation kinetics of silica.
4. Treating the brine with agents to prevent reaction of silica deposition co-products.
5. Removing silica from brine using precipitants such as lime.
6. Controlled precipitation of silica to prevent monomeric and polymerising silica deposition.
7. Cooling or rapid thermal quenching of geothermal brine.
8. Treating brine with silica scale inhibitors and dispersants.

In New Zealand, silica scaling has traditionally been avoided by method 1 above; keeping the geothermal brine at a high enough temperature that supersaturation is not an issue. This is an effective measure but the downside is that a significant amount of useable heat is not utilised. A greater power

output could be achieved if the re-injection temperature of the brine could be lowered while still controlling silica scaling.

Another prevention measure used in New Zealand is method (3) above, that of acid-dosing the geothermal fluid before it is passed through the power station. Acidification slows down the amorphous silica polymerisation process to a time scale long enough for the brine to be re-injected without scaling occurring in the plant. The dosing of the acid must be carefully controlled to provide the optimal conditions that prevent scale formation and minimise pipework corrosion due to reaction with the acid.

1.4. Research Objectives

The research described in this thesis was sponsored by Mighty River Power, one of the major companies in New Zealand that operate geothermal power stations. This project was to be the first in a series of research projects with an overarching goal of better understanding the silica scaling process so that novel solutions to the problem can be developed.

The aim of this project was to design and build a silica scaling test rig that can form silica scale using synthetic brine. The rig was to be able to vary a number of hydrodynamic conditions with controllable synthetic brine characteristics. Future research projects are to use this rig to perform experimentation that will allow a better understanding of the silica deposition process to be obtained.

1.5. Thesis Organisation

This thesis describes the development of the silica scaling test rig from the research stage to the preliminary experimentation. The background theory for silica deposition and pipe flow hydrodynamics are described in Chapter 2 and the literature on silica scaling experimentation is reviewed in Chapter 3. Chapters 4-6 describe the development of the new method of silica scaling experimentation and the design, construction and commissioning of the silica scaling test rig that can perform this experimentation. Chapter 7 describes the development of the colloidal silica production method for making the synthetic brine. The various side experiments performed and the preliminary experiments conducted in the silica scaling test rig are described and discussed in Chapter 8. The conclusions made in the thesis are given in Chapter 9 and the recommended future work is listed in Chapter 10. The thesis utilises the IEEE referencing method and a full reference list is given after Chapter 10.

Chapter 2. Background Theory

2.1. Amorphous Silica Thermodynamics and Kinetics

The source of the silica in geothermal systems is from the quartz in the surrounding rocks of the reservoir. At high temperatures and pressures the quartz dissolves into the hot water, reaching an equilibrium condition with the reaction:

$$SiO_2(s) + 2H_2O \Leftrightarrow H_4SiO_4(aq) \quad \text{Eq. (2.1)}$$

Quartz Silicic Acid

As the geothermal fluid rises in the well and into the power station at the surface, the temperature and pressure are both lowered significantly. The solubility of quartz decreases under these conditions causing the fluid to become super-saturated. At lower temperatures and pressures the precipitation kinetics for quartz are very slow. Under typical conditions for geothermal power stations, the solubility of silica is controlled by amorphous silica (AS), which has a higher solubility than that for quartz [3].

Exploitation of geothermal resources depends on this characteristic. Initially, the reservoir is saturated with quartz but under-saturated with AS. Once the geothermal fluid has been brought to the surface, quartz is unlikely to precipitate and the fluid is likely to remain under-saturated with AS. This prevents silica scale forming in the production wells and further heat can be removed before the AS equilibrium solubility is reached and silica scaling becomes a possibility.

The reaction between AS and silicic acid is similarly described by:

$$SiO_2(s) + 2H_2O \Leftrightarrow H_4SiO_4(aq) \quad \text{Eq. (2.2)}$$

Amorphous Silica Silicic Acid

The method of calculating the dissociation constant for Eq. (2.2) is widely available (e.g. [4]).

2.2. Amorphous Silica Colloid Formation

For geothermal fluid super-saturated with AS, the formation of colloidal particles is likely. Typical sizes for particles found in geothermal systems are in the range 3-3000nm [4]. A general name for a suspension of colloidal particles in a liquid medium is a sol. The formation of particles in a sol involves three steps: Nucleation, Ripening and Growth.

2.2.1. Nucleation

Spontaneous nucleation of AS occurs in fluids with a super-saturated state. The greater the degree of supersaturation, the faster the nucleation proceeds. Under some conditions of silica concentration and pH, an induction period may be observed where polymerisation does not begin immediately but only after some time.

First, silicic acid molecules begin to polymerise to form dimers:

$$H_4SiO_4 + H_4SiO_4 \Rightarrow H_6SiO_2 + H_2O$$

Eq. (2.3)

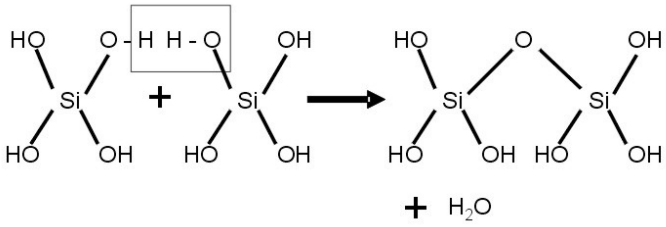

The dimers will then continue to polymerise forming trimers, tetramers and longer chains. The particular hydroxyl group where bonding occurs is random which causes the polymer to have an amorphous, rather than crystalline, structure. The polymer tends to maximise the number of Si-O-Si bonds and minimise the Si-OH groups. Therefore, as the polymer chain continues to grow in the presence of silicic acid monomers it tends towards the compact shape of a sphere with internal Si-O-Si bonds and SiOH groups remaining on the outside. This growth continues until the degree of supersaturation decreases to a point where the monomeric silica concentration is near to the equilibrium solubility for those conditions.

2.2.2. Ripening

This mechanism is often referred to as "Ostwald Ripening" and occurs after the nucleation stage has occurred. During nucleation, the nuclei formed will have a range of diameters. The smaller particles are more soluble than the larger particles and will tend to dissolve back into solution. This results in a slight increase in supersaturation causing further growth of the larger particles. This will continue until a critical size is achieved, dependent on the temperature. This mechanism tends to produce a monodisperse sol; that is, a sol containing particles of uniform size.

2.2.3. Growth

If the solution moves toward a super-saturated condition after a stable sized monodisperse sol has already been produced, the already formed particles will tend to grow in size. Less energy is required for monomers to attach to the existing particles than to form new nuclei and so the former process is favoured. If the level of supersaturation is high enough, new nuclei may form but Ostwald Ripening will occur again, causing them to dissolve and the existing particles to grow. The solution may move towards a super-saturated condition due to the further addition of monomeric silicic acid or due to a decrease in solubility such as from a decrease in temperature or pH level.

2.3. Silica Deposition

Iler proposes three mechanisms by which deposition of AS may occur: Direct, Colloidal and Biogenic [5].

2.3.1. Direct Deposition

This form of deposition occurs solely from monomeric silica under super-saturated conditions. The rate of silica deposition increases with the degree of supersaturation. The reaction proceeds above pH 8 and as the reaction is catalysed by hydroxyl ions such that it progresses faster with increasing pH. The silicic acid reacts with available hydroxyl groups on the material surface according to the following reaction:

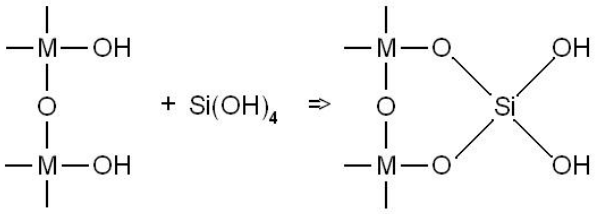

Eq. (2.4)

where M is a metal that can form a silicate at the pH involved. Once the first layer of silica is put down on the material surface, further layers of silica will deposit upon it causing a film growth.

The pipe-work in geothermal power stations is usually made from mild steel such that various phases and oxide products involving Fe will be involved in this reaction. The scale formed is hard, dense and vitreous with a typical scaling rate in the order of 0.5 mm/year [4].

2.3.2. Biogenic Deposition

Some living organisms are able to remove silica from dilute solutions and deposit solid silica within themselves in regular structures. In geothermal systems, the diverse range of thermophilic bacteria, in particular diatoms, which populate them can cause biogenic deposition. Microbes appear to provide a substrate on which silica can aggregate leaving behind a mould of its structure. The mechanisms involved are not well understood, particularly whether the role played by the microbes is active or passive [6]. Some unexpected results in experimental studies of silica deposition in New Zealand have been attributed to microbial influence [7].

2.3.3. Colloidal Deposition

The deposition of colloidal particles also occurs under super-saturated conditions. Increasing levels of supersaturation drives the nucleation and growth of the particles which may then deposit on a surface. It is suspected that both direct and colloidal deposition happen simultaneously in cases where there are particles and monomeric silica present [5]. For particulate deposition there are two steps involved: Transport and Attachment.

2.3.4. Transport

For deposition to occur the particles must be transported from the bulk flow to the surface. A number of forces and influences must be taken into account in this process. An important parameter for characterising the types of forces that are dominant for a particular particle transport situation is the dimensionless relaxation time, t_p^+ [8]. This is obtained by scaling the relaxation time, t_p, of a particle within a fluid by the friction velocity, u_τ (defined in the next section), and the kinematic viscosity of the fluid, ν.

$$t_p{}^+ = \frac{t_p(u_\tau)^2}{\nu} = \frac{\rho_p {d_p}^2 (u_\tau)^2}{18\mu\nu} \qquad \text{Eq. (2.5)}$$

where ρ_p is the density of the particle, d_p is the diameter of the particle, and μ is the dynamic viscosity of the fluid.

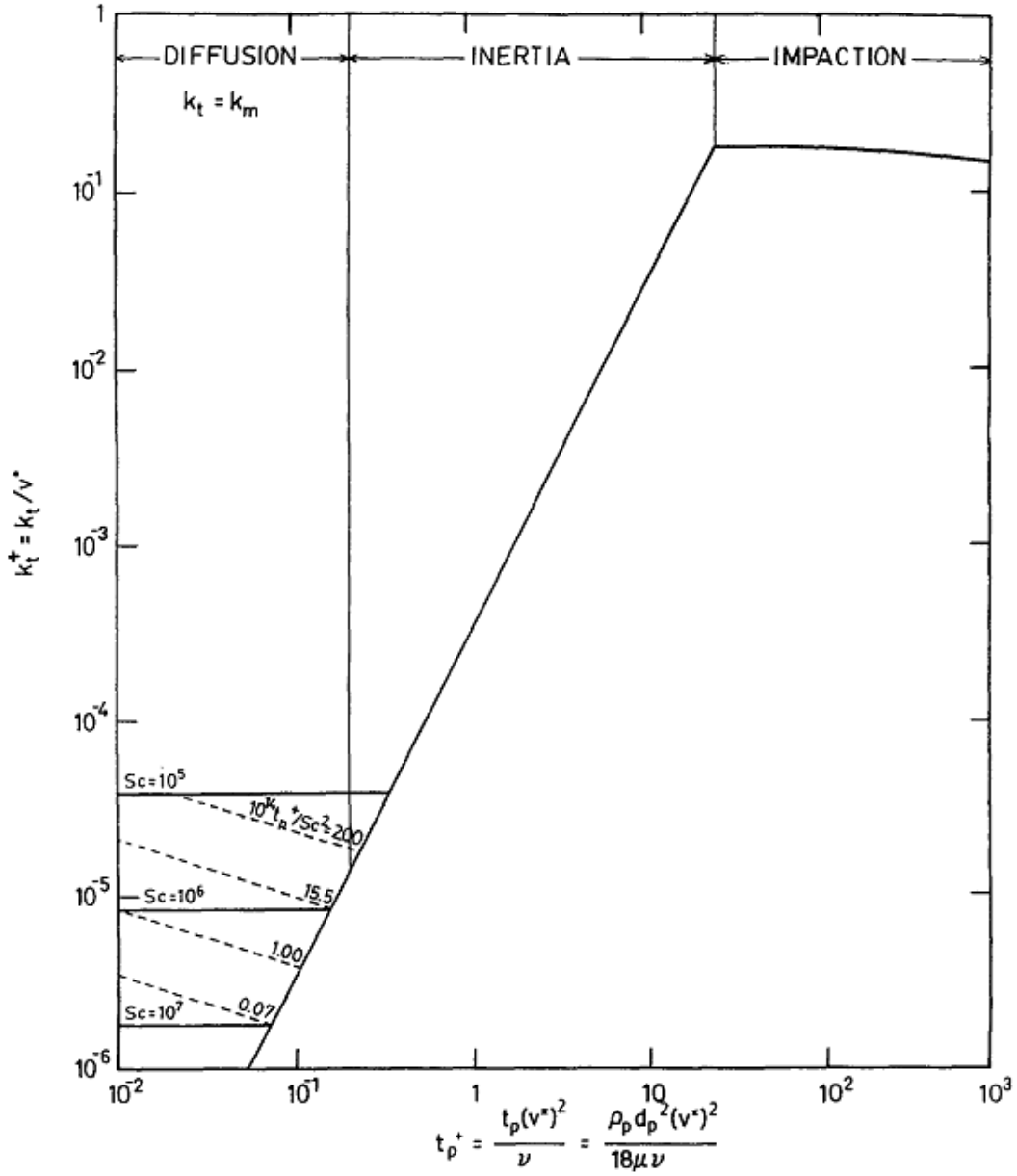

Figure 2.1: Particle Transport Regimes. Source: [8]

The transport of particles in a fluid medium has been well studied and Figure 2.1 shows a typical, generalised way that results are presented. The vertical axis is the dimensionless transport coefficient, k_t^+, which corresponds to rate at which particles are transported from the bulk flow to the deposition surface. The horizontal axis is the dimensionless relaxation time and the axis title shows an identical equation to Eq. (2.5) except for a different symbol, v*, used for the friction velocity. Also included in the chart are different lines corresponding to different Schmidt numbers, Sc, which is the ratio of viscosity to mass diffusivity.

The chart shows the three characteristic regimes that particle transport situations are split into: Diffusion, Inertia and Impaction. In the Diffusion regime, the particles are so small that they will tend to always follow the fluid streamlines except for diffusional effects such as Brownian Diffusion (see below). In the inertia regime, the particles are of sufficient size that particles will start to deviate from the fluid streamlines where there is a curvature in the streamlines. With increasing particle size this effect becomes increasingly important until the Impaction regime is reached, where particles become "sluggish" to the changes in streamline direction.

Within these three regimes there are a number of important mechanisms which are involved in particle transport. Many have listed and described these, such as Zipfel [9] and Epstein [8]. Important particle transport mechanisms include:

- **Brownian Diffusion** – the particles follow random, chaotic motion due to collisions between them and the surrounding fluid molecules. Averaged across very large numbers of particles there is a diffusional force driving particles from areas of high concentration to areas of low concentration. The rate of diffusion increases with increasing temperature and decreasing particle size. Brownian diffusion has little effect on particles outside of the Diffusion regime.
- **Turbulent Diffusion** – the particles become entrained in eddies and are transported throughout the flow. A lot of mixing occurs in turbulent flows causing the concentration of particles to become uniform in the bulk flow. If there is particle depletion happening at the wall surface this will cause a local decrease in the particle concentration on the near-wall side of the boundary layer. The turbulent mixing will then tend to cause the concentration to become uniform in this area, effectively providing a diffusional force transporting particles from a high concentration in the bulk flow to low concentration in the near-wall region.
- **Inertial Impaction** – the inertia of the particle causes it to continue along its same trajectory despite a directional change in the flow stream. This occurs for large particles, typically with relaxation times $t_p^+ > 0.1$. When turbulent flow provides a particle with sufficient momentum towards the direction of the wall, the particle will travel across the boundary to reach the surface.
- **Turbophoresis** - a turbulence intensity gradient exists in channel flow where there is a decreasing level of turbulence intensity from the centre of the pipe to the pipe wall. Particles

will tend to migrate down the turbulence intensity gradient towards the wall. This too occurs for larger particles, typically with $t_p^+ > 0.1$

- **Gravitational Settling** – for horizontal channels, large and heavy particles will tend to settle on the bottom of the channel over time. These particles will have $t_p^+ > 1$
- **Electrostatic Force** – charged particles, depending the sign of their charge, will be either attracted or repulsed from charged surfaces. This force can be important for tiny particles but it only acts over a short range and as the particle size increases, an increasing magnitude of electrostatic force is required to influence transport. The charged surface may arise from the thermoelectric effect where a heated surface may induce an electromotive force in the cooler bulk flow with sufficient charge carriers.
- **Thermophoresis** – when the pipe surface is at a different temperature to the bulk flow of the fluid a temperature gradient will exist. Particles will tend to move down this temperature gradient; cool surfaces will attract particles while hot surfaces will repel them.
- **Saffman Lift Force** – when a particle is in a shear flow (such as in the viscous layer, see below) there is a velocity distribution such that the velocity at the top and bottom of the particle will differ. This difference in flow over the top and bottom of the particle results in a lift force. When the particle is travelling slower than the shear flow, the force will act in the direction of increasing velocity, which is usually towards the bulk flow. When the particle is travelling faster than the shear flow, the force will act in the opposite direction, usually towards the wall.
- **Magnus Lift Force** – when the particle is rotating in an external flow, a lift force is experienced perpendicular to the streamline of the flow. This also results from a difference in the flow velocity over top and bottom of the particle.

The particular forces that act on a particle suspension will depend largely on the flow conditions. The average bulk fluid velocity, surface roughness, channel shape and the channel dimensions all influence the flow structure that will exist in each particular case. The development and characterisation of flow conditions is given in Section 2.4 below.

2.3.5. Attachment

Once the particle has been transported to the wall it needs to attach to the surface for deposition to occur. The surface forces that exist between the particle and the wall surface will influence the potential for the two to bond together. The theory that describes this interaction is called the DLVO theory and it takes into account two major forces:

1. London-van der Waals forces – due to the fluctuating motions of electrons around nuclei, spontaneous electrical and magnetic polarisations will occur about the nuclei. When two neutral particles are in close proximity to each other these polarisations will induce a fluctuating electromagnetic field providing an attractive force between them.

2. Electrical Double Layer forces – when particles are immersed in an electrolyte a diffuse layer of counter-ions will surround the particle, causing the potential at the edge of the diffuse layer to be different to that of the nucleus. This is known as the zeta potential. When the particles move, the diffuse layer moves with it and the double layer surface potential has a large influence on the interaction forces between particles

When the particle and the wall surface both have zeta potentials of the same sign, a repulsive force will be experienced as they are brought together. This is the case for a colloidal silica particle attaching to a surface that already contains a silica deposit. As the particle is brought closer to the surface, the repulsive force will increase and a greater interaction energy will exist between them as shown qualitatively in Figure 2.2 below. Once the particle is brought within sufficient proximity, the London-van der Waals forces start to act and result in an attractive force favouring the attachment of the particle to the surface. Figure 2.2 shows that there is an interaction energy barrier required to be overcome for the particle to be brought close enough for attachment to occur. This energy must come from the transport mechanism of the particle if deposition is to occur. The total deposition rate experienced depends then on both the rate of transport to the surface and also the rate that particles attach to the surface. The slower of these two mechanisms will dictate the overall deposition rate. Many factors influence the shape and magnitude of the interaction energy curve shown in Figure 2.2 such as: ionic strength of solution, zeta potential, pH, temperature, morphology of surface and any externally applied electric field.

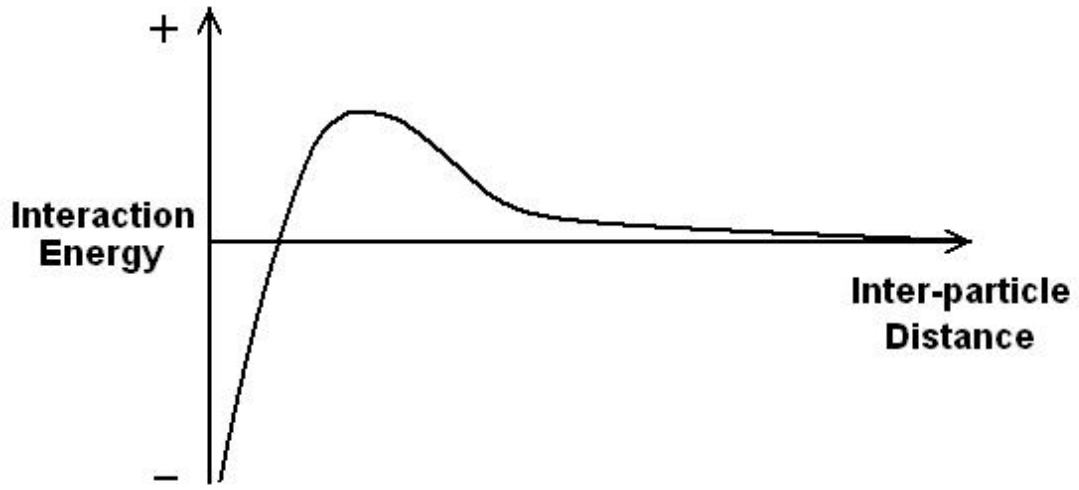

Figure 2.2: Interaction energy between two particles of like charge with inter-particle distance

2.4. Pipe flow theory

The geometry of the hydrodynamic flow of interest in this thesis is that of a cylindrical channel, generally called pipe flow. The hydrodynamics of this situation have been well studied due to its wide application across many industries.

2.4.1. Developed Flow Characterisation

The type of flow experienced in a pipe can be characterised by a dimensionless number called the Reynolds number, Re, which gives the ratio of the inertial force to the viscous forces in the flow:

$$Re = \frac{DU}{\nu} \qquad \text{Eq. (2.6)}$$

where D is the pipe diameter, U is the average fluid velocity and ν is the kinematic viscosity of the fluid.

A developed flow in a channel is one where the velocity profile across the channel does not change in the flow direction. When a uniform flow enters a pipe of fixed diameter, the velocity profile will begin to change due the viscous forces experienced from interaction with the pipe wall. As the distance from the inlet increases, the velocity profile will continue to develop until a steady condition is reached. The form of the developed velocity profile depends largely on the Reynolds number. The length of pipe required for a developed velocity profile to be obtained is called the entrance length, L_E.

2.4.2. Laminar Flow

For Re<2000 a laminar flow will exist in the pipe. In a laminar flow, the fluid will travel as smooth streamlines with no disruption or mixing between layers. Only molecular diffusion provides transport of fluid molecules between layers. The developed flow has a parabolic velocity profile which can be determined analytically and is often referred to as Poiseuille Flow. The entrance length for a laminar flow is given [10] by:

$$L_E = 0.065ReD \qquad \text{Eq. (2.7)}$$

2.4.3. Turbulent Flow

Once the Reynolds number starts to exceed 2000, fluctuations in the flow, vibrations of the pipe and roughness elements on the pipe wall will start to make disturbances in the flow. Turbulent eddies will start to form which disturb the smooth and parallel laminar streamlines and cause mixing to occur. For 2000<Re<4000 the flow will randomly oscillate between being laminar and being turbulent – this is commonly called the transition range.

For Reynolds numbers greater than 4000, a fully turbulent flow will exist in the pipe; there will be no laminar streamlines but eddies in the flow will be continuously produced and propagated. A developed turbulent flow looks very different to a developed laminar flow. Instead of a parabolic profile spanning

the whole pipe, there are different regions with different time-averaged correlations for the velocity profile as shown in Figure 2.3 below.

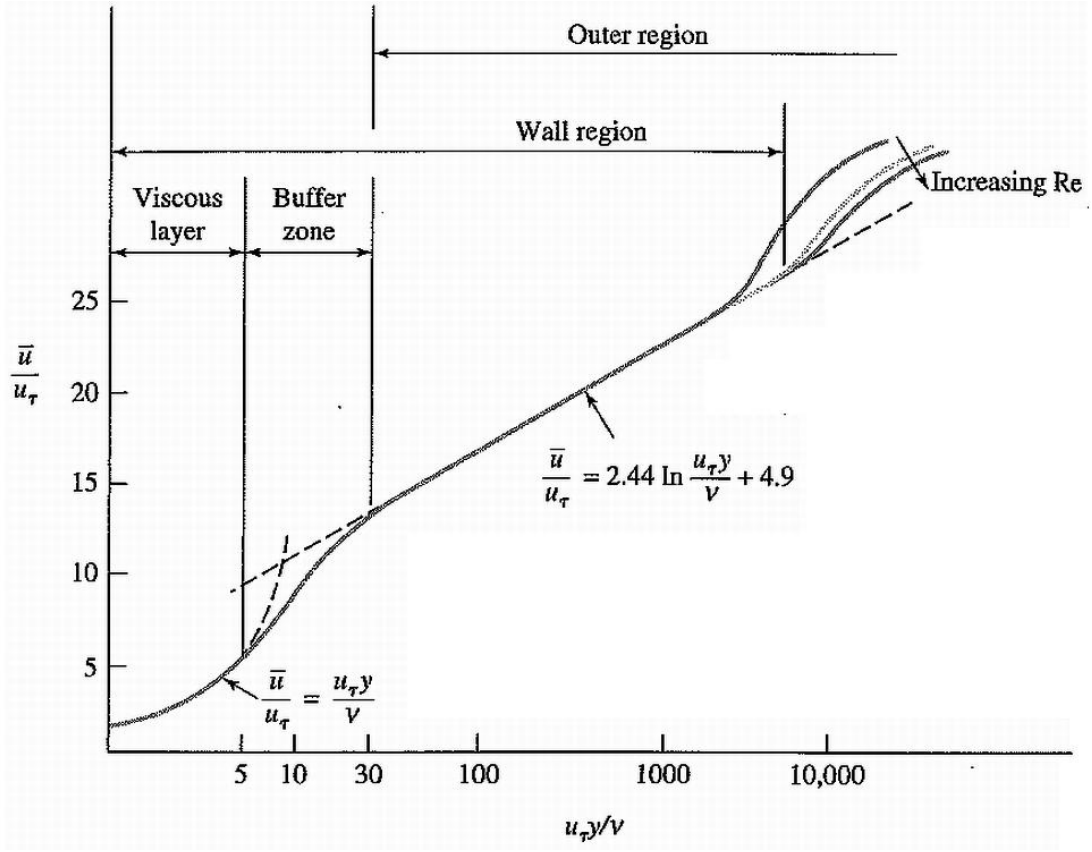

Figure 2.3: Dimensionless mean velocity profile in the near-wall region of fully developed, turbulent pipe flow. Source: [10]

In Figure 2.3 the horizontal co-ordinate is the dimensionless distance from the wall where y is the distance from the wall, ν is the kinematic viscosity and u_τ is the friction velocity which is defined below and is constant for a particular flow. The vertical co-ordinate is the dimensionless time-averaged local velocity where ū is the time-averaged local velocity.

The two empirical correlations for the dimensionless mean velocity profile within the wall region are shown in Figure 2.3. The viscous layer lies very close to the wall and a linear velocity profile exists. A logarithmic correlation holds for the area where the outer and wall regions overlap. The velocity profile in the buffer zone is a blend of these two correlations. Outside of the wall region a power law profile holds.

The wall region is of particular interest in turbulent pipe flows as this is where most of the turbulence is produced by the bursting process. Bursting starts with disturbances in the viscous layer causing vortical structures to be formed in the otherwise laminar flow. These vortical structures get ejected into the outer region of the flow resulting in turbulent eddies. A rush of fluid then sweeps in to take the place of the ejected fluid [11].

For a particular pipe situation, the thickness of the different wall region layers can be estimated from the empirical correlations. The friction velocity is defined as:

$$u_\tau = \sqrt{\frac{\tau_0}{\rho}} \qquad \text{Eq. (2.8)}$$

where τ_0 is the wall shear stress and ρ is the density of the fluid. The shear stress can be found from a common correlation for the dimensionless wall shear stress called the Darcy Friction Factor:

$$f_D = \frac{\tau_0}{\frac{1}{2}\rho U^2} \qquad \text{Eq. (2.9)}$$

where U is the average bulk fluid velocity. For laminar flow in a pipe the friction factor is given simply by:

$$f_D = \frac{64}{Re} \qquad \text{Eq. (2.10)}$$

For turbulent flows, the friction factor has been determined empirically and presented in charts such as the Moody diagram. A number of correlations have also been developed to determine the friction factor by calculation. An accurate solution over a wide range of conditions is the solution produced by Serghides [12]:

$$A = -2\log_{10}\left\{\frac{\frac{e}{D}}{3.7} + \frac{12}{Re}\right\} \qquad \text{Eq. (2.11)}$$

$$B = -2\log_{10}\left\{\frac{\frac{e}{D}}{3.7} + \frac{2.51A}{Re}\right\} \qquad \text{Eq. (2.12)}$$

$$C = -2\log_{10}\left\{\frac{\frac{e}{D}}{3.7} + \frac{2.51B}{Re}\right\} \qquad \text{Eq. (2.13)}$$

$$f_D = \frac{1}{4}\left(A - \frac{(B-A)^2}{C-2B+A}\right)^{-2} \qquad \text{Eq. (2.14)}$$

where e is the roughness of the pipe.

The required entrance length of pipe for a fully developed turbulent flow has been well studied and depends upon the conditions used to define the fully developed condition. For the full development of the mean velocity profile, an entrance length of 70-100 pipe diameters is required for a Reynolds number on the order of 10^5 [13]. The velocity profile development is affected by the pipe inlet conditions [14] but the overall development length is of the same order. For the development of all of the turbulence characteristics, in particular the development of large scale turbulent structures, a larger entrance length is required [15].

2.5. Water Tunnels

To perform hydrodynamic experiments in a laboratory a specially designed device is used called a water tunnel. The design of the water tunnel will vary widely depending on the application but, in general, their purpose is to produce desired, reproducible flow conditions at the test section to investigate hydrodynamic phenomena. The desired flow conditions may be a uniform axial velocity profile, such as in [16], or a fully developed channel flow, such as in [13]. Water tunnels bear a close resemblance to wind tunnels, for which much more literature has been produced. A basic schematic of a water tunnel showing the main features is given in Figure 2.4.

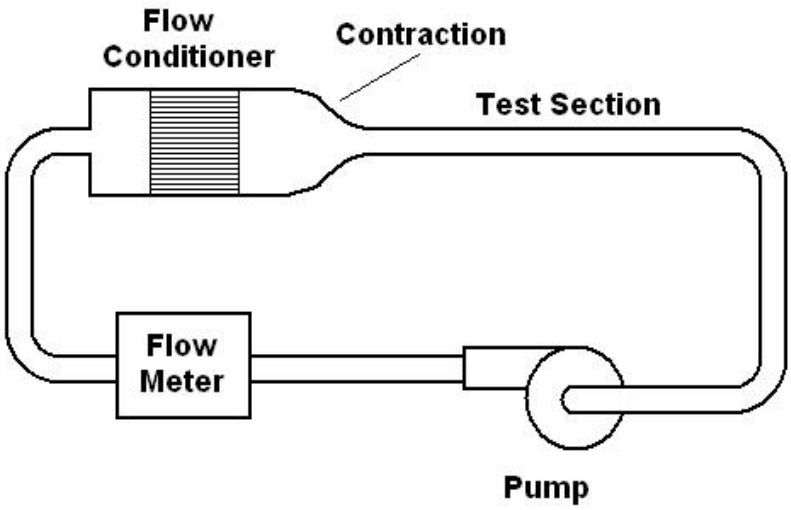

Figure 2.4: Generic Water Tunnel Schematic

The flow is circulated around the water tunnel from a pump, usually running to maintain a constant flow rate. As the flow travels around a number of bends, the velocity profile will be perturbed by secondary flows that can take a long travelling distance to dampen out. For this reason, a Flow Conditioner is placed before the test section, to make the flow become close to uniform. The flow conditioning device can take many forms including a tube bundle, a honeycomb or a perforated plate. A settling chamber exists downstream of the flow conditioning device to dissipate the turbulence produced.

Following the settling chamber is a smooth contraction that takes the channel dimensions down to the test section size. The contraction profile is designed to prevent any separation occurring in the profile and to produce a uniform velocity profile at the outlet. In Klein's review of turbulent, developing pipe flow experiments [14], the area contraction ratios that were used ranged from 4:1 to 25:1.

From the inlet of the test section the uniform velocity profile will start to develop into the fully a developed profile as described in the previous section. For experiments requiring a uniform flow, the test location of interest will be near the inlet. For experiments requiring a fully developed flow, the test section will be of sufficient length for the velocity profile to fully develop. For turbulent flows a trip is sometimes used at the test section inlet to reduce the length required for the flow to develop.

Chapter 3. Literature Review: Silica Deposition Experiments

The deposition of amorphous silica in geothermal development applications has been investigated for more than fifty years. A wide range of methodologies has been used to obtain various research outcomes. As the purpose of this thesis is to develop an experimental rig to test silica deposition it is of use to review the various methods that have been used and to what end.

3.1. Field experiments

3.1.1. Experiments at Ohaaki, Rotokawa, and Wairakei geothermal fields

Mroczek reviewed a number of experiments that were performed at Ohaaki, Rotokawa, and Wairakei geothermal fields in New Zealand [17], most of which are summarised below[1].

Experiments to qualitatively determine the amount and morphology of silica deposits from typical Wairakei fluid was investigated by Mroczek and McDowell[1]. A wooden tank partitioned into many sections was used to "hold up" the fluid by providing a torturous path that ensures the fluid remains inside the tank for 120 minutes. Five control valves were placed at different positions in the tank corresponding to different residence times. Each valve had a length of steel pipe with the valves set to provide the same flow rate. The pressure and temperature of the brine was varied in three experiments. In the pipes, a compact, white silica deposit was found which differed from the non-uniform, soft, porous and loosely adhering scale found in the tank. In general, the scaling rate was observed to increase with residence time. They proposed that aeration and turbulence had an influence on the different scaling rates found between experiments.

P. A. Taylor[1] performed tests to determine likely silica scaling rates at a geothermal field by creating a rig that simulated a re-injection pipeline from a separator to a re-injection well. The rig consisted of a hold-up vessel and a tube bundle. A controlled velocity vessel, consisting of a sequence of pipes varying in diameter, was also used to determine whether deposition depended on velocity or turbulence. The scale deposited inside the tube bundle was hard and black, and up to 50% of the thickness consisted of corrosion product. Inside the hold-up and controlled velocity vessels a soft, dirty white deposit was found. Less deposition formed at higher Reynolds numbers and more scale formed on protrusions to the flow, such as the outside edge of bends. Mroczek shows that the deposition formed must be from direct deposition as only monomeric silica would have been present in the experiments.

Mroczek and McDowell [18] investigated the effects of varying temperature and flow rate of geothermal fluid through pipes and gravel beds. Experiments were run for approximately a month and

[1] Where a reference is not given the research information has come from company reports, the details of which are given in Mrozcek's report.

then the sections of the pipe were cut out at selected positions and the scale scraped off for analysis and measurements of the scaling rate. At the higher temperatures silica was mainly present in monomeric form while at the lower temperatures polymerisation of the silica was found to occur. In the pipe flow they found little difference in overall rates of deposition when the flow rate or temperature was varied. However, they did notice for those at lower temperatures that there was a large reduction in the deposition rate between the pipe inlet and outlet. This was explained as the polymerising silica rapidly depositing near the inlet which quickly depleted the monomeric concentration and resulted in lower deposition rates downstream.

Mroczek and Reeves [19] investigated the effects on deposition from mixing aged polymerised silica with fresh un-polymerised silica. Some brine was taken from the main flow and held up in an aging tank which was then mixed back into the original stream to obtain various ratios of monomeric to total silica. The mixed fluid was passed through stainless steel tubes and glass tubes packed with glass beads for about 40 days. The amount of silica deposited was determined by drying and weighing the tubes. They found that the scaling rate and scale morphology is greatly affected by the concentration of monomeric silica. Figure 3.1 below shows the normalised weight of silica deposited in the experiments and describes the morphologies observed. The maximum deposition rate occurred at 80% monomeric and 20% polymerised. They surmise that the particle size may not be as important to scaling as the monomeric silica concentration.

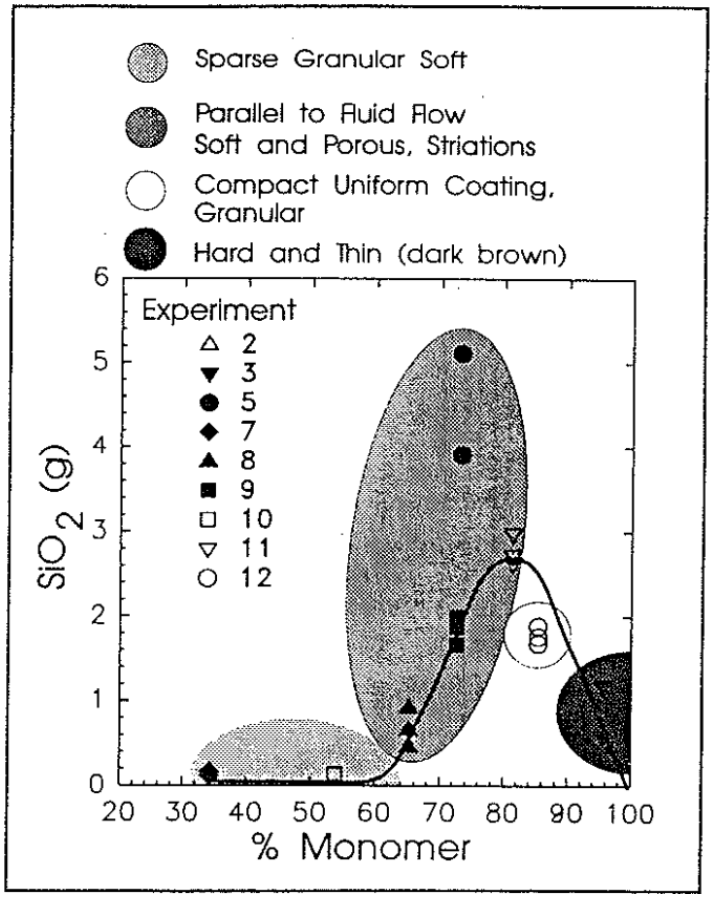

Figure 3.1: Weight of silica deposited (normalised) vs. amount of monomeric silica in mixed solution. Source: [19]

A variety of experiments were performed by Rothbaum et al [20] at the Broadlands and Wairakei fields in New Zealand. Geothermal brine was taken and held up for various lengths of time in holding tanks. Two types of test section were used: steel pipe and semicircular ceramic tile channels that were open to the air. Tests were also performed where the pH of the brine was lowered from pH 8-9 to about pH 4-5 under a couple of arrangements. Different experiments were run for different lengths of time, ranging from a couple of months to half a year. Silica scales were scraped off the pipe and ceramic tiles to analyse the composition and to measure the scaling rates. The composition and morphology of scales varied widely and quartz was even found in some deposits. They concluded that:

- Polymerisation had little effect on the quantity or chemical constitution of the scale produced
- Ageing New Zealand geothermal waters is not an effective method of scale control
- Aeration of geothermal waters greatly increases the scaling rate and it was suggested that this might be caused by the rapid oxidation of ferric hydroxide which then initiates nucleation of colloidal silica
- Acidification of geothermal waters can reduce the scaling rate by up to one hundred times

The effect of aeration on silica scaling was later investigated by Brown and McDowell [21]. Geothermal brine was passed through steel pipes held at different temperatures with oxygen or nitrogen injected into the stream. Scaling rates were determined again by scraping scale off sections of pipe. They found there was no effect on silica deposition from the injected gases. This was accounted for by noting that injection occurred before polymerisation started whereas in the experiments of Rothbaum et al, the degree of polymerisation was higher owing to the brine being held up. Greater quantities of deposition were found at the lower temperature experiments and the deposition mechanism was proposed to be that of colloidal particles attaching to the surface followed by cementing in place by further direct deposition.

Mroczek's review focussed mainly on monomeric deposition but did also discuss the influence of colloidal deposition where appropriate. His conclusions from reviewing these New Zealand field experiments include:

- Monomeric silica deposition occurs readily, even before polymerisation
- Only a small fraction of the total silica in the brine deposits as scale
- Deposition remains constant or increases with increasing fluid residence time
- Once scale has been formed by any mechanism scaling will then proceed rapidly
- Hydrodynamics play an important role in deposition
- Deposition rates onto clean iron pipe surfaces decrease after a given period (assumed to be when the surface is uniformly coated with scale)
- Deposits formed at high temperature tend to be tougher and more adherent

3.1.2. Ageing Experiments

The effect of ageing a polymerised solution to minimise the amount of silica was investigated by Rothbaum et al [20] due to the earlier work in Japan by Yanagase et al [22]. Silica scaling was found to be a problem in the Otake geothermal field in Japan and Yanagese et al found that the polymerisation in discharged waters occurred mainly in the first 60 minutes after discharge. For this reason they constructed a rectangular tank containing a baffle arrangement that forced the fluid to take a torturous path and be held up for about 60 minutes before passing to an outlet pipe. The retaining system reduced the quantity of scale formed in the discharge pipeline by a factor of 10 and this effect was further enhanced when the brine was agitated.

Following on from this research another study, reviewed by Mroczek, was conducted by W. A. J. Mahon, L. E. Klyen and G. D. McDowell in 1975[2] to investigate the feasibility of employing a retaining tank in New Zealand fields. A retaining tank was created that allowed a residence time of one hour to be obtained. The effect of deposition in the discharge pipe was investigated with undiluted brine and brine diluted 1:1 with cold water. In this study, the silica scaling rate was only reduced by a factor of 2 to 3, probably due to the fact that polymerisation had barely begun after 1 hour. They did find, however, that holding up diluted brine reduced the silica scaling rate.

The use of a retaining tank has been investigated at the Nesjavellir geothermal site in Iceland. After finding that ageing the separated brine for two hours considerably reduced the concentration of monomeric silica a large retaining tank was built [23]. The tank consists of a 144m long horizontal pipe that is 2.39m in diameter and, at the design flow rate, can hold up the fluid for two hours. Using the retaining tank was found to halve the level of supersaturation in the fluid. Opening the tank after four years, they found that the tank was coated by a <1 to 3mm layer of deposited silica and the system has been deemed successful.

3.1.3. Packed Channel Experiments

Silica scaling in the formation rocks of re-injection wells is of particular concern as it reduces the ability to inject the waste water back into the geothermal reservoir. This may potentially lead to the abandonment of the well. Many experiments have attempted to simulate this process in a simple way by packing a cylinder with some material and forcing brine through. Some such experiments have already been mentioned above.

Itoi et al [24] passed brine from the Otake geothermal field through a 550mm long, 50mm diameter cylindrical column packed with 2mm diameter aluminium beads. A number of manometer tubes were installed in the vertical column to measure the change in pressure over time. Experiments were run for 90 minutes and then the column was pulled apart and the areas where beads were stuck together by scale were sampled, dried and weighed to determine the amount of silica deposited. The flow rate was observed to decrease gradually with time to about 25% of the initial value over the course of the

[2] Details of this report are given in [17].

experiment. Silica scale was deposited chiefly in the first 10cm of the packed column, decreasing the permeability at this point by a factor of two. At the lower portions of the column (flow was from top to bottom) very little silica was deposited.

Later experiments have been performed in Japan by Kiyota et al [25] who investigated the effect of pH modification on the silica deposition in packed columns. Five columns (200mm long, 20mm in diameter) were connected in series, packed with rock fragments and had geothermal brine passed through them for one week. Two rock fragment sizes were used: 0.8mm and 2mm in diameter. The location of maximum deposition was found to be in the first column and the deposition rate decreased as distance through the column series increased. The pH modification tests involved lowering the pH of the brine from about 6.7 to 5.5. These experiments yielded a constant deposition rate in all five columns and an overall reduction in the total deposition rate of around 70%. They estimated that this would increase the life of the re-injection wells by about three times.

Similar packed bed experiments have also been performed at the Wairakei geothermal fields in New Zealand to predict the lifetime of re-injection aquifers [26]. In these experiments lengths of 25mm pipe were packed with 2mm diameter ceramic zirconia beads, chosen for low silica content and stability in hot, high pH fluid. Brine was passed through the beds and the beads were sampled at selected positions. The deposition rate was found to be slow and, for most experiments, was reasonably constant down the length of the packed bed. Deposition in these experiments was likely to be only monomeric as the residence time in these pipes was shorter than the induction period required for silica polymerisation to occur.

3.1.4. Other Field Experiments

Experimentation was performed at an El Salvador geothermal site to test the pressure drop in a waste water pipe line due to silica scaling [27]. Brine was taken from a separator, held up in a retention tank for polymerisation to occur and then passed through a series of pipes with decreasing diameter but at a constant flow rate. Pressure tappings were made at regular intervals along the pipe and the change in pressure was monitored over the course of the experiment, which lasted for seventeen days. As expected, the pressure drop increased substantially as scale was formed.

There are a number of silica scale inhibitors and dispersants available on the market and some have been designed for geothermal applications. The companies who produce the chemicals will often publish results from laboratory testing, such as [28], but the results of testing these additives on geothermal sites is not always published. One example of results that have been published is that of the use of the organic additive, Geogard SX, in the Botong geothermal field in the Philippines [29]. They describe the effects of adding the chemical to their fluid collection and disposal system, deeming it a success. Gallup [30] also describes successful field and laboratory experiments where organic inhibitors were used.

3.2. Laboratory Experiments

Silica deposition experiments, with geothermal applications in mind, have also been performed in laboratories using synthetic brine.

Colloidal seeding is a common method used to determine the rate of deposition of monomeric silica. A colloidal silica sol with known particle size and concentration is added to a solution of known monomeric silica content. The deposition of monomers onto already formed particles is favoured over the creation of new nuclei. Due to this, the decrease in monomeric silica can be measured over time and the deposition rate onto amorphous silica surfaces can be measured. Such experiments have been performed by Weres et al [31] and Fleming [32]. With geothermal relevance in mind, Bohlmann et al [33], also determined monomeric silica deposition rates in a similar fashion except using packed beds of various forms of crystalline and amorphous silica. When compared to deposition rates in geothermal fields, the models of Weres et al and Bohlmann et al were found to agree poorly but were usually within an order of magnitude of field rates [17].

Weres and Tsao [34]created a small continuous flow system to test the deposition of polymerising amorphous silica. They used synthetic brine that was made to simulate geothermal brine from the Cerro Prieto geothermal field. Two solutions, one containing sodium metasilicate and the other containing hydrochloric acid and various salts, were continuously mixed together to create the synthetic brine. The brine was then passed once through joined segments of 3mm diameter quartz tubing at a slow flow rate. Quartz tubing was chosen because it is nearly chemically identical to silica scale and theoretically should provide steady state deposition from the start. The total transit time for fluid was about 7 minutes and the experiment was run for 1.5 to 2 hours. At the end, the segments of tubing were rinsed, dried and weighed; the difference in weight before and after providing the weight of silica deposited. The deposition rate was high at first and then dropped off rapidly with distance down the tubing. From this they concluded that rate of monomeric deposition must then control the overall deposition rate. The rate of deposition here was one or two orders of magnitude greater than that determined by Were's monomeric deposition model in [31]. The deposition mechanism proposed was that first colloidal silica first attached to the wall and then monomeric deposition occurred which made the deposit solid and non-porous.

With a view of preventing silica scale build-up in geothermal heat exchangers in mind, Sugama and Gawlik [35] investigated deposition on coatings made of polyphenylenesulfide (PPS) and polytetrafluoroethylene (PTFE)-blended PPS. Coated and non-coated steel panels were immersed for up to 7 days in a sodium metasilicate solution at 200°C. Deposition completely covered the non-coated steel samples whereas the coated samples were free of scale except for some contaminants that were easily removed by rinsing.

Fouling in heat transfer equipment was tested more substantially by Chan et al [36] by investigating the change in thermal resistance as silica scale built up. A specialised corrosion resistant rig capable of

high pressure (1.58MPa) and high temperature (190°C) was constructed. The closed loop system involves the fluid passing through a boiler into a brine tank and then through the titanium tubes of a shell and tube heat exchanger. On the shell side of the heat exchanger is a separate loop circulating distilled water at a measured flow rate. The brine tank has a secondary loop which passes through two vertical columns containing a high grade silica gel and other chemicals. Silica dissolves into the brine and the system is controlled to get the desired brine conditions. Silica deposition occurs on the inside of the titanium tubes and the fouling resistance is measured over time with the use of a series of thermocouples and log mean temperature difference equations. The system was found to show an induction period followed by an initial drop in resistance before the resistance started gradually increasing.

Later they tested the effects of other chemicals on the fouling process, such as Fe^{3+}, Na^{+} and K^{+} [37-38]. When sodium and potassium chlorides were used, the silica fouling rate was found to increase with salt concentration. Sodium was found to cause a larger fouling rate than potassium at the same molarity. When the use of ferric chloride was investigated it was found that Fe^{3+} was the more dominant ion in increasing silica fouling. Adding a few ppm of Fe^{3+} increased the fouling resistance rate immediately and significantly, shifting the deposition mechanism from crystal growth to coagulation deposition.

3.3. Hydrodynamic Experiments

A number of the authors mentioned above have suggested that hydrodynamics have a significant influence on silica deposition. Some of the experiments performed were designed, in part, to test this and other experiments simply yielded results that could provide this interpretation. Some specific experiments and modelling studies performed in New Zealand have aimed to shed more light on colloidal silica scaling in geothermal applications and on the effect of hydrodynamics.

3.3.1. Wairakei Open Channel Experiments

Garibaldi and Freeston [39] placed stainless steel plates and cylinders in an open waste water channel at Wairakei. These geometries were chosen as the hydrodynamics of the flow around them are well known. The plate was fully submersed and placed horizontally in the channel by a suspension frame system. The cylinders were also placed horizontally but with their axis perpendicular to the flow. The deposition rate was determined by removing the sample from the drain and weighing it a number of times.

They found that the deposition rate was slow for the first 7 days and then it started increasing significantly. On the cylinders they found the highest amount of deposition along the stagnation line. There was little deposition on the top and bottom of the cylinder but a significant deposit was found on the back of it. The scale on the front half was fibrous when looked at through an electron scanning microscope and was different to the back half, which developed a cellular structured deposit. The flat

plate showed different scale morphologies: the first 10mm from the leading edge was free of scale, the next 150mm had a fibrous deposit and the rest of the plate showed scale with a rippled surface.

The deposition rate was concluded to be higher for low velocities and where laminar boundary layers exist. They also concluded that laminar boundary layers produce fibrous deposits while turbulent boundary layers produce the ripple pattern. It must be noted here that the deposition in this experiment may have been influenced by thermophilic bacteria that were found to be present in the drain channel by a later study [40].

3.3.2. Numerical Models

A numerical model of monomeric and colloidal silica deposition in turbulent flow in a duct was created by Jamieson [41]. The two scaling processes were assumed to add to the total deposition independently and the monomeric deposition was assumed to follow the model of Bohlmann et al [33]. Attachment forces were neglected in this model and four transport mechanisms were considered for particle deposition:

A. Transport from bulk flow to viscous layer
    1. Turbulent diffusion
B. Transport through viscous layer to wall
    2. Inertial Impaction
    3. Brownian diffusion
    4. Convection due to turbulent bursts

Empirical and theoretical equations from literature were used for each of these mechanisms and they were combined using a network model to give an effective overall mass transfer coefficient for deposition. The model was applied to a number of field tests in New Zealand and Iceland with some success although a number of assumptions had to be made about the degree of polymerisation in each case. Pertinent conclusions from his research include:

- In nearly all the cases he simulated, small or newly nucleated particles (<6nm diameter) were involved in deposition. The dominant particle transport mechanism that controlled the deposition rate was Brownian diffusion through the viscous layer. He concludes that variation in scaling rates due to hydrodynamic effects are likely to be primarily due to changes in the viscous layer thickness.
- Scaling is reduced when high polymerisation rates allow large particles (>20nm diameter) to form.
- Surface roughness was not studied but it was speculated that for rough surfaces, where the viscous layer is completely broken up by surface irregularities, turbulent diffusion would dominate.
- Rippled, spiky, or massive deposits only form when colloidal deposition dominates over monomeric deposition.

Another numerical simulation of colloidal silica deposition was later created by Pott [42]. The model was designed to investigate the initial deposition phenomenon on a flat plate taking into account the effects of the boundary layer development from the leading edge. Only particle deposition was included and the only transport mechanism considered was that of Brownian diffusion. Attachment assumed to occur when the particle reached the plate and particle concentration at the surface was assumed to be zero. The results of the model showed that:

- Deposition rates increase with decreasing particle size.
- Initially, silica colloids mainly deposit at the leading edge of the plate and the deposition rate decreases rapidly with distance from the leading edge.

3.3.3. Controlled Hydrodynamic Tests

Following on from the previous research performed in New Zealand, a pilot plant incorporating a water tunnel was built at Wairakei. A schematic of this plant is shown in Figure 3.2 below.

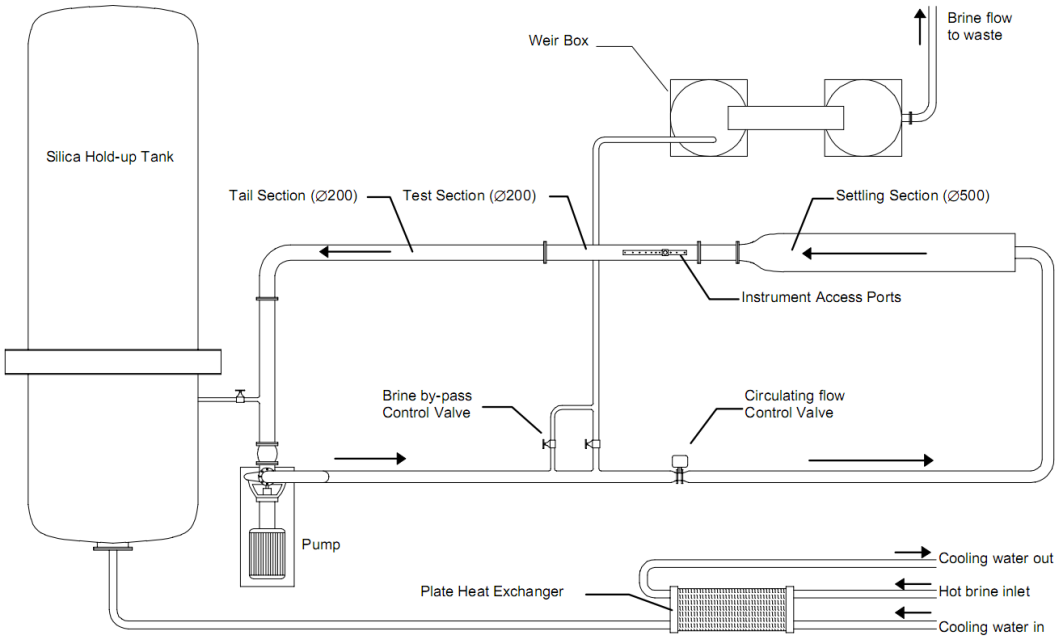

Figure 3.2: Schematic of the Pilot Plant used at Wairakei. Source: [7]

Geothermal brine was passed through a plate heat exchanger to cool the fluid, causing nucleation to occur. The fluid was then passed to the hold-up tank which allowed the particles to grow and stabilise at the desired size before being passed into the testing loop of the rig. By controlling the temperature in the heat exchanger the particle size was able to be manipulated to be between 10-125nm.

In the testing loop, the fluid is mostly re-circulated with a small fraction drawn off and replaced with freshly treated geothermal brine. The average residence time in the circuit is between 7 and 35 minutes depending on the make-up flow rate. The plant is capable of providing a fluid velocity in the test section of 0.5m/s to 3m/s and it was measured to have a uniform velocity profile in the bulk flow.

Small cylinders and flat plates were suspended in the middle of the test section and left for silica to build up on them under constant hydrodynamic conditions. After the experiment was completed the test sections were removed and analysed for deposition, visually and with an optical microscope.

The first experiments were performed by Brown and Dunstall [7], who investigated the effects of velocity and particle size. 250mm long mild steel plates were installed vertically in the test section. The leading edge was sharpened to a knife edge and one side had a trip wire installed 5mm behind the edge to compare the effects of having laminar and turbulent boundary layers.

Surprising results were found with one of the tests and further testing showed that the protective zinc coating on the plates greatly increased rate of silica deposition. They proposed that the precipitation of this scale was mediated by thermophilic bacteria. Outside of these extra tests they found there was no observable influence on deposition from hydrodynamics but it did appear that larger particles caused a greater scaling rate.

The next round of experimentation involved 25mm diameter cylinders mounted vertically and spanning the test section diameter. The cylinders had no zinc coating and, based on the morphology of the scale formed on them, they were deemed to form typical geothermal silica scale without biotic mediation. Experiments were run for three weeks using large (~125nm), medium (~65nm), and small (~10nm) particles at fast (~2.5m/s) and slow (~1.0m/s) fluid velocities. A number of interesting features were observed:

- The deposition rate increased markedly with particle size.
- No deposition was found on the stagnation line. The silica free zone width was wider for lower velocities (but with same particle size) and for smaller particles (with same velocity).
- The half of the cylinder facing the flow had substantial deposition that showed a “picket fence” effect. The scale showed ridges or “fences” parallel to the length of the cylinder and perpendicular to the flow. The ridges pointed into the flow.
- The back half of the cylinder, facing away from the flow was free of deposition.
- Near the top and bottom of the cylinders, near the test section pipe wall, the silica free stagnation line vanishes and a U-shaped scale formation was observed.
- No difference in scaling was observed between top and bottom sections, ruling out gravitational forces as having an effect.

As the highest rates of deposition occurred for large particles with large fluid velocity, inertial impaction over Brownian diffusion was concluded to be the dominant transport mechanism acting.

The hydrodynamics of silica scaling around these cylinders was investigated further by Zipfel with Brown and Dunstall [9]. Zipfel reviewed the literature about turbulent flow around circular cylinders and described the various flow regimes, the influence of free stream turbulence and surface roughness, the skin friction and pressure distributions, and the methods for predicting the location of the separation point.

A cylinder with pressure taps was created that could be inserted in the test section and rotated. The pressure variation over the surface of the cylinder could then be measured at the different flow velocities corresponding to the previous tests. The location of where the flow separated from the back of the cylinder could also be determined.

The cylinders from the previous tests were analysed under a microscope to determine the height of the silica deposit around the cylinders and the angle where silica deposition ceased. These results were then compared with pressure measurement results showing that deposition ceases close to where the flow separates. It was found that the angle from the stagnation line to where the maximum thickness of deposit occurred increased with decreasing particle size.

One of the cylinders had a partly corroded surface in the location where silica scale formed. The silica deposition height across this region was compared with that of the corresponding region on the other side of the stagnation line, which had a smooth surface. It was found that the corroded surface had a greater deposit thickness and this was attributed to the greater surface roughness.

The "picket fence" deposition pattern was analysed more closely and it was found, for tests with larger particles, that there existed major silica rows with smaller silica rows between them. The width of the silica rows was measured around the cylinder to obtain a distribution with angle. The position of maximum row width was found to correspond to the position of maximum silica height.

The skin friction distribution around the cylinders was assumed to be comparable to Achenbach's results [43] which were obtained from experiments conducted under similar hydrodynamic conditions. It was stated that the location of greatest shear stress could be obtained from finding the highest positive gradient of the skin friction function. This was found to be close to where the silica deposit was the thickest and, assuming that silica scaling is a function of time, the location where silica scaling initiated. The location of greatest shear stress was also stated to be where the minimum boundary layer thickness occurs.

Another scaling experiment was performed (75nm particle size, $Re=9.36x10^4$, 3 weeks duration) using a cylinder that had a tripping wire installed 45° from the stagnation line. Deposition was found to be absent for about 10° downstream of the wire. This result was found to approximately agree with other results from literature and it appeared that the tripping had no effect on the silica deposition rate downstream of the reattachment.

Based on all of these findings, Zipfel hypothesised:

- Inertial impaction is the dominant particle transport mechanism. Larger particles are more likely to deposit than smaller particles.
- No deposition occurs on the stagnation line because as it is region of highest pressure, minimum velocity and highest streamline curvature.

- Where the flow separates, the concentration boundary layer also separates, bringing fewer particles to the near-wall region to be deposited. Hence negligible deposition beyond the cylinder separation point and in the small region after the tripping wire.
- Deposition first occurs at the location of minimum boundary layer thickness as there is the least distance to travel across, promoting higher diffusion and inertial transport rates. The silica deposit at this position continues to grow forming a row parallel to the stagnation line. This acts as a small tripping wire causing separation and then reattachment and deposition a short distance downstream, forming further silica rows. As the rows build up, the local surface roughness will increase promoting further deposition.

3.3.4. Note on Zipfel's Analysis

It appears that there was some confusion between Skin Friction Drag, obtained by integrating the local shear stress, and the Skin Friction Coefficient, which is a dimensionless form of the shear stress. Achenbach provided the distribution of the Skin Friction Coefficient in his results and not the Skin Friction Drag. Finding the largest positive tangent of this distribution does not provide the location of the maximum shear stress; that occurs at the largest value of the distribution. Due to this, the location of thickest silica deposit was at a location of relatively high, but not highest, shear stress.

Also, the distribution of the boundary layer thickness around a cylinder in the sub-critical flow regime is given by Schlichting and Gersten [44]. From the stagnation point, the boundary layer thickness increases slightly with increasing angle and then starts to increase rapidly as the separation point is approached. Thus, the stagnation point is the location of minimum boundary layer thickness and the boundary layer thickness would have been slightly larger at the location where greatest silica deposition occurred.

This mostly affects his hypothesis on the onset of silica deposition. If deposition did initiate at the location of the thickest deposit, which is quite plausible, it was not because that location had the maximum shear stress and thinnest boundary layer; some other explanation must be provided.

Chapter 4. New Silica Scaling Experiments to Test Transport Hypotheses

4.1. Aim of new research

As the literature review has shown, many field experiments on silica deposition have been performed obtaining a range of conclusions, some of which are contradictory. To draw precise conclusions from a field experiment is complicated due to the many complex factors involved in silica scaling. Each geothermal site has its own unique chemistry and operational conditions, which may contribute to the large range of scale morphologies observed and deposition rates recorded. Also contributing was the effect of the polymerisation state of amorphous silica; despite this often being known, unexpected and as yet unexplained experimental results were still found. Not only were there many differences between the deposition results from different geothermal sites, but laboratory determined results were also hard to correlate with those from the field.

Despite advances in the control of silica scaling, there are still many unknowns. A number of the underlying mechanisms involved have been identified and described. However, the type and quantity of deposition that one may experience at any particular geothermal field cannot yet be accurately predicted. There is a need for further research to isolate and test in a controlled manner the different parameters that have already been identified as playing a significant role.

The aim of the new silica scaling experimentation, described in this thesis, is to understand in greater detail the mechanisms by which colloidal silica particles deposit.

4.2. Analysis of vertical cylinder experiments

The vertical cylinder experiments of Brown, Dunstall [7] and Zipfel [9] have produced the most convincing evidence for the influence of hydrodynamics on silica scaling. The conclusion from these experiments was that the most important transport mechanism for the colloidal silica particles was inertial impaction. For this to be the case it would be expected that the dimensionless particle relaxation time for the situation would be greater than 0.1 based on Figure 2.1.

To determine the dimensionless particle relaxation time for the experimental conditions, the friction velocity is required and hence, from Eq. 2.8, the shear stress is required. The shear stress in this case is different from Eq. 2.9, which is for a pipe wall. Instead, the shear stress on the surface of the cylinder is required and this can be obtained from the skin friction coefficient:

$$C_f = \left(\frac{\tau_0}{\rho U^2}\right)\sqrt{Re_c} \qquad \text{Eq. (4.1)}$$

The Reynolds number in this case is not for the whole test section pipe but for the flow around a cylinder of diameter D_c, which is given by:

$$Re_c = \frac{D_C U}{\nu} \qquad \text{Eq. (4.2)}$$

From the results of Achenbach [43], for hydrodynamic conditions similar for that in Test No. 2, the maximum skin friction coefficient is about 3. For the following analysis, this value will be assumed to hold for all the experimental cases as it will yield results of the correct order of magnitude.

Table 4.1: Analysis of vertical cylinder experiments, from [9]

Experimental Parameters							
Test No.		**1**	**2**	**3**	**4**	**5**	**6**
Experiment Duration	days	21	34	21	21	17	29
Fluid velocity, U	m/s	1.22	1.96	1.08	1.69	1.15	2.04
Temperature	°C	72	66	58	58	57	55
Particle size, d_p	nm	125	125	65	65	10	10
Kinematic Viscosity, ν	m^2/s	4.10E-07	4.50E-07	5.60E-07	5.10E-07	5.30E-07	5.30E-07
Reynolds number, Re_c		73,400	106,000	54,300	82,200	55,900	96,000
Fluid Density, ρ	kg/m^3	977	980	984	984	986	986
Test Cylinder Diameter, D_c	mm	25	25	25	25	25	25
Particle Density, ρ_p	kg/m^3	1500	1500	1500	1500	1500	1500
Calculations							
Dynamic Viscosity, μ	Pa.s	4.01E-04	4.41E-04	5.51E-04	5.02E-04	5.23E-04	5.23E-04
Skin Friction Coefficient, C_f		3	3	3	3	3	3
Shear Stress, τ_0	Pa	16.10	34.69	14.78	29.41	16.55	39.73
Friction Velocity, u_τ	m/s	0.1036	0.1521	0.0993	0.1400	0.1050	0.1627
t_p^+		8.51E-05	1.52E-04	1.12E-05	2.70E-05	3.32E-07	7.97E-07

The largest dimensionless particle relaxation time was for Test No. 2 and its value was three orders of magnitude lower than that required for the Inertia particle transport regime. For these conditions the regime should be Diffusion and no inertial effects should be expected, especially due to the very low value of the relaxation time. A particle size of at least 10,000nm would be required for the transport regime to be that of Inertia. This directly contradicts the conclusions drawn from these experiments.

The major evidences for why inertial impaction was proposed to be the most important mechanism were:

- Larger particles caused a greater deposition rate than smaller particles.
- Deposition occurred on the half of the cylinder facing the flow.
- Location of maximum silica deposition height was at a greater angle from the stagnation line for smaller particles.

These results strongly suggest that inertia is the dominant transport mechanism. If diffusion was the more important transport mechanism, smaller particles would be expected to have a greater deposition

rate. Deposition would also be expected on the back half of the cylinder as re-circulating eddies transport particles close to the wall to be diffused across the turbulent boundary layer.

Schlichting and Gersten [44] have provided data and empirical equations for a subcritical flow around a cylinder at Re=1.9x10^4. From this information the total velocity and acceleration profiles at the outer edge of the boundary were plotted in Figure 4.1 below.

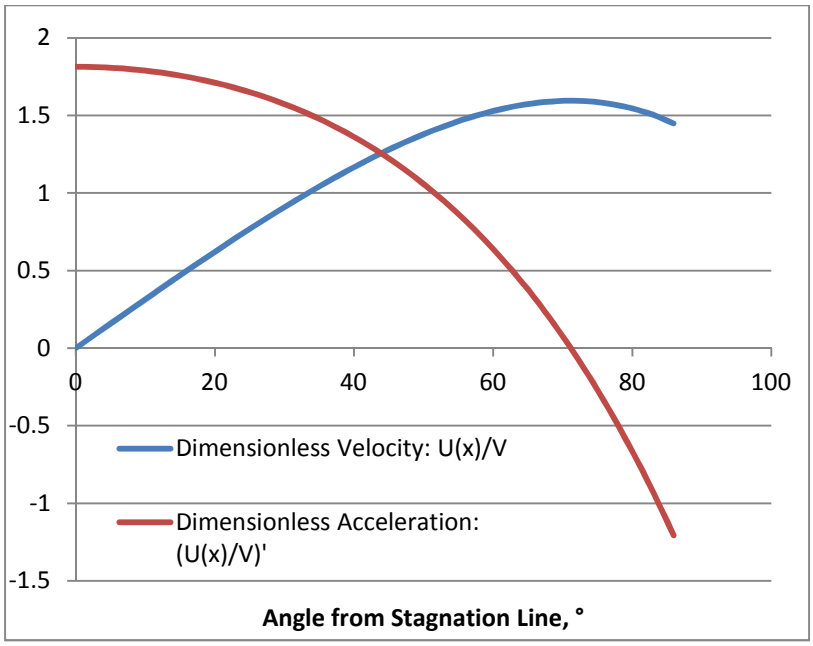

Figure 4.1: Velocity and Acceleration at outer edge of Boundary Layer for flow around circular cylinder at Re=1.9x10^4 using results from [44]

This result shows that, while the velocity at the edge of the boundary layer at the stagnation point is zero, the acceleration of the fluid is at a maximum. Near the stagnation point, the streamlines outside of the boundary layer have a maximum rate of curvature. For inertial impaction, it would be expected that deposition would occur at locations of high acceleration and high streamline curvature where the particles would deviate from the streamline and travel across the boundary layer. This would be on the half of the cylinder facing the flow, which is what the experimental results yielded. Also, particles with larger inertia would be expected to arrive at the cylinder surface at a smaller angle from the stagnation line as they will be more likely to be able to deviate from the streamlines.

If it is the Diffusion transport regime that holds for these experiments, then these findings must be able to be explained without the inertial impaction mechanism. Possible explanations may include:

- Attachment forces may favour large particles over small particles.
- Aggregation of small particles to form micron sized particles may have occurred in experiments.
- Some of the other transport mechanisms may hinder the transport of smaller particles. The Saffman lift force in particular has been shown to be a dominant factor in the particle concentration distribution near the wall for nanoparticles under certain conditions [45].

4.3. New Experiments

The new set of silica scaling experimentation will be able to provide results that will allow further conclusions to be drawn on particle transport mechanisms. The contradiction between the vertical cylinder experimental results and the theoretical expectations will be able to be tested again and hopefully resolved.

The method of testing will involve the use of a synthetic colloidal silica sol in a water tunnel, based in a laboratory. This has several advantages over previous silica scaling experimentation performed in the field:

- Better control of and ability to alter the chemical conditions.
- Better control of the hydrodynamic conditions.
- Better able to monitor, control and adjust experimental conditions.

The silica scaling test section will be cylindrical pipe as part of the water tunnel. This will yield different results to that of a vertical cylinder submersed in a flow. The parameters to be varied are:

- Particle size
    - The colloidal sol will be made to have desired size before running experiment.
- Reynolds Number, Re
    - Varied by changing the flow velocity and pipe diameter.
- Boundary layer thickness
    - Varied predominantly by changing the flow velocity and also by pipe diameter.

A variety of experiments can be performed by varying these three parameters. The Reynolds number can be varied to provide laminar and turbulent flows. These flow regimes can both be tested with small and large particles. For turbulent flows, the Reynolds number can be altered while holding the boundary layer constant (and vice versa) by the careful choice of flow velocity in pipes with different diameters.

The Reynolds number represents the ratio of inertial to viscous forces in the fluid. Maintaining a constant Reynolds number when using pipes of different diameter ensures that the flow is hydrodynamically similar in each case. The rationale for controlling the boundary layer thickness is that it represents the distance that particles must diffuse through or travel across by inertial impaction. The ratio of the timescale for this transport to other important timescales, can then be varied. The effect of Reynolds number and boundary layer thickness on deposition can be tested independently.

Depending on whether the particle transport is dominated by Brownian Diffusion or Inertial Impaction, the effect of changing these parameters is hypothesised in Table 4.2 on the following page. These hypotheses are based on the assumption that the deposition process is not limited by the attachment process.

Table 4.2: Hypotheses for influence on deposition rate in cylindrical channels due to varying parameters

		Influence on Deposition Rate	
		Brownian Diffusion	**Inertial Impaction**
Laminar Flow	**Increasing Particle Size**	Decrease – Brownian Diffusion is inversely proportional to particle size	Decrease – Inertial impaction should not act in laminar flow due to all streamlines being parallel to the walls, only Brownian Diffusion
	Increasing Re	No Change – Brownian Diffusion is independent of flow velocity	No Change – Brownian Diffusion is independent of fluid velocity
Turbulent Flow	**Increasing Particle Size**	Decrease – Brownian Diffusion is inversely proportional to particle size	Increase – Inertial forces are higher for larger particles
	Increasing Boundary Layer Thickness (constant Re)	Decrease – Brownian Diffusion rate is inversely proportional to distance diffused through	Decrease – Greater distance to travel across requires higher particle inertia.
	Increasing Re (constant Boundary Layer Thickness)	No Change – Brownian Diffusion is not affected by pipe diameter or flow velocity; distance diffused across has greatest effect.	Increase – Higher ratio of inertial to viscous forces in the fluid should provide greater inertial forces for particles

The laminar experiments will provide useful information on the transport and attachment process of the silica particles. If the hypotheses above are not confirmed experimentally, it will likely be that the attachment process has a significant influence on the deposition of different sized particles. This influence could be quantified by comparing the experimental results with the theoretical transport rates for a laminar flow. Deposition experiments using static fluid could also be performed to determine Brownian Diffusion transport and deposition rates for different sized particles.

The turbulent flow experiments may allow the dominant transport mechanism to be identified. Testing with different particle sizes will yield the clearest results but definitive conclusions can only be obtained if the attachment forces can be shown not to limit the deposition process. Hence, the laminar experiments should be conducted first.

For the Boundary Layer Thickness and Reynolds number experiments, proving the hypotheses correct by experimentation would suggest that the transport mechanisms have been understood correctly. The constant Boundary Layer Thickness with increasing Reynolds number experiment is the only one that will allow the transport mechanism to be identified. However, the influence on deposition from the turbulence characteristics of the flow has not been considered when developing these hypotheses. Characteristics that may influence the results include the turbulence intensity, eddy size spectrum and burst size and frequency. Future work will possibly need to include an investigation into the turbulence characteristics of each flow situation and their effects on the transport process.

Chapter 5. Design of Silica Scaling Test Rig

After the generic plan for the experimentation was decided, the detailed design of the silica scaling test rig was initiated. The design process was iterative with the generic plan and rig design being continually modified as practical considerations were realised. This chapter outlines the final design of the rig, the reasons for the design choices made and the capabilities achieved, not necessarily in chronological order.

5.1. Design Intent

With the method of experimentation decided, a number of factors were identified that the silica scaling test rig must address:

- Rig is to be sited at the University of Canterbury in available laboratory space.
- Rig is to be safe for operators and bystanders.
- Rig able to be left unattended for long periods of time.
- Synthetic brine to be used, preferably to be manufactured on site.
    - Silica particles of different size able to be produced.
- Rig must be able to fulfil the experimentation plan requiring:
    - Fully developed turbulent and laminar flows able to be repeatedly produced.
    - Test section pipe diameter able to be modified.
    - Flow rate and temperature of fluid able to be changed and controlled.
- Experiments must produce silica scale that can be quantified and analysed.

5.2. Detailed Design

5.2.1. Piping & Instrumentation Diagram

The first step in designing the rig was to plan out the major components, how they would connect to each other and what types of measurements were required to be made. This was performed by creating a Piping and Instrumentation Diagram (P&ID) which shows conceptually the design of the rig without describing all of the physical details of the construction. As the design developed, more and more detail was added to the P&ID and Figure 5.1, shown on the following page, is the seventh and final revision.

The rig consists of a main loop that has, in order: the Mixing Tank, pump, throttling valve, flow meter, Flow Conditioner, test section, and a line that returns to the Mixing Tank. A number of measuring devices are located in the Mixing Tank and in the main loop. A secondary loop, used for splitting the flow, bypasses the test section and returns fluid back to the Mixing Tank. A once-through line also exists, coming from a compressed nitrogen tank to the top of the Mixing Tank and then vented to the atmosphere after passing through a water trap.

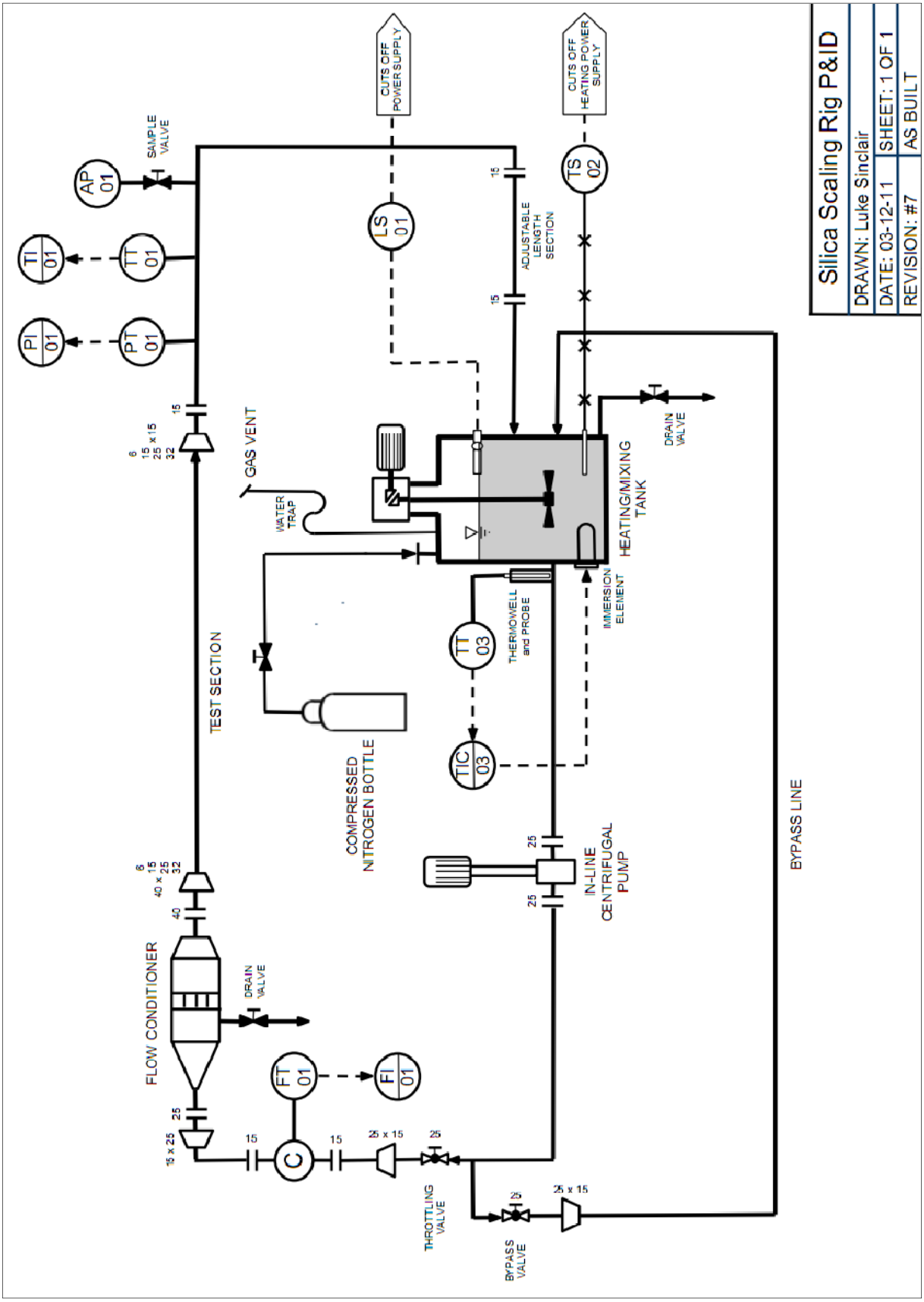

Figure 5-1: Silica Scaling Test Rig Piping & Instrumentation Diagram

5.2.2. Computer Aided Design Model

A model of the rig was created on the Computer Aided Design software package SolidWorks. The model was used to experiment with different designs for the whole layout and to illustrate the overall size and structure. It was also used for the detailed design of the Mixing Tank, Flow Conditioner and the stand for the tank and pump. Detailed engineering drawings of these components were created and submitted to workshops for the items to be fabricated. An assembly drawing of the whole rig at a later stage of design is shown in Figure 5.2 below.

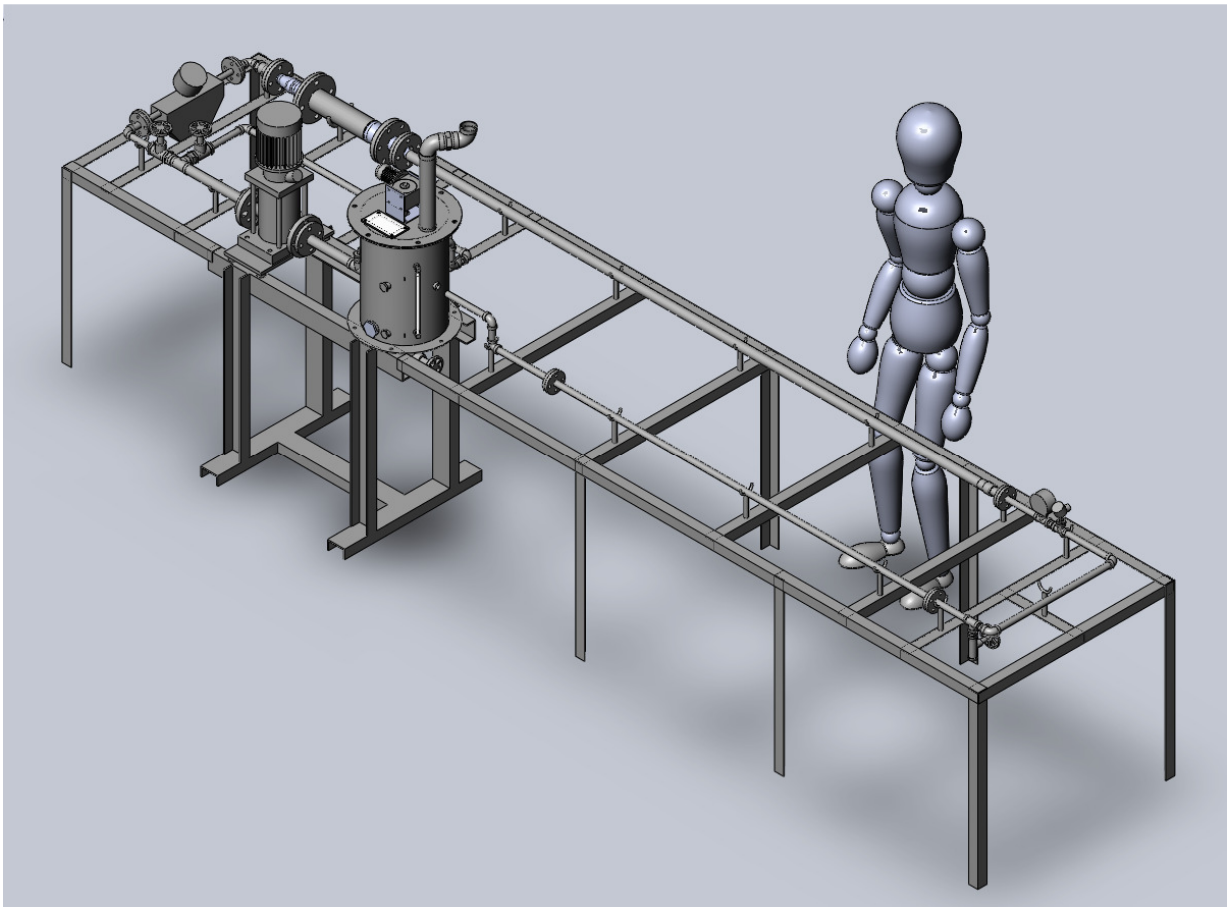

Figure 5.2: SolidWorks model of Silica Scaling Test Rig

5.2.3. Limitations to design

As the design process was begun, a number of limitations to the construction of the rig were identified which had an influence on the design decisions that were made.

Location of Rig

In line with the design intent, the rig was to be located within a laboratory at the University of Canterbury. This allowed the rig to be regularly accessible for monitoring and controlling. Also, the resources and equipment required for experimentation to be performed and modifications to be made would be in close proximity.

After reviewing the available options for rig location in the Mechanical Engineering Department, the best option appeared to be the North Calorimeter Room. The room was vacant, unfrequented by other staff or students, temperature controlled and contained a water supply with drain. These factors were ideal for setting up a rig that could be left running unattended for long periods of time.

Due to the size and shape of the room, the rig had to be limited to a maximum length of about 7 metres. Also, any materials used to construct the rig had to be able to be transported through the corridors, staircases and doors to get to the room.

Fluid Volume

As the test section diameter and length increases, the volume of fluid in the loop will increase. The volume of the Mixing Tank will, correspondingly, also need to increase (details described in Section 5.2.7 below). It was soon realised that the major limitation to the maximum size of the test section diameter would be the amount of synthetic brine that could be produced. After an initial survey of what equipment could be used to make large batches of colloidal silica, but before any such batches were made, it was decided that 20 litres would be a feasible quantity to produce. This limited the maximum test section diameter to be a nominal bore of about 32mm (NB32).

Rig Temperature and Pressure

Initially the rig was planned to be able provide similar temperature and pressure conditions as that experienced in geothermal power station re-injection systems (for example, 130°C, 5 bar). As the experimentation plan was developed and the vertical cylinder experiments were investigated further, it was realised that this was not necessary for understanding the transport mechanisms. The vertical cylinder experiments were conducted between 55-72°C and the influence of hydrodynamics on silica scaling was noticeable. As the purpose of the new experiments is to better understand the transport processes and not to exactly simulate scaling in power plants, it appeared that this could be done at lower temperatures. Another advantage of operating at lower temperatures was it is easier and cheaper to find equipment that can operate under the design conditions.

To create a rig that operates above atmospheric pressure would require all components and seals to be able to withstand the pressure. Extra safety equipment would be required, such as pressure relief valves, pressure wave tanks and overflow tanks. It was quickly realised that operating the rig above atmospheric pressure was going to complicate the design, require more onerous safety procedures and probably increase costs beyond the budget provided. Due to all these factors, the rig was designed to be open to the atmosphere, necessarily limiting the maximum temperature to 100°C. A number of components were limited in the maximum fluid temperature that they could withstand and so the maximum experimental temperature was chosen to be 80°C and a safety feature would be used to shut the system down should it exceed 90℃.

At higher temperatures Brownian Diffusion will have a larger effect and it is likely that the attachment forces will differ to those at lower temperatures. The effect of increasing temperature could be

partially investigated in the new silica scaling test rig and, if it was found to be significant, this could be a recommended avenue of research in the future. The effect on particle transport mechanisms at pressures above atmospheric is unknown; however, due to the relative incompressibility of water it may be insignificant.

5.2.4. General Features

Rig Materials

The rig will likely be used for a number of years to perform the planned, and possibly other, experimentation. Long-lasting materials were required; particularly those that would not corrode when full of water and also after exposure to air during regular draining procedures. Stainless steel was selected for its resistance to corrosion, ability to withstand high temperature and the availability of components.

As far as possible the rig was designed to be made completely from stainless steel. Two grades of stainless steel were used depending on what the purchased component was made from: the common 304 grade and the 316 marine grade. The only other wetted materials are: neoprene (gaskets), nitrile rubber (O-rings and lip seal), PFA tubing (sight gauge and cooling coil), TIG welding product (on thermowell), Teflon impregnated with Nickel (stainless steel threadseal tape), Loctite 577, Nickel (Heating Element is plated with it), and acrylic (Rotameter cylinder). Descriptions of the locations and purposes for these items are given in this section.

Connections

The pump and the Coriolis flow meter required flanged fittings for their connection. Apart from connections to these two components and the Flow Conditioner, all other pipe fittings were chosen to be BSP tapered thread fittings. There is a wide range of BSP fittings and they are readily available, easy to seal and easy to assemble and disassemble. For the same reasons, Swagelok fittings were chosen to be used for the smaller tube components, such as the thermocouples and PFA tubing.

The standard pipe diameter used in the rig was Schedule 40 NB15. This size was the smallest Schedule pipe available, and hence requires the least fluid volume. Using Schedule 40 allowed sufficient wall thickness to cut a BSP thread into it and could also be easily welded. Furthermore, stainless steel BSP threaded fittings for this size were cheap and easy to source. Schedule 40 NB25 pipe was used on either side of the pump to match the required size of its connections.

Seals

Loctite 577 was used for most of the stainless steel BSP threaded connections. The product is a Dimethacrylate Ester and is designed for locking and sealing metal pipes and is particularly suitable for stainless steel. As the majority of the fittings had no need for regular disassembly, a thread locker was useful for ensuring that the connection would stay free of leaks despite vibrations and accidental movement during the disassembly of other parts.

When the rig needs to be disassembled it can be broken down into a few sections, each containing a number of individual fittings. For the threaded connections at which these sections are broken apart, stainless steel threadseal tape was used instead of Loctite. This was because it is easier to apply and re-apply the tape and requires less effort to undo the connection. Stainless steel threadseal tape is similar to regular Teflon threadseal tape except that it is thicker and is impregnated with Nickel, which prevents stainless steel connections from seizing over time.

For flanged fittings, standard neoprene gaskets that matched the flange type were used. Neoprene is a common material for this application and can withstand the maximum rig temperature range. Some flanged fittings in the Flow Conditioner used nitrile rubber O-rings to seal the connection; the reason for their use is explained below. The Mixing Tank has a number of seals, described in its section below: an EPDM gasket for its lid, a neoprene gasket for sealing the window, a nitrile rubber lip seal for the mixer shaft, and Teflon threadseal tape for the riser connections.

Insulation

Insulation was required for the rig to reduce heat loss while operating at high temperatures and as a safety measure to prevent contact with hot components. Armaflex nitrile rubber foam insulation was used throughout the rig and the thickness recommended by the supplier for this application was 19mm. Two types Armaflex product were used: an Armaflex sheet was cut to shape to wrap around the Mixing Tank and preformed pipe sections were used to insulate all of the pipes. Cut-offs were then used to cover all other components, such as flanges and elbows.

Mounting Frame

For the ease of the operator, the rig was designed to be at about hip height. The two heaviest components were the Mixing Tank and the Pump, which were conveniently adjacent to each other. A mounting frame was constructed out of mild steel channel section for these two items allowing both to be directly bolted to the frame.

The other components of the rig were relatively light and could be supported by creating a frame out of a proprietary, industrial shelving angle section produced by Dexion. The angle section was selected as it was light-weight, locally available and had an array of bolt holes and slots that allowed great flexibility in assembly. A box-like frame was created that attached to the mounting frame for the Mixing Tank and the Pump. Bolts were used in all of the connections which allowed to the frame to be easily adjusted, disassembled or modified. Legs of the frame were screwed, in pairs, to lengths of wooden board to ensure that correct spacing was maintained and to provide extra support. The Dexion angle section could also be used to create supports for certain components of the rig that attached onto the main frame.

Draining

The lowest point in the rig was designed to be the Mixing Tank and a drain was placed on the bottom surface of the tank. As can be seen in Figure 5.2 above, not all of the main loop will be able to drain

into the tank. Due to this, a drain was also designed to be located near the end of the main loop and it was to double as a sampling point for experimental fluid. The main loop was then to be constructed in such a way that all the fluid would drain towards this second drain. Draining would also be possible out of a BSP Union in the bypass loop and the pipe was to be connected in such a way that fluid would drain out of the Union.

It was always anticipated that there would exist some dead volume in the rig that could not be drained out. This will occur within the flow meter, the pump and within some fittings. The rig will need to be thoroughly flushed with clean water whenever fluid is replaced. If the dead volume can be determined, then the diluting factor can be properly accounted for in the experimental analysis.

5.2.5. Test Section

The test section was chosen to be cylindrical pipe for the practical reasons that that they are readily available to be purchased and the hydrodynamics of flow inside them is well understood. Mild steel was chosen as this is the most common pipe material and deposition regularly occurs in geothermal power stations on such pipe. Seamless pipe was selected over welded pipe as this ensured there was no internal obtrusion that could affect the hydrodynamics. Also, welded pipe has a heat affected zone around the weld that has a different chemical composition and grain structure to the rest of the pipe.

To use commercial pipe as the test section limits the diameter to that of the standard sizes. As mentioned above, the maximum pipe size chosen for the rig was NB32. The outside diameter for this type of pipe is fixed and the inside diameter depends on the wall thickness, which is specified by the Pipe Schedule. Schedule 40 pipe was chosen as this is a common size and the wall thickness is sufficient for a range of welding processes to be performed on it, allowing it to be easily modified. At this Schedule the inside diameter is about 35mm. The standard length for this pipe is 6 metres and so two 3 metre long test section lengths could be obtained from each piece, utilising all the material. This corresponds to about 86 pipe diameters which should be sufficient for the mean velocity profile to become fully developed.

The minimum size for Schedule pipe is NB15; to obtain a test section with a smaller diameter than this requires using commercial tube. The smallest tube size available has an outside diameter of 9.5mm and a wall thickness of 1.6mm providing an inside diameter of 6.3mm. When using this tube, a test section of 1 metre in length would provide 159 pipe diameters which would be sufficient for a fully developed flow.

Commercial tube is produced by rolling a strip of steel and welding it together. Due to the small thickness of the tube only a small weld seam is produced, which is substantially smaller and protrudes less than that in Schedule pipe. The chemical composition and grain structure near the weld seam will be different to that in the rest of the pipe. The chemical composition of the tube will also be slightly different to that of the seamless pipe, the latter having a slightly higher carbon content. Future work could involve investigating the pre-coating of test sections with monomeric amorphous silica. This

may speed up the deposition rate of silica and would minimise the weld seam effects in the tube test sections.

To accommodate for the different test section diameters and lengths, the rig needs to be able to be easily adjusted. The Flow Conditioner was designed to have an interchangeable contraction section that ensured a smooth transition from the Flow Conditioner diameter to that of the test section. Standard threaded fittings were selected for use on the downstream end of the test section to step the diameter up or down to connect to the permanent part of main loop. As can be seen on the P&ID shown in Figure 5.1, there is a section of pipe called the "Adjustable Length Section" which is near to the Mixing Tank and on the opposite side of the loop to the test section. Appropriate lengths of pipe can be inserted here to ensure that the loop connects up when test sections of different lengths are used. The right hand side of the loop will remain fixed as a single piece, whose position will move depending on the test section length.

5.2.6. Flow Conditioner

The Flow Conditioner is one of the most important components in the rig as it allows repeatable hydrodynamic conditions to be reproduced in the test section. Figure 5.3 below shows a section view of the SolidWorks model that was used to create the drawings that were sent to the workshop to fabricate it. The Flow Conditioner consists of four parts: the main body, the tube bundle, the expansion section and the contraction adaptor piece.

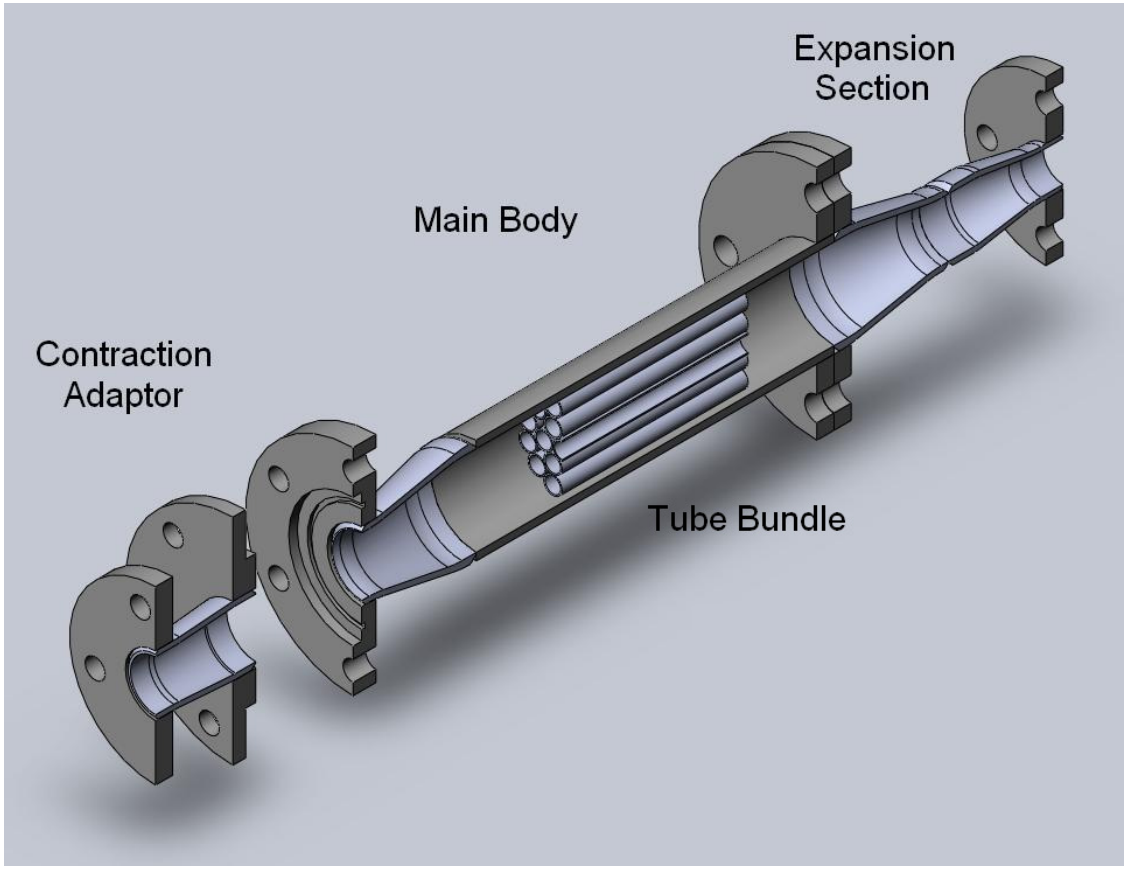

Figure 5.3: Section View of Flow Conditioner, Flow direction is from back right to front left

Main Body

The main body of the Flow Conditioner is a 250mm length of Schedule 40 NB65 pipe (Outside Diameter: 73.0mm, Wall Thickness: 5.16mm, Inside Diameter: 62.7mm). The size was chosen to provide a sufficient contraction ratio to the test section, allow a tube bundle to be fitted inside, and to minimise the volume of fluid it holds. For the largest test section diameter, NB32, the area contraction ratio was only 3.2:1. This is lower than the ratios quoted in Chapter 2 but a greater ratio could not be obtained with standard pipe sizes unless a substantially larger pipe was used. For all other test section diameters, the contraction ratio will be more than sufficient.

The NB65 pipe is welded to a Schedule 40 NB65 x NB40 butt-weld concentric reducer. Welded on to the end of this reducer is a custom made slip-on flange. Welded onto the other end of the main body is a BS10 Table E slip-on flange; a commonly used type of flange.

Tube Bundle

The 19-tube bundle flow straightener is commonly used in many industries. The design for this tube bundle was taken from ISO 5167-1 [46], which is for the application of straightening the flow before the use of an orifice plate flow meter. The tube used had an outside diameter of 12.7mm and a wall thickness of 1.6mm. Lengths of 130mm were bundled together and tack welded in the 19 tube arrangement shown below in Figure 5.4. The fabricated tube bundle was slightly too large for the pipe but could easily be tapped into place with no deformation.

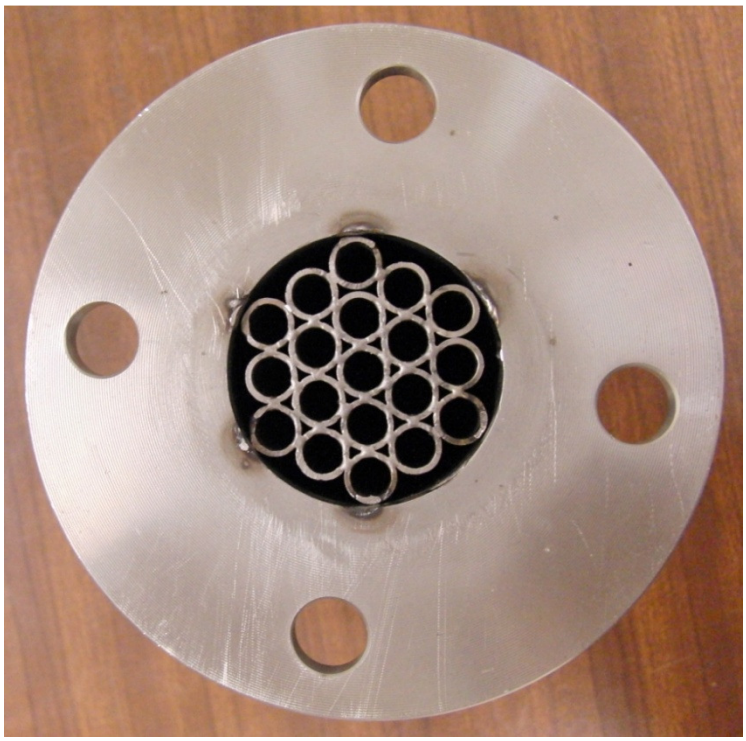

Figure 5.4: Tube bundle inside the main body of the Flow Conditioner

In the above standard, a number of factors were specified for the design of the tube bundle. Most of the parameters depended on the inside diameter of the pipe the bundle was to be inside. In this case it was D=62.7mm.

- Tube diameter, $d_t \leq 0.2D$
  - d_t = 12.7mm; 0.2D = 12.54mm
- Tube wall thickness, $t \leq 0.025D$
  - t = 1.6mm; 0.025D = 1.58mm
- Bundle diameter, d_B: $0.95D \leq d_B \leq D$
  - d_B = 63.5mm; D=62.7mm
- Length of tube, L = 2D
  - L=130mm; 2D = 125.4mm

The current design of the tube bundle is slightly outside of the specified parameters in a few cases. However, the standard applies to the use of tube bundle flow straighteners to provide accurate flow measurement. As this is not of concern, and as the bundle is regular in shape and symmetrical, the current design should provide an adequate flow straightening effect.

Expansion Section

The purpose of the expansion section is to increase the diameter smoothly to that of the main body. Smooth expansion reduces the amount of separation and turbulence formed when compared to a sudden expansion. Just upstream of the Flow Conditioner, a standard BSP threaded fitting takes the main loop diameter from the nominal size of NB15 to NB25. Off-the-shelf components were used to decrease costs and it was found that no single item could make the expansion in one step. Therefore, two butt-weld concentric reducers were welded together in series: NB65xNB32 and then NB32xNB25.

Respectively sized BS10 Table E slip-on flanges were welded onto each end of the reducers. Flanged connections were chosen as they allowed the Flow Conditioner to be easily disassembled in position. These flanges are both sealed by using the appropriate sized gasket. Having a flanged connection between the expansion section and the main body also allowed easy access for cleaning the Flow Conditioner, in particular the tube bundle.

Contraction Adaptor Section

To accommodate for the use of test sections of different diameters, the contraction needed to be able to be easily changed to provide the correct diameter. Again, no single item could be found to reduce the diameter from NB65 to all the desired test section diameters and so it was achieved in two steps. The first step involved taking the diameter down to NB40, which was achieved on the main body section. From NB40 there exist butt-weld concentric reducers that can take the diameter down to NB32 and NB15, which are two anticipated test section sizes. To reduce the diameter smaller than this, such as for tube sizes, will require the construction of a custom reducer.

Figure 5.3 above shows the contraction adaptor section with an NB40xNB32 reducer. This size has been fabricated for the initial testing of the rig. On the larger side of the reducer a custom slip-on flange is welded on and on the other side there is an NB32 BS10 Table E slip-on flange.

The contraction adaptor needed to have smooth connections to the Flow Conditioner and the test section to prevent any flow disturbances. This was achieved by using custom flanges with a spigot to ensure concentric alignment between the contraction adaptor and the main body. By using an O-ring in a groove to seal this connection, the surfaces of the two custom flanges were flush, preventing any gap existing on the inside surface of the pipe. The other side of the adaptor used a standard flange and was sealed with a gasket. However, after construction, it was realised that this did not provide a smooth connection and an O-ring groove was cut.

A locator shaft was created to ensure that the contraction adaptor piece would join concentrically with the test section. The method for using this tool is shown in Figure 5.5 below. The shaft is concentrically stepped to fit tightly against the inlet and outlet diameter of the adaptor piece as well as to the inside diameter of the test section. The flanges can be bolted together with the shaft in place to obtain a concentric connection. The shaft can then be removed and the whole thing can be joined to the main body of the Flow Conditioner and is aligned via the spigotted custom flanges.

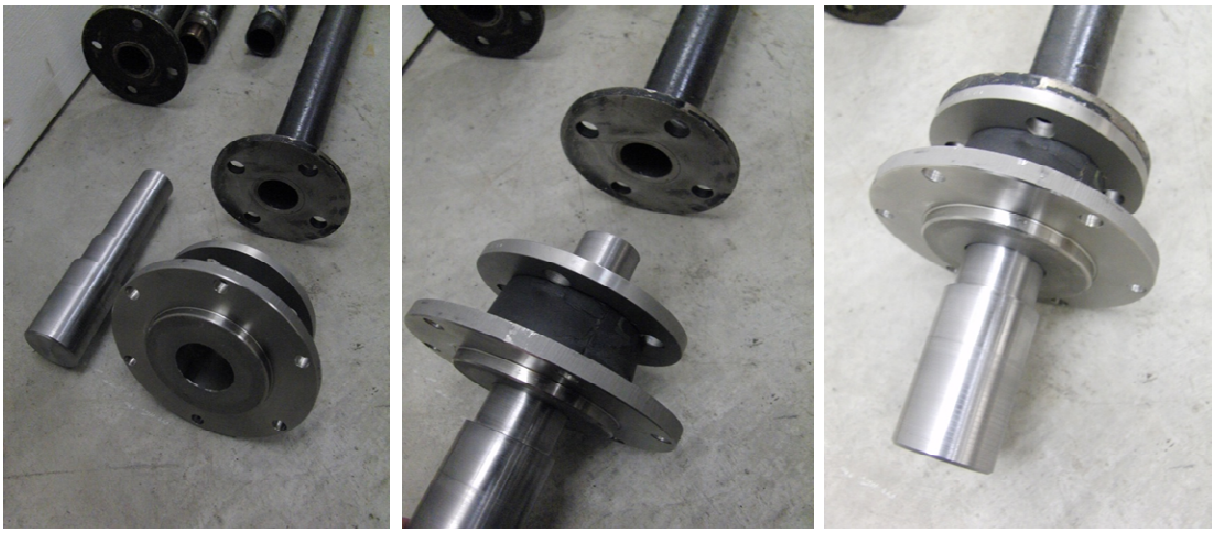

Figure 5.5: Method for using locator shaft to connect the contraction adaptor piece to the test section

Modifications

After the Flow Conditioner had been fabricated a number of modifications were made to it. Initially there was a substantial step in the main body between the pipe and the reducer, which is likely to have occurred due to the inside diameters of the two components not matching. Also, a large plate was welded downstream of the tube bundle to keep it in place. Both of these protrusions are not desirable in the downstream half of a flow conditioner and so were remedied.

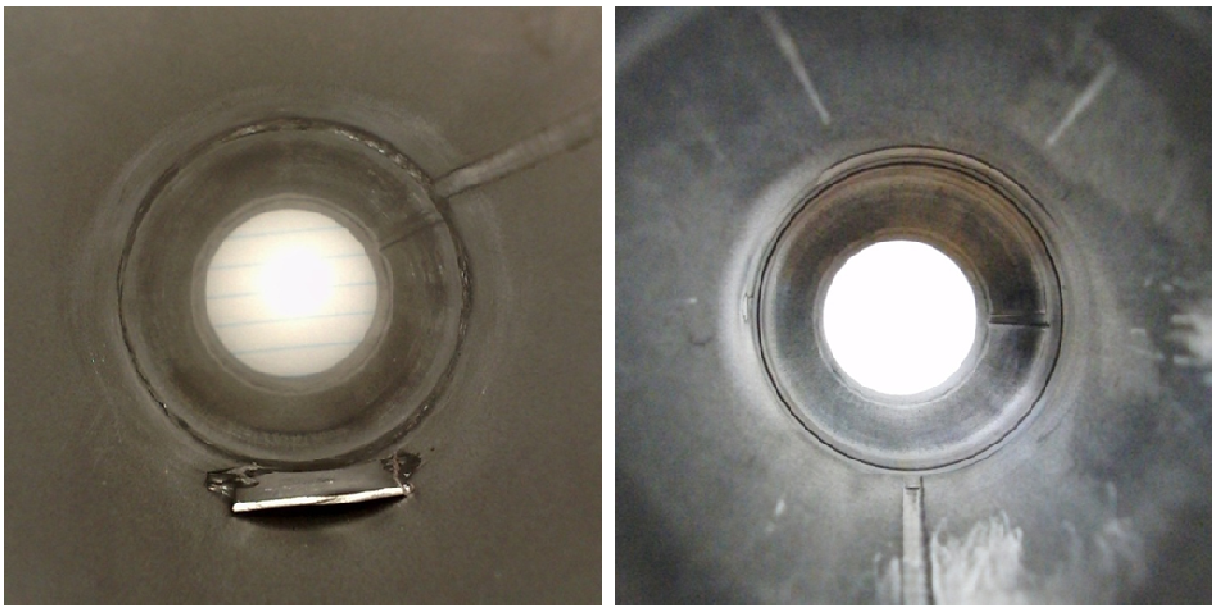

(a) (b)

Figure 5.6: Internal transition between main body pipe and reducer: (a) - before, (b) - after

The main body of the Flow Conditioner was cut in half near the plate and both the plate and the step were removed on a lathe. The presence of the plate and step as well as the final result after smoothing them off can be seen above in Figure 5.6(a)-(b). To connect the two pieces together again, a spigot arrangement was created using a lathe. The internal diameters of the pieces were bored until they matched and were then welded together.

The pieces were difficult to bore and as a result the inside diameters were not perfectly circular causing a slight lip to exist in places once the pieces were welded back together. Another asymmetry in the Flow Conditioner is in the custom flange attached to the end of the main body section. The internal transition of this connection is smooth but the angle it is welded on is slightly skewed. This causes the test section to veer off at a slight angle to the Flow Conditioner.

After the whole rig was constructed and experiments were begun, it was found that the fluid could not be drained very easily from the Flow Conditioner. An NB8 weld nipple was welded to the underside of the main body, underneath where the tube bundle sits, to allow a ball valve to be threaded onto it to act as a drain.

5.2.7. Mixing Tank

The Mixing Tank is named so for only one of its purposes. Having a large reservoir of fluid was useful for a number of reasons:

- Temperature is easier to control in a reservoir than for fluid continuously flowing past in a loop.
- Having a reservoir tends to homogenise the fluid, whereas the composition of fluid in a loop may vary with position.

- Holding up fluid in a reservoir easily allows the system to be open to the atmosphere and to be accessible for monitoring and control.
- When other chemicals are added, mixing in a reservoir ensures that the concentration will be more quickly dispersed.

The Mixing Tank contains many features and each of the parts is identified in Figure 5.7.

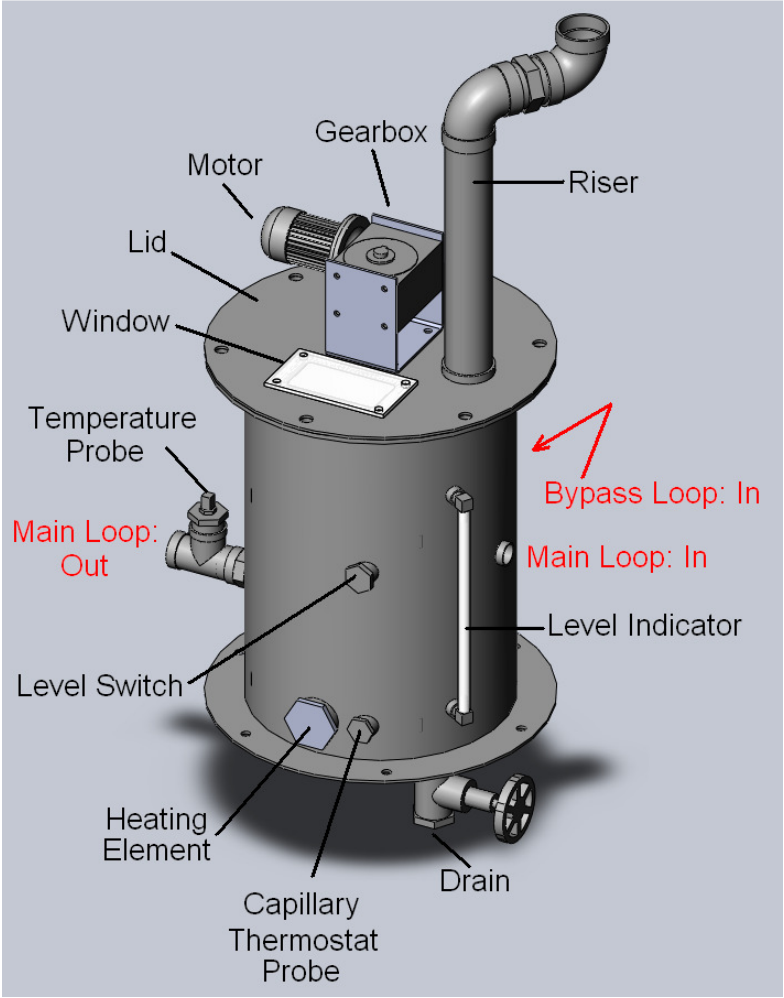

Figure 5.7: SolidWorks model of the Mixing Tank with labelled components

Sizing of Tank

The size and shape of the Mixing Tank was designed to provide constant, light stirring of the fluid. This will keep the fluid in the tank at the same temperature, allow homogenisation of colloidal sol and allow added chemicals to be quickly mixed in uniformly. The tank volume was chosen to be at least three times greater than the volume of fluid in the main loop to ensure the system behaved as a reservoir rather than a continuously circulated volume. Initially, the volume of fluid in the main loop for the largest test section size was estimated to be about 5 litres. Because of this, the tank volume was chosen to be 15 litres.

A standard design for such an agitation system is to have a vertically mounted propeller rotating in a cylindrical tank with baffles on the side walls. Optimal mixing configurations have been well studied

and the recommended sizes for the components are given by set ratios between the various tank dimensions. The dimensions selected for the Mixing Tank are given in Table 5.1 and the dimension ratios are compared to those of a Standard Agitation System from [47]. The Mixing Tank design does not deviate very far from the standard ratios and thus is expected to provide a reasonable degree of mixing.

Table 5.1: Mixing Tank dimensions and comparison to standard ratios

Dimension	Value (mm)	Standard Ratio	Actual Ratio
Tank Inside Diameter, D_T	269		
Liquid Height, H	265	$\frac{H}{D_T} = 1$	$\frac{265}{269} = 0.99$
Propeller Diameter, D_P,	100	$\frac{D_P}{D_T} = \frac{1}{3}$	$\frac{100}{269} = 0.37$
Height of propeller above bottom of tank, E	140	$\frac{E}{D_P} = 1$	$\frac{180}{100} = 1.4$
Propeller Blade Width, W	17	$\frac{W}{D_P} = \frac{1}{5}$	$\frac{17}{100} = 0.17$
Baffle Width, J	25	$\frac{J}{D_T} = \frac{1}{12}$	$\frac{25}{269} = 0.09$

Mixing

When fluid is mixed in a cylindrical tank, there is a possibility that swirling flow may occur where all the fluid has a tangential velocity following the impeller. Baffles are used to prevent this occurring which ensures that efficient mixing occurs. Four baffles were deemed sufficient for this small tank and they were offset from the wall by 5mm and offset from the bottom of the tank by 5mm. This improves the mixing action and prevents sediments at the bottom of the tank getting caught and building up on the baffle. The design fluid level in the tank was chosen to just cover the top of the baffles.

The impeller used in this rig was an old six-bladed propeller that was used for mixing demonstrations and experiments in a teaching laboratory. As can be seen from Table 5.1 this propeller is well sized for the Mixing Tank. The material that the propeller is made from is unknown but it is suspected to be some kind of stainless steel. A stainless steel shaft was made and two flat sections were ground onto the bottom end of the shaft for the propeller to clamp onto it via two grub screws.

The mixer components can be seen in Figure 5.8 below. The shaft was driven by a 0.09kW 3-phase AC Baldor Motor which was controlled with a frequency converter. The output shaft of the motor was directly coupled to the blue 25:1 worm-drive reducing gearbox. This allowed the speed of the output shaft from the gearbox to be controlled between 0-56 RPM. The propeller shaft was designed to slip over the top of the gearbox output shaft and was connected by using grub screws that clamp into the output shaft's keyway.

Figure 5.8: Mixer components on top of Mixing Tank

The motor and gearbox were held in place by a bracket that was bolted to the Mixing Tank lid. Clamped between this bracket and the tank lid was a shaft seal housing that was fabricated from a stainless steel round. A circular hole was bored into the top surface of this round to provide a press fit for a nitrile rubber lip seal. This allowed the shaft to rotate while still maintaining a seal. An O-ring groove was cut into the bottom surface of the round to provide a stationary seal between the housing and the lid. All of the bolt holes were sealed with the use of an O-ring at the base of the bolt head clamped on to the underside of the Mixing Tank lid.

The largest flow rate that the pump can provide the system is 1.8m^3/hour (see Chapter 6). The time that it takes to empty the tank can be used as an estimate for the average residence time of fluid in the tank, hence:

$$Average\ Residence\ Time = \frac{Volume}{Flow\ Rate} = \frac{0.015m^3}{(1.8m^3hr^{-1})\left(\frac{1\ hr}{3600s}\right)} = 30s$$

Although the stirring in the tank is not vigorous, with a minimum average residence time of 30s it was assumed that homogenisation would occur.

Temperature Control

The Mixing Tank provided the most convenient location for the temperature control system. The heating element used was a 1000W U-shaped, nickel plated copper resistive heating element. By placing it at the bottom of the tank, a convection current is created which further adds to the mixing effect.

The heating element size was chosen after estimating the heat loss from the rig at the maximum experimental temperature. Under conditions of negligible air movement in the laboratory, the heat loss was estimated to be about 2100W without insulation and about 120W with insulation. The calculations and assumptions made for this estimation are given in Appendix A. Based on these calculations, a 1000W heating element should be sufficient to keep the system at the maximum temperature. Time to heat fluid up was another important parameter and it was estimated that this heating element would be able to heat the fluid from room temperature (20°C) to maximum temperature (80°C) in about 80 minutes, which was deemed sufficient.

The temperature was monitored at the outlet of the tank by a PT100 temperature probe submersed with the tip in the centre of the flow stream. The location of this probe is visible in Figure 5.7 above. The probe was connected to a Dwyer 16-C digital temperature controller which controlled the heating element via a relay. A junction box was used to cover and exclude water from the heating element electrical connections.

Connections

The Mixing Tank has inlets for both the main and bypass loops and an outlet that leads directly to the pump. BSP threaded sockets were welded into the tank wall which allowed the pipe lines to be directly connected to the tank.

The outlet was designed to be near the bottom of the tank so that the hydrostatic pressure would tend to drive fluid into the pump. This aids the pump priming procedure and decreases the likelihood of cavitation occurring. To increase the natural tendency for mixing to occur in the tank, the two inlets were chosen to be placed as far from the outlet as possible and near the design fluid level height. The inlets were designed to be fully immersed at all times to prevent the entrainment of air.

Safety Features

A number of the safety features for the entire rig were located in the Mixing Tank:

Level Switch

There is a high possibility that a leak may develop somewhere in the rig during an experiment. If all the fluid is to drain out from this leak then damage may occur to the equipment. If the pump were to operate in air rather than water than the impeller may over-speed and cause the motor and electronics to overheat and become damaged. Also, if the heating element were to operate in air it would quickly burn out, resulting in a significant electrocution risk.

This is prevented by the use of a level switch which was designed to be fully submerged at the design fluid level. If the fluid level begins to drop then the float of the level switch also drops, causing it to trip when it reaches about the height of the main loop inlet. This switch cuts off power to the entire rig and will not switch back on unless a sufficient fluid level is restored. An indicator light on the electronics box is lit when the fluid level is too low.

Level Indicator

To allow quick identification of the fluid level in the tank, a level indicator was used. This was simply constructed from a piece of clear PFA tube and two Swagelok elbows. The elbows then screwed into two BSP threaded sockets that were welded into the tank. Unfortunately, the elbows were longer than expected such that at the design fluid level, the fluid level cannot be seen in the level indicator. The fluid level that the level switch cuts off at can be seen and it is about 40mm below the top of the indicator.

Window

A window on the tank lid was included in the design to allow the condition of the fluid in the tank to be seen. The window was constructed out of a sheet of clear Perspex that was bolted onto the tank lid. The bolt holes were sealed with O-rings around the bolt heads on the underside of the tank lid and a pipe flange gasket was modified to provide a gasket to seal the window. Once experimentation was begun it was quickly found that the visibility was too poor to be of use due to the condensation that formed on the inside of it.

Capillary Thermostat

A backup, mechanical temperature safety device was used alongside the digital temperature control system in case of hardware/software failures or an incorrect set point value entered. A capillary thermostat was chosen which had a probe that could be inserted into a thermowell in the Mixing Tank.

A BSP threaded socket was welded into the tank at the same level as the heating element. Having the thermowell close to the heating element ensured that it would be in the region of hottest fluid in the rig. The thermowell was constructed from a BSP threaded cap with a hole drilled into it to fit a short length of stainless steel tube. One end of the tube was pinched and welded together and then the tube was welded to the cap to make it water tight. The capillary thermostat probe was covered in thermal paste and inserted into the thermowell, which protrudes well into the tank. The capillary thermostat switches when the set temperature is exceeded and stays switched until it is manually reset. An indicator light on the electronics box turns on under these conditions. The set temperature can be changed as required.

Riser

When the rig is operating at the higher temperatures, hot, condensate laden air will rise from the tank, potentially causing burns to anyone nearby. To minimise the risk of injury, the tank was sealed and a riser was used to direct the vapour away from anyone near the tank.

An EPDM gasket was made to fit the Mixing Tank flange and the seals for all other components on the Mixing Tank lid have been described above. The only opening on the Mixing Tank lid is then the riser. To prevent pressure building up inside the tank from the riser becoming blocked up, it was designed to have a reasonably large bore. This would also be useful for the riser's other purpose; the location where chemicals or fluid could be added to the rig.

Plans were made to construct the riser from PVC pipe and use some BSP fittings to allow safe addition of chemicals. However, after the preliminary experiments it was soon realised that an oxygen exclusion system needed to be installed and the riser would need to be used for a slightly different function.

5.2.8. Pump

The pump selected for the rig was a Grundfos CRNE 1-3 vertical, multi-stage, inline centrifugal pump. This pump was selected for a number of reasons:

- Centrifugal pumps provide steady, non-pulsating flow rates. This is desirable when trying to set up a steady, fully developed flow in the test section.
- The pump had variable speed control allowing lower flow rates to be produced at lower pressures.
- The motor and electronics of the pump had integrated overload and temperature protection, ensuring the pump would not be damaged if there was a blockage or if all fluid leaked from the rig.
- A larger model of this same pump had been used in a field silica scaling test rig and expertise was available for cleaning it should significant scaling occur.
- The temperature limit of the fluid was 90°C which covers the desired experimental conditions
- The inline connections simplified the mounting and coupling of the pump to the rig.

As the fluid in the rig is continuously circulated there is no net system head. The head that the pump produces only needs to exceed the pressure losses experienced as the fluid travels through the loop. For this reason, the 1-3 was selected as it was the smallest pump in the Grundfos CRNE collection. The rated flow rate and head for this pump are 1.8 m^3/hr and 14.8m, respectively.

The pressure loss in the rig was estimated using a simple analysis of the theoretical pipe friction and loss through fittings. The method of calculation is given in Appendix A. The results from this analysis are shown in Figure 5.9 below where the pressure loss in the rig is superimposed onto the pump duty curve provided by the manufacturer. The red curve is for when the throttling valve is fully open and the blue curve is for when the throttling valve is one quarter open. The blue region corresponds to the operating range of the pump and the lines ranging from 25% to 100% show the pump duty at different motor speeds.

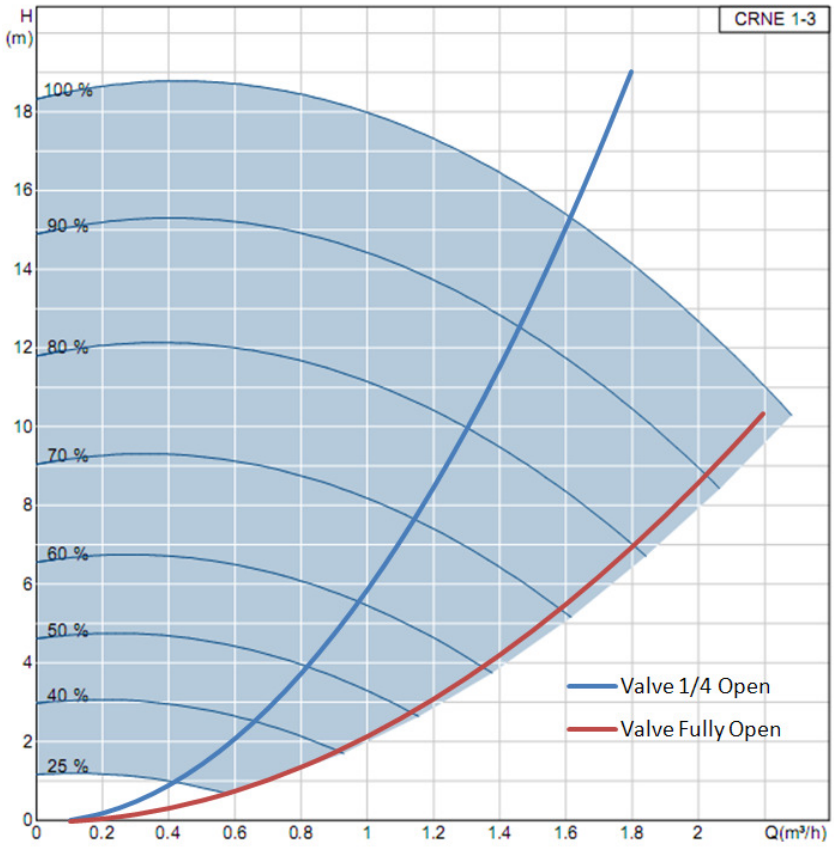

Figure 5.9: Pressure loss in rig (H) with flow rate (Q) superimposed on CRNE 1-3 pump duty chart

These results show that the pump is well-sized for the application and that the pump should never be pushed to operate outside its operating region. With the throttling valve fully open, the maximum flow that the rig can achieve appears to almost be the maximum that the pump can also achieve, about 2.2 m^3/hr. The pump manufacturer's duty curve suggests that the flow rate can be brought right down to zero and the most efficient way to do this would be to decrease the motor speed down to 25%.

In the case of the pump having difficulty operating at very low flow rates, the bypass line was added to the rig. This acts as a flow splitter, allowing the pump to operate at a higher flow rate while still maintaining a very low flow rate through the test section.

The net positive suction head (NPSH) required for the pump to prevent cavitation was also estimated and the analysis is given in Appendix A. Cavitation is most likely to happen when the fluid is at higher

temperatures and so the analysis was conducted at 90°C, the maximum operating temperature before the heating system would shut down. The NPSH available for the pump under these conditions was calculated and the results are shown as the blue line in Figure 5.10 below. The results are superimposed onto a chart of the NPSH requirements for the pump as provided by the manufacturer. The black lines correspond to different motor speeds in the same fashion as for Figure 5.9 above.

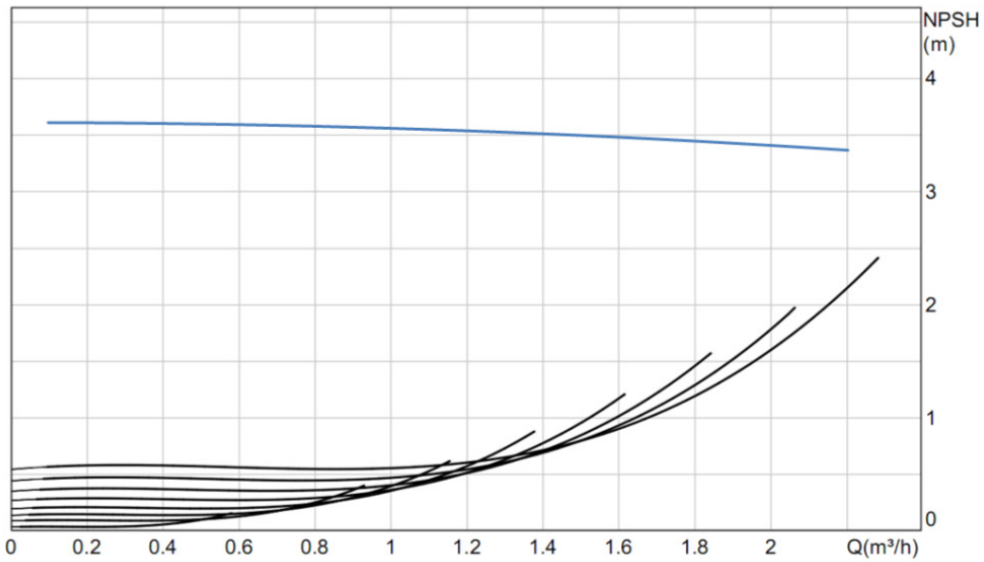

Figure 5.10: Net Positive Suction Head available for rig (blue) superimposed on the NPSH requirements at different pump speeds for the CRNE 1-3

These results show that, even in the most extreme conditions, the NPSH of the system is always greater than the NPSH required for the pump not to cavitate. Thus, it is anticipated that cavitation will never be a concern in the operation of the rig.

5.2.9. Flow meter

Mighty River Power made available for use a Micro Motion F050 Coriolis flow meter. This flow meter was suitable for the silica scaling test rig for a number of reasons:

- It does not require any flow conditioning or straight pipe runs preceding it, so can be placed anywhere in the rig.
- It has no moving parts that could become covered in silica scale and affect its performance.
- Maximum flow rate is 8.16m^3/hr.
- Maximum fluid temperature is 204°C.
- The flow rate can be logged over time to measure consistency of the flow rate.

There is no minimum flow rate for this flow meter but the accuracy of the measurement starts to deteriorate rapidly when the flow rate decreases below 1/40 of the maximum flow rate. For this flow meter, this occurs when the flow rate is less than 3.4 litres/min and the accuracy at this point is ±0.26%. The planned experiments for the rig are given at the end of this section and for some of the

experiments the flow rate is below this threshold. The accuracy of flow measurement for these experiments is unknown and it may have to be validated using another flow measurement method, such as the bucket and stopwatch method or the use of a small rotameter.

The measurement made in a Coriolis flow meter depends largely on the known mass of the tubes inside it. If scale were to build up in these tubes then this will increase the mass and affect the measurement of the flow. The use of the other flow measurement methods mentioned above could be used to calibrate the flow meter and provide a means of seeing whether its output strays over time.

5.2.10. Throttling Valves

The fluid flow rate is controlled by the pump speed and by the use of a throttling valve. Globe valves were used for both the throttling valve and the bypass valve. This type of valve is commonly used for the fine control of the flow rate and they still perform well even after silica scale has formed in them [48].

5.2.11. Test Section Pressure Measurement

The static pressure in the test section was desired to be known for use in any models that simulate experimental results from this rig. This was achieved by using a Dwyer DPG-203 digital pressure gauge mounted on the permanent section of the main loop just downstream of the test section outlet. The pressure range for this transducer is 0-30PSI (0-20.7 m H_2O) which is sufficient to cover the maximum head that the pump can produce of 19m. The output of this transducer can be logged to determine the consistency of the pressure within the test section.

The maximum fluid temperature that this transducer can withstand is 70°C. This is lower than the desired maximum experimental temperature and so a cooling coil was added. The coil was constructed from a length of PFA tube attached to the main loop and pressure gauge with Swagelok fittings. The fluid within this coil will be stationary.

As the pressure transducer is located on the permanent part of the rig the pressure will be slightly different to that in the test section. There will have been some pressure loss through the fittings at the end of the test section and pipe friction losses as the test section was traversed. These can be estimated using the simple relationships that were used to estimate the pressure loss in the entire rig in Appendix A.

The pressure measurement given by the transducer may not exactly be the static pressure in the rig. A BSP threaded tee was used to attach the fitting for the PFA tube and there may be a re-circulating flow in the branch. The measurement of pressure within this re-circulating region may well be different to the static pressure of the flow. This connection may need to be modified to obtain a more accurate static pressure measurement.

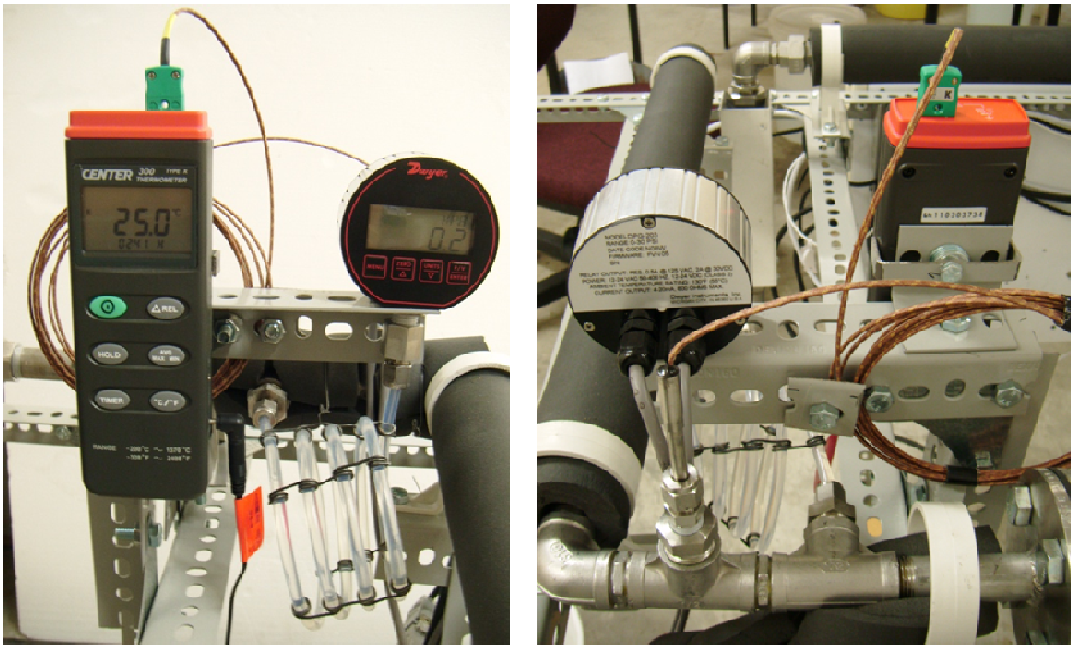

Figure 5.11: Temperature (rectangular) and Pressure (circular) meters and measurement devices

5.2.12. Test Section Temperature Measurement

The fluid temperature within the test section is also desired to be known for modelling purposes. This was achieved by the use of a Type K thermocouple and a Center 300 Digital Thermometer placed just downstream of the pressure measurement section as can be seen in Figure 5.11 above. The thermocouple extends through the Swagelok fitting with the tip in about the centre of the flow. Due to the test section being well insulated, this measurement will likely be close to the average temperature within the test section. The thermometer also has logging capabilities and so the temperature variation within the test section over each experiment can be determined.

5.2.13. Electronics Box

Once the components of the rig had been determined and the P&ID had been drawn, the electrical connections and controls were designed. An electrical schematic was drawn up and supplied to the electrical technician assigned to this project. The electrical technician improved on this design, ordered the appropriate components and performed all the electrical aspects of the rig construction. The rig complies with all relevant electrical standards for safety.

The test section thermometer had its own power supply connection but all of the electronics for the rest of the rig were housed in the electronics box that was built by the electrical technician. The power requirements for the entire rig were low enough that it could be run off a single connection to a 10A domestic power point. The main features contained within this electronics box are:

- Emergency Power Switch to shut down entire rig (except for test section thermometer).
- Power supplies for all components.
- Relay switch system for shutting down rig if the level switch goes off.

- Relay switch system connecting the temperature controller to the heating element.
- Thermostat switch arrangement to shut down the heating system should over-temperature occur in the capillary thermostat.
- Two fault lights: over-temperature and low fluid level.
- The temperature controller and frequency converter are mounted in the box.

5.3. Hazards and Operability (HAZOP) Study

At the request of Mighty River Power, a Hazards and Operability (HAZOP) study was performed on the rig to ensure that it would achieve a high level of safety for operators and bystanders. The HAZOP method was developed in, and is regularly used in, the chemical process engineering industry. It is a systematic method for analysing the effects that could occur in every part of system due to a deviation from the designed for parameters. This study was performed using the application guide standard, BS IEC 61882:2001 [49].

This HAZOP study was conducted after the P&ID had been developed but before the detailed design had commenced. This allowed any major safety flaws to be avoided before too much work had been performed and allowed the safety features of the rig to be designed in conjunction with the rest of the rig. The initial steps of this analysis were performed with Paul Siratovich from Geological Sciences, another sponsored student from Mighty River Power. A summary report of the study findings was produced and is given in Appendix C. The detailed design was then completed and the HAZOP study was revisited and updated to take into account the changes that had been made. The summary report of the Revision #1 HAZOP study is also given in Appendix C.

5.3.1. HAZOP Study Methodology

Parts

The HAZOP procedure involves the systematic analysis of each part in the system. In order to perform this analysis the P&ID was split up into 20 different parts, usually separated by some kind of connection. For example, between the pump and the Coriolis flow meter there were six parts: pump, pump outlet pipe, bypass tee, throttling valve, NB25x15 contraction, Coriolis flow meter. Part 1 was the Mixing Tank and this contained Parts 1a-1h; the various components inside it or connected to it.

Elements

Each part was attributed with a number of “elements” which the standard defines as a “constituent of a part which serves to identify the part’s essential features”. All parts in this study, except for 1a-1h, contained the elements:

- Fluid – that is, the presence of fluid in the part
- Temperature – the temperature of the fluid in part and of the part itself
- Pressure – fluid pressure in part
- Flow – the flow of fluid through the part

Depending on the part, other elements would be included. For example, “Pressure Reduction” was an element of Part 6 (Throttling Valve) and “Pressure Measurement” was an element of Part 13 (Pressure Sensor).

Parts 1a-1h did not contain the experimental fluid within them. For this reason, the four elements mentioned above did not apply and their elements were mainly that of their function. For example, “Rotation” was an element of Part 1a (Mixer Motor), and “Heating” was an element of Part 1f (Heating Element).

Guide Words and Deviations

For each element of each part, a number of guide words were applied to identify potential ways that deviations from the design intent could occur. The basic guide words identified in the standard were used and are given in Table 5.2 below.

Table 5.2: Basic guide words and their generic meanings. Source: [49]

Guide word	Meaning
NO OR NOT	Complete negation of the design intent
MORE	Quantitative increase
LESS	Quantitative decrease
AS WELL AS	Qualitative modification/increase
PART OF	Qualitative modification/decrease
REVERSE	Logical opposite of the design intent
OTHER THAN	Complete substitution

The identification of the deviations is a creative process using the guide words as a “trigger” to allow a possible application of the guide word to an element to be envisaged. For example, when applying the guide word, ”NO”, to the element, “Pressure Reduction”, of Part 6, a possible deviation would be “Throttling Valve does not reduce the pressure”. There may be more than one form of deviation for each particular combination of guide word, element and part.

For each deviation, all of the possible causes and consequences that could be envisaged were then recorded. Usually several of these were identified for each deviation and each one is then referred to as a hazard.

Operation Stage

The purpose of this study was to ensure that operators of the rig and bystanders would be safe whenever they are near the rig. At different operation stages of the rig, different hazards are present and so this study incorporated the analysis of what deviations could occur during three stages of operation: Set-up, Operational Steady State, and Shut-down/Draining.

Risk Evaluation

A scoring system was created to evaluate the level of risk for each hazard. This system was created by modifying the University of Canterbury Health & Safety Hazard Assessment system. The scoring system is given in Table 5.3 below. Each hazard is scored based on three criteria:

1. Frequency – How often the hazard can possibly occur.
    - For example, a leak can only occur when there is fluid in the rig. During an experiment the hazard of a leak is "Constantly".
2. Likelihood – How frequently the hazard occurs when it is actually possible.
    - Given that there is fluid in the rig, this is the chance that a leak may then occur.
3. Severity – How severe the consequences (to people and equipment) are if the hazard were to occur.
    - If the rig did develop a leak, what the consequences would be and how significant they would be.

Table 5.3: Scoring system for risk evaluation

Frequency	Score	Likelihood	Score	Severity	Score
Annually	1	Rare	1	Minor	1
Monthly	2	Unlikely	2	Moderate (first aid only)	2
Daily	3	Possible	3	Severe (serious harm)	3
Hourly	4	Likely	4	Major (permanent disabling injury)	4
Constantly	5	Almost Certain	5	Catastrophic (loss of life, >$1m costs)	5
Scores are multiplied to give total risk					
Risk	**Score Range**	**Action**			
Low	1 to 10	Negligible, can be ignored			
Medium	11 to 30	Mitigation required to minimise score as much as possible			
High	31 to 80	Mitigation compulsory to reduce risk			
Critical	81 to 125	Mitigation compulsory to reduce risk			

The risk to the experiment was also identified in this analysis and was labelled according the system shown in Table 5.4

Table 5.4: Experimental Risk Evaluation

Negligible	Negligible effect on experimental results or ability to carry out experiment
Noticeable	Noticeable effect on experimental results or ability to carry out experiment
Significant	Significantly affects results or ability to carry out experiment
Devastating	Renders results useless or prevents experiment being carried out

Risk Mitigation

For all hazards with a Medium risk or higher, mitigation was required to reduce it as much as possible. For each hazard, various safeguards were identified and possible forms of mitigation were envisaged. With all of these in place, the risk level was re-evaluated, usually obtaining a Low risk level. However, in some cases, the risk could not be reduced to be less than Medium but they were still deemed safe as the severity was minor and was not likely to cause harm to people.

The mitigation methods and procedures that were identified but had not yet been incorporated into the rig design were marked in the "Action Required" column. The end goal of the HAZOP study was to have all hazards at an acceptable risk level with no further actions required.

5.3.2. HAZOP Study Results

The HAZOP study was completed in full with every part analysed for every combination of element and guide word. The risk levels ranged from Low to High in the study and all risks were successfully reduced to either Low or to Medium with only a Minor severity. The completed worksheet contained over 2000 rows but there was a significant amount of repetition with some element/guide word combinations. An example of the study worksheet is given in Appendix B.

The preliminary study results are summarised in Appendix C and contributed to the rig design by:

- Identifying Generic Mitigation procedures that could be built into the rig design to prevent or minimise many hazards occurring.
- Identifying and providing tasks for a number of checklists for Rig Commissioning, Start-up, Operational, Shutdown and Maintenance stages.
- Identifying the need for a temperature controlled switch, which resulted in the addition of the capillary thermostat.
- Identifying the need for an emergency shut off switch, which resulted in the main power switch on the electronics box.
- Identifying the need for multiple draining points around the rig.
- Providing some design considerations for the heating system, the Mixing Tank, and whole rig.
- Providing some ideas and considerations that should be pursued further to improve the safety and functionality of the rig.

The Revision #1 study was performed at the end of the detailed design stage when the complete design of the rig had been settled upon. The results from the preliminary study were then modified to incorporate all of the subsequent changes to the rig design. Another summary report was produced, given in Appendix C, which detailed:

- How the results of the first study had been incorporated into the rig design. If they had not been incorporated, justifying reasons were given.
- The further modifications that were made to the Generic Mitigations and Checklists.

- Some further changes to be made to the rig design.
- Recognition of a number of factors that could not be resolved until construction had begun.

5.3.3. As-Built Deviations from HAZOP Revision #1 study

As the rig was progressively constructed, various considerations caused the actual configuration to differ from the original design. Also, the factors that could not be resolved until construction was underway were then able to be resolved. The deviations from the HAZOP Revision #1 study include:

- Capillary Thermostat dial was not physically limited to prevent it being set higher than 90°C.
    - The dial was located inside the thermostat box and could only be accessed by using a screwdriver. Hence, no chance of accidentally bumping it.
- Temperature controller was not put inside a box to prevent it being accidentally bumped.
    - The button used to adjust the set point is small and requires a firm prod to activate it. Also, the set point increases in 0.1°C increments so is unlikely to accidentally be set dangerously high.
- Fluid mass loss to evaporation is deemed irrelevant as preliminary experiments show that it is negligible. A distilled water feed system for the Mixing Tank was hence deemed unnecessary.
- Bypass valve is not left partially open at all times to relieve pressure should complete blockage of main loop occur.
    - Due to the pump selected having sufficient safety features, a complete blockage in the main loop is not as harmful as initially suspected.
- Permanent orifice plate to increase pressure loss in main loop was found to not be required as the pump duty was always within its operating region.

Changes to the generic mitigations include:

- All electrical equipment was installed by a qualified electrician and was checked and found to be safe. No further safety features were required for the electrical equipment.
- Wooden boards were used as leg spacers for the mounting frame.
    - Although these are flammable, the risk of fire resulting from one of the electrical components was very low and as the boards were against the ground they were not deemed a significant fire risk.
- Warning signs were not set up around rig.
    - The North Calorimeter room is only frequented by those involved with this project. A Hazard Register for the room is placed on the door; this was deemed to be sufficient warning.

5.4. Experimentation Plan

Once the detailed design of the rig had been completed and the range of operational parameters had been determined, the experimentation plan could be developed. The new set of experiments described in Table 4.2 were analysed and the conditions required to achieve these experiments in the rig were determined. The calculation procedures and assumptions made when performing this analysis are given in Appendix A. All experiments were planned to be performed at 30°C. This is higher than room temperature to keep the heating system constantly operating but low enough that there is no risk of harmful burns.

Four experiments using laminar conditions were developed and they are summarised in Table 5.5 below.

Table 5.5: Planned Laminar Experiments

		Experiment No.:			
Parameter	**Unit**	**1**	**2**	**3**	**4**
Pipe Inside Diameter	mm	35	35	35	35
Particle size	nm	100	10	100	10
Flow rate	l/min	1.0	1.0	2.0	2.0
Reynolds Number		760	760	1510	1510
Required test section length	m	1.7	1.7	3.4	3.4

These experiments test the deposition of large and small particles at two different flow rates. Schedule 40 NB32 pipe was selected for these experiments because it is the largest size that can be used with the rig. As the pipe size increases, a laminar flow rate can be sustained at higher flow rates and higher flow rates will be easier to set up and measure in the rig.

With this pipe size, the required test section length for experiments No. 3 and No. 4 was 3.4m but only 3m lengths would be used in the experiments. The laminar flow will not be fully developed in this case but should be very close to developed conditions. Another potential problem is that the Coriolis flow meter may not be able to accurately measure the flow rates of 1.0 and 2.0 litres/min. Another method of flow measurement may be required.

Table 5.6: Turbulent experiments to test the effect of particle size and viscous boundary layer thickness on deposition

		Experiment No.:					
Parameter	**Unit**	**5**	**6**	**7**	**8**	**9**	**10**
Pipe Inside Diameter	mm	35	35	17	17	6.3	6.3
Particle size	nm	100	10	100	10	100	10
Flow rate	l/min	20.0	20.0	10.0	10.0	3.5	3.5
Reynolds Number		15,100	15,100	15,500	15,500	14,700	14,700
Viscous Boundary Layer Thickness	mm	0.378	0.378	0.173	0.173	0.062	0.062
Required test section length	m	2.8	2.8	1.4	1.4	0.5	0.5

Table 5.6 shows how the effect of particle size on deposition can be tested with three pairs of experiments at different flow conditions. Each pair of experiments uses a different pipe size and a different flow rate. These conditions have been carefully chosen to yield a Reynolds number in all experiments of approximately 15,000. The thickness of the viscous boundary layer varies with each pair of experiments and so the results obtained will provide information about the influence of this parameter on deposition. As each experiment is performed twice using two particle sizes, the influence of particle size can also be ascertained.

Further turbulent experiments can be performed that have a constant viscous boundary layer thickness with a varying Reynolds number. The conditions for such experiments are given in Table 5.7 below.

Table 5.7: Turbulent experiments to test the effect of Reynolds number on deposition

		Experiment No.:		
Parameter	**Unit**	**11**	**12**	**13**
Pipe Inside Diameter	mm	35	17	6.3
Particle size	nm	100	100	100
Flow rate	l/min	30.0	6.0	0.7
Reynolds Number		22600	9300	2900
Viscous Boundary Layer Thickness	mm	0.262	0.275	0.272
Required test section length	m	2.8	1.4	0.5

Experiment No. 13 may not be suitable for analysis due to its low Reynolds number of 2900, which places it in the Turbulent Transition region. A higher Reynolds number could not be used because Experiment No. 11 would need to have a higher flow rate to provide the same viscous boundary layer thickness. However, experiment No. 11 is currently at the maximum flow rate for the rig and it can't be increased further. Also, the flow rate for Experiment No. 13 may not be able to be accurately measured with the Coriolis flow meter and may require another measurement device.

Chapter 6. Construction and Commissioning of Silica Scaling Test Rig

6.1. Rig Construction and Modifications

The rig was constructed according to the design given in Chapter 5 and a picture of the finished rig is given in Figure 6.1 below. A number of modifications were made to the design as the construction process proceeded and they are described in this section.

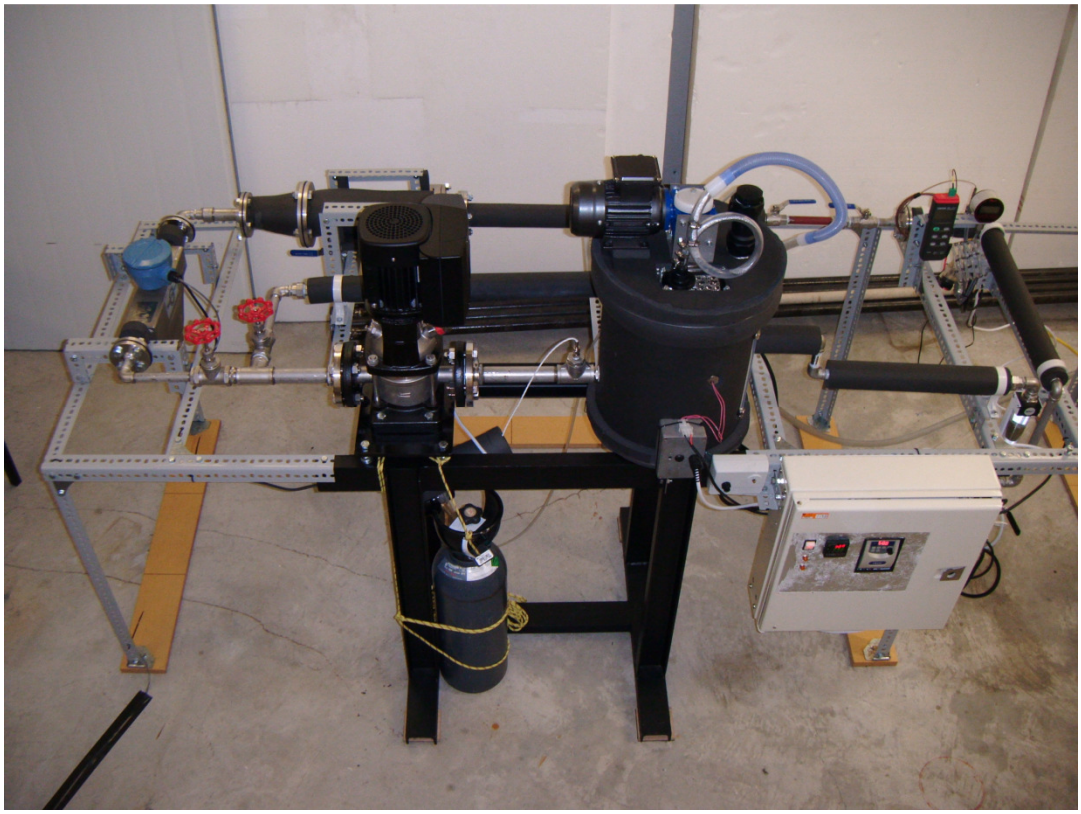

Figure 6.1: The Constructed Silica Scaling Test Rig

6.1.1. Rotameter

After the rig had been constructed and commissioning tests were begun it was discovered that the planned communication method with the Coriolis flow meter would not work. It was anticipated that it would take some time to solve this problem and so a rotameter was installed to take flow measurement readings in the meantime. The rotameter was installed at the location of main loop drain and can be seen in Figure 6.1 at the lower right corner of the rig. As the bottom of the rotameter was now the lowest point in the main loop, it was convenient to attach the drain onto the bottom of it using some BSP threaded fittings.

The rotameter measurement scale covers the flow rate range of 4-40 litres/min. This size of rotameter was chosen as it would allow measurements to be made for nearly all of the planned turbulent experiments and also for the maximum achievable flow rate in the rig. It could also be used to

calibrate the Coriolis flow meter over this range. It will not be able to provide an accurate flow rate measurement for the laminar experiments and for the turbulent experiments that use 9.5mm tube as the test section.

The rotameter tube is made of acrylic glass and its recommended temperature limit was 60°C. The capillary thermostat was set to 60°C to ensure that the rotameter could not be damaged during experiments. When the Coriolis flow meter can finally be used for measurement, the rotameter can be removed and the capillary thermostat can be set to 90°C.

6.1.2. Preliminary test section configuration

It was initially expected that there could be some issues with corrosion of the mild steel test pieces. It was also not known what the silica deposition rate would be or even if silica deposition would actually occur. To gain an understanding of the corrosion and silica deposition characteristics, the test section was modified to allow some preliminary experiments to be performed before using the full size test sections. The preliminary test section configuration is shown in Figure 6.2 below.

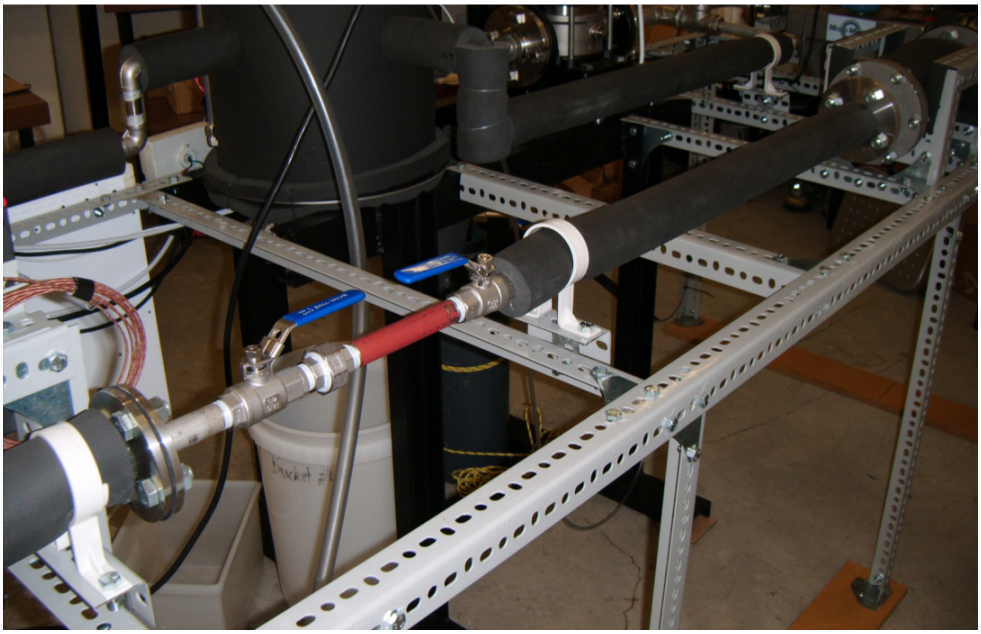

Figure 6.2: Preliminary test section configuration with 150mm long, red, mild steel pipe section

A blind flange with an NB15 pipe stub was made to connect to the Flow Conditioner contraction adaptor piece. This caused a sudden contraction from NB32 to NB15 to occur at the outlet of the Flow Conditioner. The stub was then connected to a length of stainless steel Schedule 40 NB15 pipe followed by a 150mm length of mild steel NB15 pipe. Using a small mild steel test section reduced the material cost for the preliminary experiments and decreased the amount of potential corrosion products travelling through the rig. The total length of this section was 1m, the test section length to be used for the experiments using the smallest test section diameter.

The mild steel test piece is connected to a ball valve on one side and to a BSP Union on the other side which is then connected to another ball valve. When the rig is shut down, the valves can be closed and the test piece can then be easily removed with only the loss of the fluid that was inside this small section. After inspection the test piece can be either re-inserted or swapped for a new piece and the experiment can be restarted.

Because of the short length of the test section and the presence upstream of a ball valve and abrupt contraction, the hydrodynamic conditions in the mild steel test piece will not be fully developed. This condition is not necessary to gain an understanding of the level of corrosion and silica deposition that will occur in the rig.

6.1.3. Oxygen Exclusion System

The results from the preliminary experiments are described later in Chapter 8 and it was found that significant corrosion did occur in the mild steel test pieces. The corrosion was likely to be due to the high level of dissolved oxygen (DO) in the fluid, which was measured with a YSI 550A DO meter to be 6.9 mg/litre or about 85% of saturation for those conditions. An oxygen exclusion system was created to solve this problem.

Oxygen Scavenger

Sodium sulphite, Na_2SO_3, is an oxygen scavenger and is commonly used in steam generation boiler systems to prevent corrosion of steel components. Sodium sulphite reacts with dissolved oxygen according to the reaction:

$$2Na_2SO_3 + O_2 \rightarrow 2Na_2SO_4 \qquad \text{Eq. (6.1)}$$

The theoretical ratio of sodium sulphite required to consume all of the dissolved oxygen, by weight, is:

$$\frac{2(126\ \text{g/mole}\ Na_2SO_3)}{32\ \text{g/mole}\ O_2} = 7.88 \qquad \text{Eq. (6.2)}$$

For 20 litres of fluid containing 6.9 mg/litre of DO, about 1.1 g of sodium sulphite would be required to remove all of the oxygen. A greater dose than this (~4 times) was added to the experiments to take into account incomplete reaction and to react with any further oxygen that may enter the system. The sodium sulphite used came as a powder that could be directly added to the fluid and, after mixing, started to react with the oxygen within minutes according to DO meter readings.

Nitrogen Blanket

The sodium sulphite would remove the dissolved oxygen from the fluid but if the Mixing Tank was left open to air, more oxygen would dissolve in and the problem would continue. This was solved by creating a nitrogen blanket in the top of the Mixing Tank, the only interface between the fluid and air.

The nitrogen was supplied from a regulated gas bottle located underneath the tank and shown in Figure 6.3(a) below. The diaphragm valve regulator was connected to a needle valve, which allowed very fine control of the nitrogen flow rate.

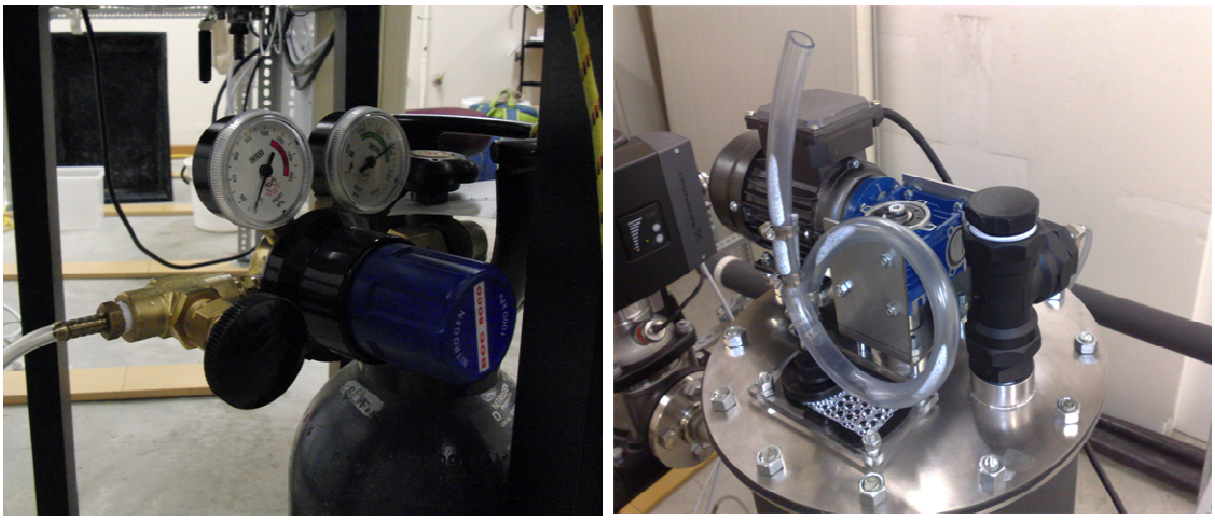

(a) (b)

Figure 6.3: Oxygen Exclusion system: (a) - Nitrogen bottle and connections, (b) - Header and water trap on top of Mixing Tank

The gas is conveyed through the plastic tubing to the black header at the top of the Mixing Tank that is displayed in Figure 6.3(b). The header is constructed from BSP threaded polythene fittings with one Swagelok fitting that connects to the plastic tubing. The top of the header is a BSP cap that can be removed to allow fluid or chemicals to be added to the rig.

With the header in place the tank is completely sealed, as described in Chapter 5. To allow gas to escape from the tank, an outlet was created through the Perspex window of the Mixing Tank lid. A water trap was constructed from a looped section of plastic tubing, which isolated the gas in the Mixing Tank from the outside air. The nitrogen bottle could then be set to provide a very low flow rate to the Mixing Tank. As the pressure builds up, the water trap will act like a manometer with the water level in the downstream section rising up. When the level reaches a certain point, a bubble of nitrogen gas is able to escape through the water trap. The water level then falls due to the corresponding loss of pressure and continues with the cycle of pressure build-up and escape of a bubble. The water trap is set to provide a positive pressure head in the Mixing Tank of about 30mm of water.

The HAZOP process was not completed on the oxygen exclusion system but the University of Canterbury Health and Safety Hazard Assessment procedure was followed. The diameter of the water trap was made to be large enough so that blockage of it is unlikely and that there is no way that pressure can build up to dangerous levels inside the tank. The outlet of water trap was connected to a length of plastic tube that conveyed the gas outside the building, eliminating the possibility of nitrogen asphyxiation in the North Calorimeter room.

6.2. Commissioning

Once construction had been completed, the safety features and operational capabilities of the rig were tested. The rig operated as expected and it was possible to control both the temperature and the flow rate of the fluid. All of the components functioned properly, except for the Coriolis flow meter which was yet to be connected.

6.2.1. Safety Features

The two major safety features were tested, and found to function as designed, in the following way:

- The Mixing Tank drain was opened during operation of the rig and once the fluid level had dropped sufficiently, the level switch cut power to the rig and lit the “Low Fluid Level” light.
- The temperature controller was set to 70°C and when the fluid reached 60.5°C, the capillary thermostat switched off power to the heating system and lit the “Overtemperature” light. The fluid then started to cool.

6.2.2. Draining

The dead volume in the rig was measured twice, both times after the rig had been completely reassembled, which ensured there was no fluid in the rig to begin with. The rig was completely filled with a measured amount of water and the system was turned on and left until steady conditions were reached. The rig was then completely drained and all of the drained fluid was weighed. The tests provided an estimated dead volume in the rig of 0.9 litres and 1.3 litres. It is likely that this fluid is located in the bottom of the pump, the Coriolis flow meter and in the pipe section between these two components.

6.2.3. Flow Rate range

The minimum flow rate that the rig can achieve could not be measured due to the lack of a suitable measuring device. The maximum flow rate that the rig can achieve was able to be measured. The flow rate with the throttling valve fully open was measured at different pump speeds.

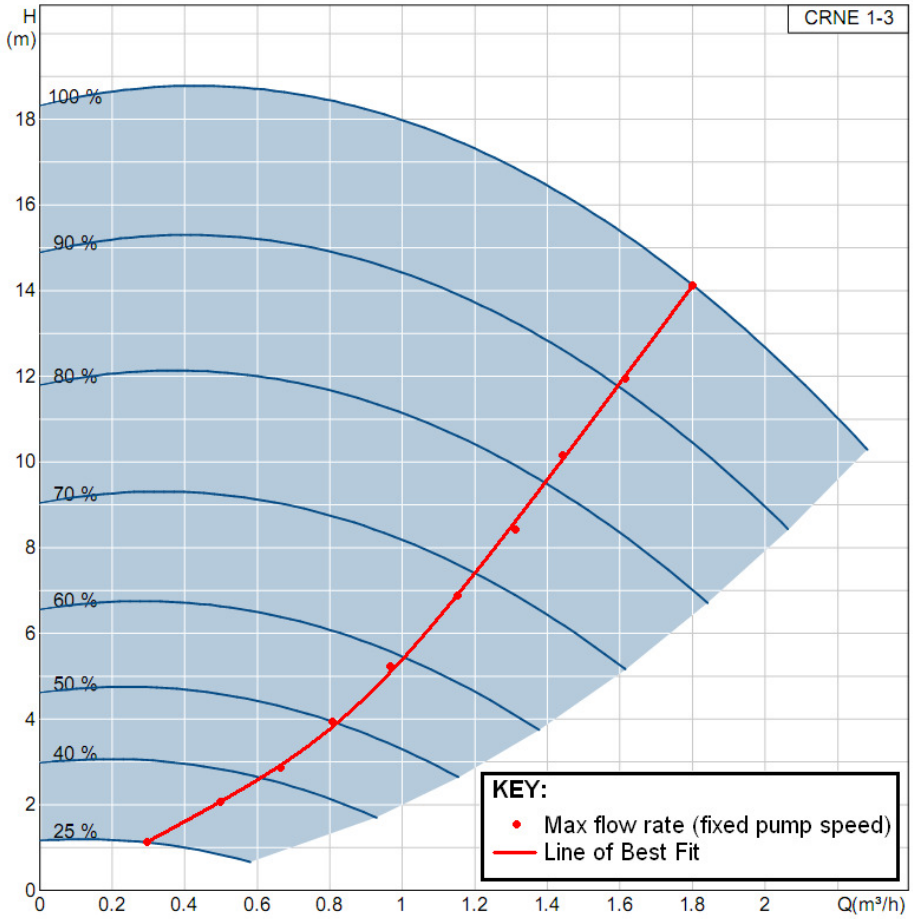

Figure 6.4: Maximum flow rate measured at different pump speeds and superimposed on CRNE 1-3 pump duty chart

The measured data was then plotted on the pump duty curve to provide Figure 6.4. The red line corresponds to the pressure loss curve for the rig and it is higher than what was theoretically predicted and shown in Figure 5.9. The maximum flow rate that can be achieved in the rig is 1.8 m^3/hr (30 litres/min) whereas it was predicted that it would be able to achieve 2.2 m^3/hr. The main reason for this is that more fittings were used in the constructed rig than were taken into account of in the theoretical model. Particularly high pressure loss that was unaccounted for occurs in the sudden contraction at the outlet of the Flow Conditioner and in the rotameter configuration. A higher flow rate can likely be achieved when the full length test section is used and the rotameter is removed.

6.3. Experimental Procedure

The experimental procedure was initially planned during the design stage and a checklist was developed from the HAZOP study. As the preliminary experiments were performed, the experimental procedure was developed and improved upon in light of the practicalities experienced. The current experimental procedure is given below.

Start-up

1. Ensure that:
    - all drains are closed
    - every piece of equipment is properly in place
    - the power supply is turned off
    - throttling and bypass valves are slightly open
2. Add 5g sodium sulphite to experimental fluid and mix. Remove the BSP cap from the nitrogen system header and add fluid using a funnel.
3. Open the pump primer valve until an uninterrupted fluid stream comes out
4. Check the rig for leaks.
5. Turn the power supply on, start pump at a low flow rate and adjust temperature set point and mixer speed as required.
6. Progressively open the throttling valve, waiting until the air bubbles in the rotameter disappear before opening further.
7. With throttling valve fully open, increase the pump speed step by step to maximum, waiting for the bubbles to disappear before doing so.
8. Set the flow rate to desired level.
9. Open the nitrogen gas bottle and turn on a high flow rate for 30 seconds to flush the air out of the Mixing Tank. Add water to the water trap and set the nitrogen flow rate to produce one bubble in the trap every 10 seconds.
10. Keep monitoring the rig until the steady state condition is reached.

During experiment – Daily Check-up

1. Check that the temperature and flow rate set points are correct and adjust as necessary.
2. Record the maximum and minimum values for temperature and pressure since last daily check-up. Reset values.
3. Check that the nitrogen flow rate is at required rate and adjust as necessary.
4. Check rig for leaks and other abnormalities.
5. Remove a small sample of fluid from the sampling point for visual inspection and testing. Measurements may include: dissolved oxygen level, pH and particle size.

Shutdown and cleaning

1. Mark the test piece so that the flow direction and the top and bottom of pipe can later be identified.
2. Turn off the main power supply on the electronics box. Shut off the nitrogen flow rate
3. If the set temperature was high, leave the solution to cool.
4. Shut off the isolating valve and carefully remove test piece, preventing spillage of the fluid inside it.
5. Set containers underneath all drains and empty the rig.
6. Add the stainless steel "dummy" test section and open the isolating valves.
7. Close all drains, fill the Mixing Tank with fresh water and repeat steps 3-7 of the Start-up procedure.
8. Once system is bled of air, simultaneously fill and drain the Mixing Tank, ensuring the water level in the tank does not over-fill or drop so low that power cuts out.
9. After 5 minutes turn off the water supply, shut down the rig and fully drain.

6.4. Conclusions

The Silica Scaling Test Rig has successfully been constructed and commissioned. The rig can be used to perform the preliminary experiments to understand the silica deposition characteristics. Once the full-length test section is incorporated the rig will be able to perform most the experiments given in Section 5.4 with controlled temperature and flow rate conditions.

There are still some issues with draining, flow measurement, and with the Flow Conditioner. Remedying these issues will enable the full set of experiments given in Section 5.4 to be performed and some experimental uncertainties will be reduced. The recommended actions to remedy these issues are given in the Future Work, Chapter 10.

Chapter 7. Colloidal Silica Production

The colloidal silica production method was initially developed during a Summer Research project by George Starling, a Chemistry graduate. The method was then refined and further developed by the author and, later, in conjunction with Pavlo Kokhanenko, the PhD student who will carry on this research.

7.1. Preliminary Work – George Starling

George Starling began his research project by reviewing the literature on colloidal silica production techniques [50]. In order to provide similarity to geothermal brines, he recommended that the methods used in this project should produce silica particles that were hydrophilic with silanol surface groups. He proposed that the hydrolysis method should be used for low concentration solutions with an ion exchange step used for concentrated solutions.

7.1.1. Hydrolysis Method

1. Sulphuric acid, H_2SO_4, is added to distilled water and the solution is brought up to the reaction temperature (typically 60°C in this research).
2. Sodium metasilicate, Na_2SiO_3, is added evenly in small doses over 15 minutes under constant agitation.
3. The pH will initially be less than pH 2 and will increase slowly as the metasilicate is added. Particle nucleation is favoured over polymerisation under these conditions, allowing many particles to form. The pH will increase slowly until a pH of about 3.5 is reached, upon which it starts to increase rapidly up to pH 8.2. The initial quantity of sulphuric added to the system was selected to neutralise the metasilicate such that at final addition the pH would rapidly increase until a pH of 8.2 was reached. Small amounts of sulphuric acid or sodium hydroxide, NaOH, may need to be added to maintain the pH at 8.2 over the course of the experiment. This pH level provides the optimum conditions for particle growth.
4. The solution is kept at constant temperature and pH conditions for 1 hour.
5. Solution is quenched to room temperature and stored in plastic bottles.

7.1.2. Ion Exchange Method

This method will need to be used if more than 10 g/litre of metasilicate is to be used in the procedure as the high salt concentration in the Hydrolysis method will start to cause aggregation. Steps 1 and 2 of the Hydrolysis method should be followed but the pH will need to be kept below pH 3.5. The solution should then be added to an ion exchange resin, such as Amberlite H form, at a ratio of about 10g of resin per 100mL of solution. The suspension should be mixed thoroughly and separated via vacuum filtration with hardened filter paper. The filtrate is then returned to the reaction vessel to be

brought back up to the reaction temperature. The pH is raised to pH 8.2 through the use of concentrated sodium hydroxide and steps 4 -5 of the Hydrolysis method can be completed as before.

7.1.3. Experimentation

George Starling produced a number of solutions using the Hydrolysis method. He found that he could produce stable solutions, without gelling, at metasilicate concentrations up to 9g/litre. He suggested that the pH is the key variable for sol stability and obtaining a smooth pH transition in Step 3 of the Hydrolysis method is necessary for a repeatable particle size distribution. He also attempted to use the Ion Exchange method but did not have suitable equipment.

7.2. Particle Size Measurement

The particle size measurements in this research were made with the zeta potential measurement device and nanoparticle size analyser, Zetatrac, sold by Microtrac Inc. The instrument uses photon correlation spectroscopy techniques to measure the particle size distribution. A small fluid sample of 1-3ml is poured into the plastic well and is left for a few minutes for the temperature to equilibrate. The Zetatrac is connected to a computer and it is operated through the use of proprietary software.

To measure a particular type of particle, a number of chemical properties are required and these were provided by the manufacturer. A number of operational settings were also required for optimal particle size measurement. These were determined based on suggestions from the manufacturer and by trial and error. A summary of the settings used for these measurements is given in Appendix D.

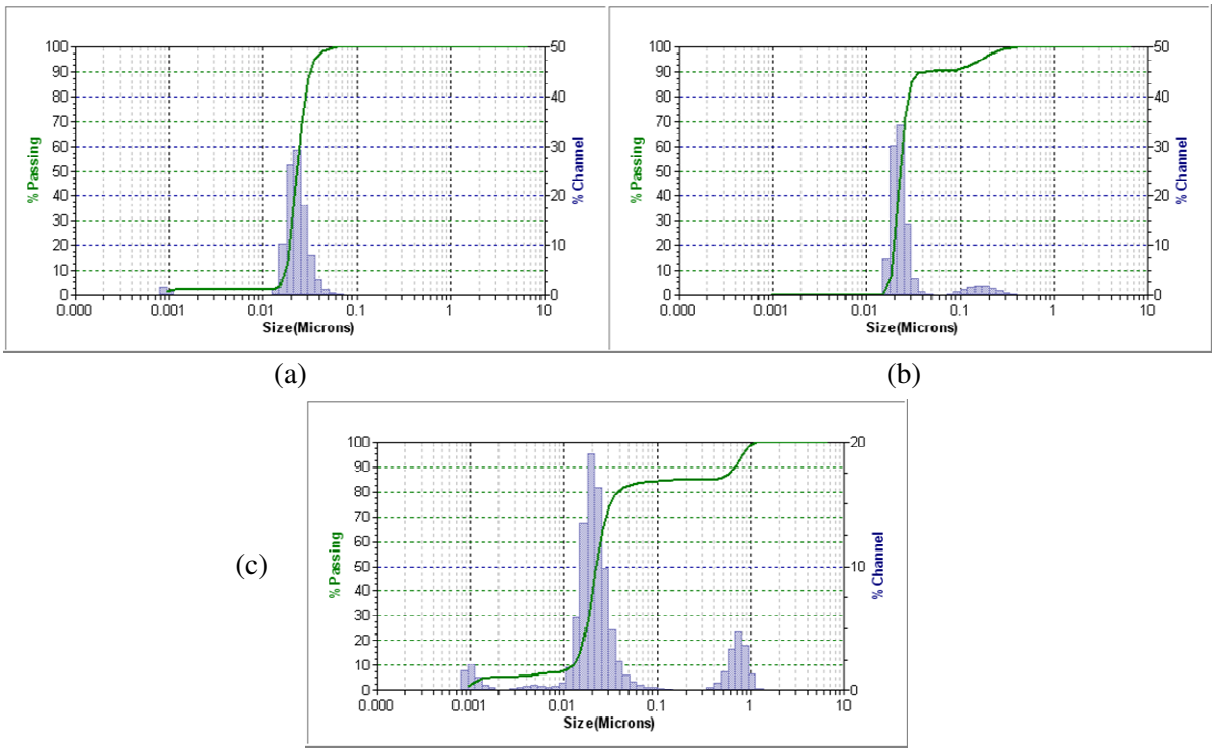

Figure 7.1(a)-(c): Typical Zetatrac output for three consecutive measurements of particle size distribution

Each sample is measured three times consecutively to obtain an average result. An example of the measurement output is shown on the previous page in Figure 7.1(a)-(c). The purple bars correspond to the percentage of the total measured signal intensity that is taken up by the signal from particles within that size range. This gives the particle size distribution and the green line shows the cumulative distribution. As silica particles are spherical in shape, the particle size refers to the particle diameter.

The above results are typical for the stable sols produced in this research. There is nearly always a large peak in the measurements and its location is repeatedly in the same position. This type of peak is to be expected for a monodisperse solution. For Figures 7.1(a)-(c) on the previous page, there is a clear peak at about 20nm and the output of software provides the location of the peaks to be 22.9nm, 22.3nm and 20.3nm, respectively. This range in peak particle size, on the order of a few nanometres, is typical for stable sol measurements.

In all three measurements small secondary peaks are present, all in different locations with different magnitudes. Due to the unrepeatability of these secondary peaks, they are assumed to be noise or from contamination. Potential causes for these peaks could be:

- Contamination of solution from dust particles or large aggregates.
- Ground vibrations upsetting the sensitive Zetatrac (North Calorimeter Room sits above a mechanical workshop).
- Electrical noise from power supply.
- Measurement signal being hard to obtain due to low particle concentration.

To improve the accuracy of particle size measurements, future work could involve: creating a vibration damper for the Zetatrac, running the Zetatrac off a well-controlled uninterruptable power supply and improving the cleanliness of measurement taking to reduce contamination.

7.2.1. Low Particle Concentration Measurements

The Loading Index is a measure of the total AC signal obtained from the light scattered from the particles. It is dependent on the particle properties, concentration and size as well as the properties of the fluid in which they are suspended. The Loading Index can be checked before particle size measurements are made and these were usually recorded in the present research.

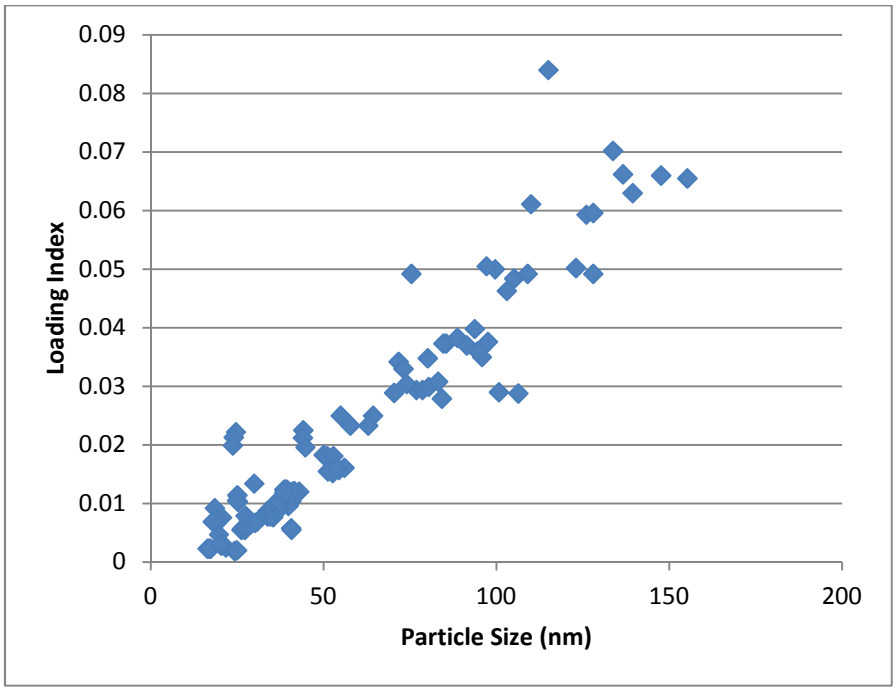

Figure 7.2: Loading Index measurements vs. particle size for Sample L11 as it grew over time

Figure 7.2 shows the Loading Index measured for Sample L11 (9g/litre metasilicate) as it grew over time. Only amorphous silica was present in this sol and the concentration would have been constant over the whole period. The Loading Index was found to be proportional to the particle size, as can be seen in Figure 7.2 above.

The manufacturer of the Zetatrac has provided concentration limits for accurate particle size measurements based on the Loading Index. The Caution Range is for sols with a Loading Index less than 0.1, which covers even the largest particle size shown in Figure 7.2. There is no lower limit for the Loading Index but with decreasing magnitude, measurements are increasingly susceptible to error. Small concentrations of large particles can have a significant effect on the particle size measured, as can rapid temperature changes and bench vibrations.

The SetZero Background Index is the initial Loading Index recorded for a clear fluid to determine the background noise in the system. Within the Caution Range it is recommended that a SetZero of less than 0.010 is used. If this value was used then, according to Figure 7.2 above, the signal from particles less than about 40nm would be counted as noise. Therefore, in this research, a smaller value for the SetZero was used, usually within the range of 0.0004-0.0008.

To measure particles on the order of 10nm in size, the Loading Index was about 0.0010. This is not much higher than the SetZero condition that could be achieved and so it would be expected that measurements will be particularly susceptible to noise in this case. As nearly all of the measurements in this research fall within the Caution Range there is a need to validate the results against other measurement techniques. These may include other types of particle size analysers and using Transmission Electron Microscopy.

7.3. Development of Colloidal Silica Production method

7.3.1. Stage 1

Following on from the preliminary work by George Starling, his version of the Hydrolysis method was repeated by the author to try and obtain reproducible results. The set-up which George Starling developed is shown in Figure 7.3.

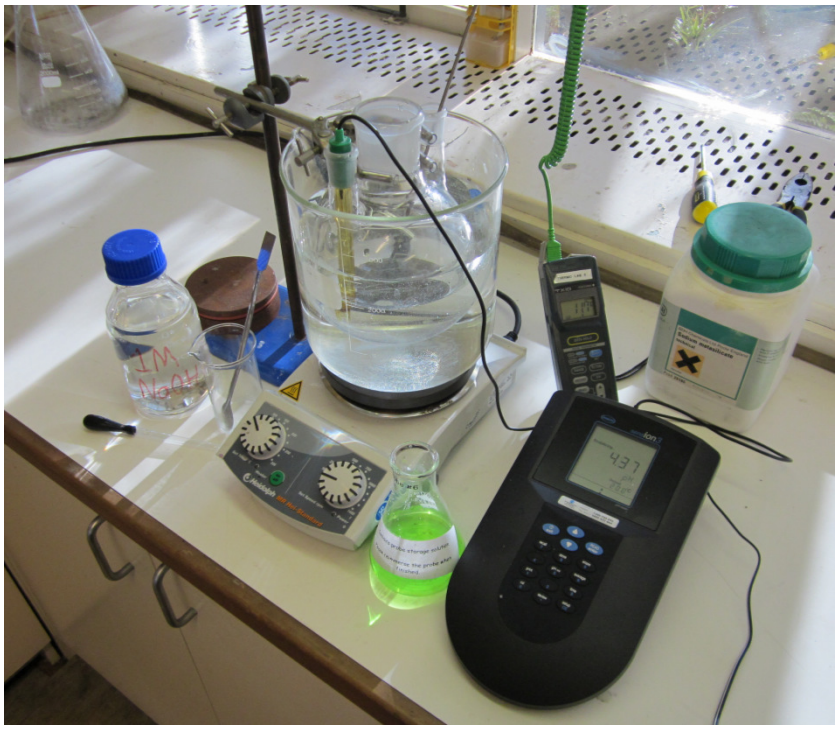

Figure 7.3: Experimental setup used to produce 500mL batches of sols

A 3-necked spherical vessel is held in a waterbath which sits up upon a magnetic stirrer/heater plate. A plastic coated "magnetic flea" is placed inside the spherical vessel which stirs the solution. Temperature and pH probes are inserted through the smaller openings and continuously monitor the conditions.

The first stage of experimentation involved creating 16 sols using the set-up shown in Figure 7.3. The volume of the sols produced were 400ml, 500ml or 600ml, depending on the storage vessel available. Sols L1-L3 were created to become familiarised with the method but no measurements were performed on them due to the disruption of the 22/02/2011 Christchurch earthquake. Sols L4-L13 were created using a metasilicate concentration of 9g/litre and the particle size and pH were measured over time. Sols L14-L16 were created with a metasilicate concentration of 3g/litre but it was found that this concentration was too low to obtain results from the Zetatrac.

The goal for sols L4-L13 was to follow the same method exactly to gain repeatable results. As the experiments were performed the production method did vary. The main variations were in the pH level achieved during different stages of the experiment and also in the amount of acid and base that was added to the solution. The way in which the pH was brought up from an acidic level to an alkaline level in Step 3 of the Hydrolysis level significantly varied between experiments. Sometimes after the addition of the sodium metasilicate the solution would remain acidic, other times it would be basic and greater than pH 8.2. Adding small amounts of acid or base to adjust the pH would sometimes achieve the desired pH in one step. Other times, too much was added and the pH oscillated about the desired level as acid and base were consecutively used for compensation. This affected the final pH of the solution once it was cooled and stored. A summary of these experiments is given in Table 7.1 below.

Table 7.1: Measurement Summary for Sols L4-L13

Sol No.	Initial Size (nm)	Growth Rate (nm/day)	pH During Experiment	Storage pH
L4	12	0.3	8.3	8.8
L5	52	23	8.3	8.8
L6	36	19	7.8	8.2
L7	11	0.2	8.5	9.1
L8	20	2.9	8.0	8.4
L9	14	1.0	8.0	8.4
L10	13	0.5	8.0	8.4
L11	17	1.1	8.0	8.4
L12	11	3.3	7.9	8.2
L13	10	0.2	8.4	9.1

The largest initial particle sizes and growth rates were found for sols L5 and L6. These had aggregated after 1 and 2 weeks, respectively, and later gelled. With the exception of these two sols, the initial particle size for all other experiments was between 10-20nm. The most stable solutions with the lowest growth rates were sols L4, L7 and L13. It was noticed that these three sols had the highest pH during the experiment and during storage. At a higher pH, the solubility of amorphous silica is higher and it was suspected that this has a great influence on the growth rate of already formed particles. Sol L5 also had a high pH but it is unknown why it behaved so differently.

7.3.2. Stage 2

The next phase of experimentation involved the testing of different experimental parameters on stability and on the effect of modifying the pH to achieve stability. Pavlo Kokhanenko was taught how to make the solutions and he conducted most of the experimental and analytical work during this phase.

The experimental parameters to be varied were:

- Increasing reaction temperature from 60°C to 75°C.
- Increasing the reaction time from 1 hour to 2 hours.
- Adding all of the metasilicate simultaneously rather than incrementally over 15 minutes.
- Producing a 5 litre batch using new equipment rather than 500ml batch.

Table 7.2: Measurement Summary for Sols S17-S28. Courtesy of Pavlo Kokhanenko

Modification	Sol No.	Storage pH	Initial particle size (nm)
None	S17	8.45	7.7
	S18	7.80	12.8
Increased Temperature	S19	8.67	11.9
	S21	8.55	14.0
	S22	8.75	8.5
	S25	8.85	10.5
Increased Reaction Time	S20	8.40	12.0
	S24	8.44	14.0
Instant metasilicate addition + Increased Temperature	S23	8.50	23.0
	S26	8.83	10.3
	S27	9.05	9.3
	S28	8.90	9.1

The initial results that were obtained from these experiments are displayed in Table 7.2. The samples that were produced in a 5 litre batch were S25 and S28. The results show that there is significant variability in the initial particle size and the storage pH even when identical conditions are used. No conclusive results were found from these experiments except that the storage pH tends to be higher when an increased temperature is used. This is to be expected as the pH level of a solution increases with decreasing temperature. This is probably due to the change in the equilibrium dissociation constant for H_4SiO_4 with temperature. All solutions were initially at approximately the same pH and so when the solution is cooled to room temperature, those that were initially at a higher temperature will result in a higher pH.

The effect of pH on stability was tested by taking the solution just after it had been cooled and splitting it into three containers. One container was left as a control and the pH was usually between pH 8-9. The other two containers had their pH adjusted with sulphuric acid or sodium hydroxide to

obtain one sample at about pH 8 and the other at about pH 9. The results for these experiments are shown in Figures 7.4-7.6 below.

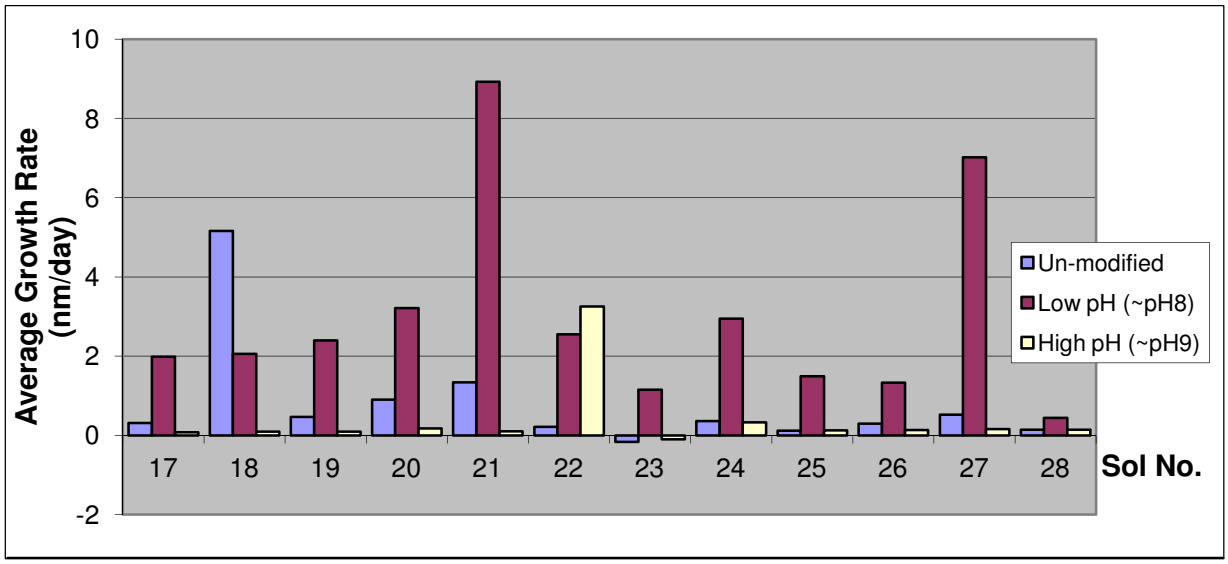

Figure 7.4: Average growth rate over one month for Stage 2 sols

The average growth rate for the Low pH samples is markedly higher in nearly every sol. One exception is the unmodified S18; from Table 7.2 it can be seen that it starts with a pH of 7.8 and so it would be expected to behave like a Low pH sol. The other exception is for the High pH sample of S22; the reason for its large amount of growth is unclear.

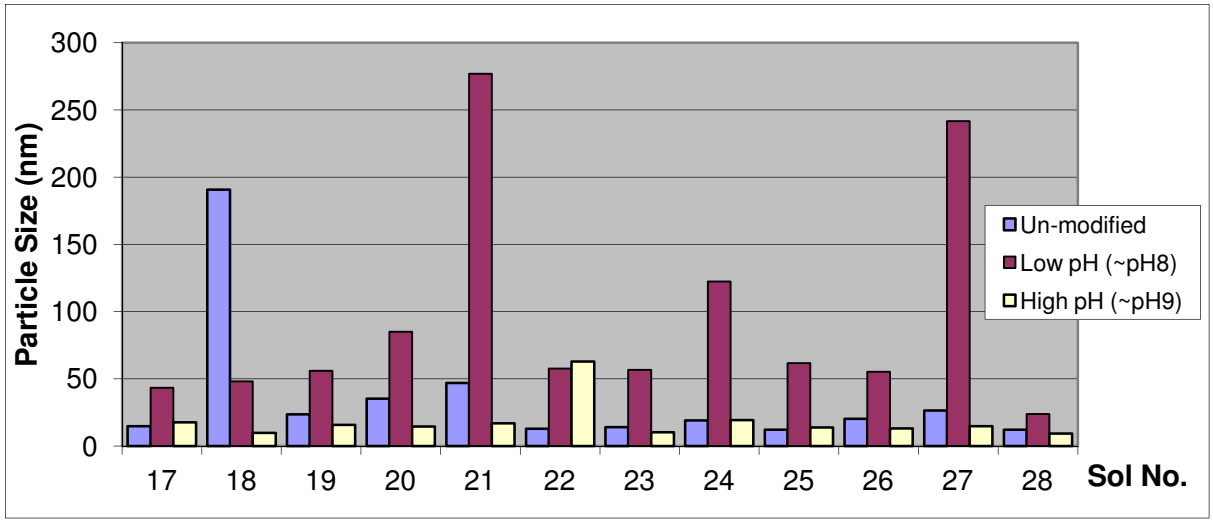

Figure 7.5: Particle sizes after one month for Stage 2 sols

After 1 month from the production of the sol, most of the Low pH samples grew to a size of about 50nm with some growing even larger, up to a particle size of about 270nm. The unmodified samples tended to grow a little and were generally larger than the High pH samples. This was to be expected as the unmodified samples usually had a pH in between the Low and High pH samples.

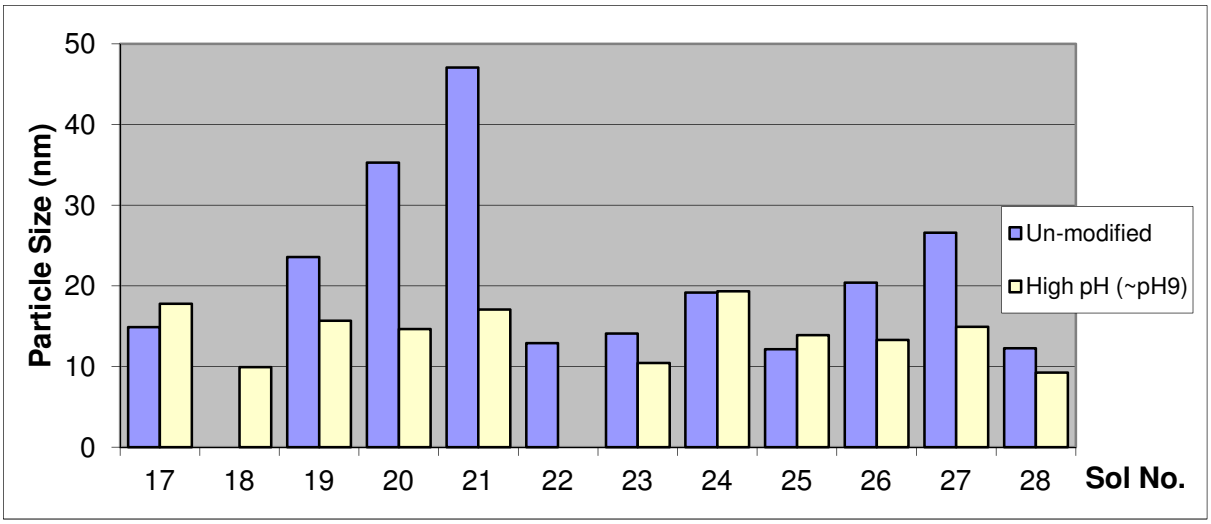

Figure 7.6: Particle sizes after one month for Stage 2 sols excluding the Low pH sols and un-modified S18 and S21

Figure 7.6 shows that after one month nearly all of the High pH samples produced sols of 10-20nm particle size, regardless of the different experimental parameters used to produce them. This will be sufficient for use in the silica scaling test rig as it is anticipated that a sol will not be used for more than a month long experiment.

This method is only able to repeatedly produce sols with particles sizes in the range of 10-20nm. In order to obtain larger particle sizes, some further experiments were performed, the results of which are shown in Figures 7.7(a)-(d). Some of the Low pH sols were split into two after significant particle growth had occurred. One part was left unmodified (blue) and the other had its pH raised to about 9 (red).

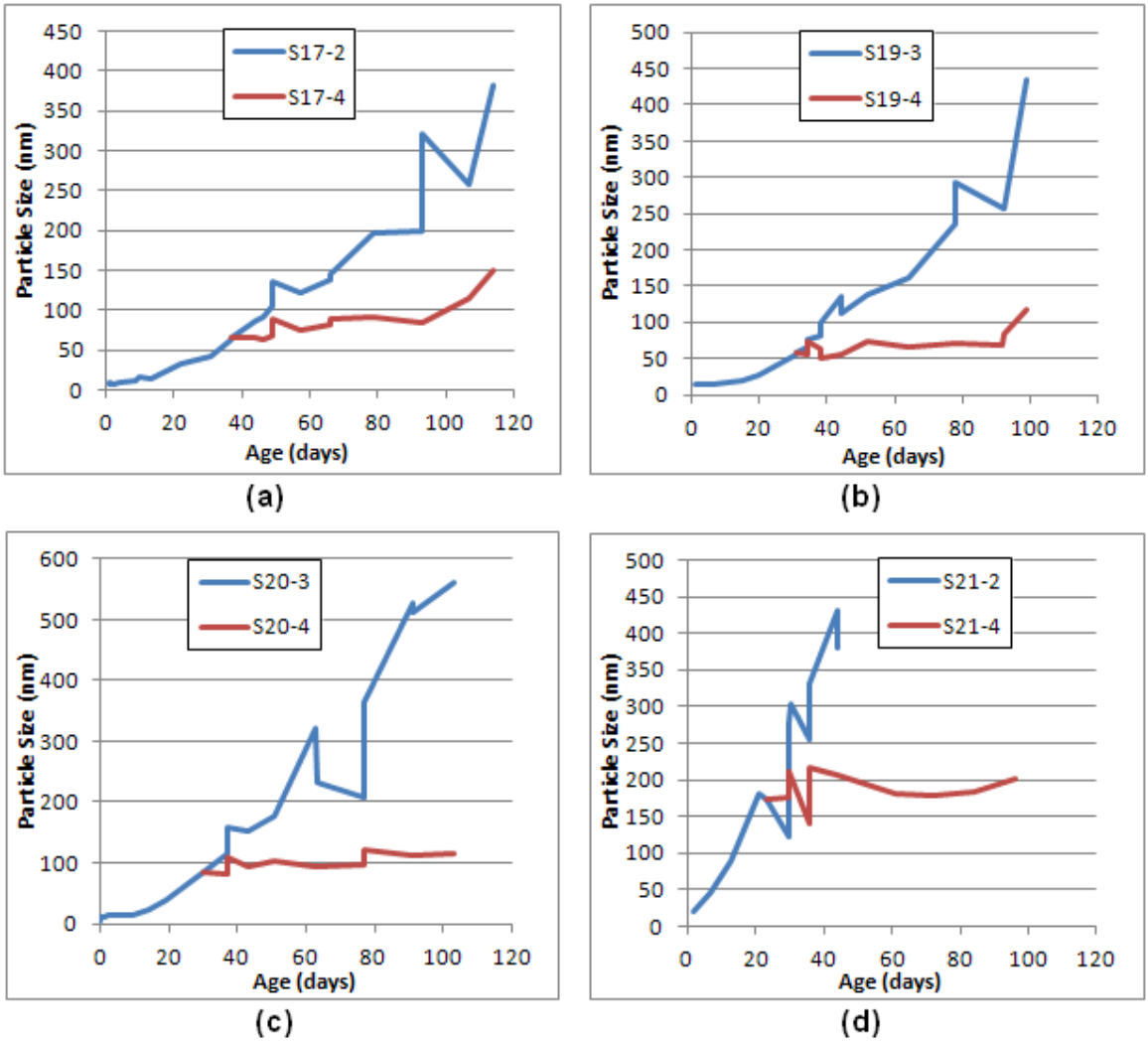

Figure 7.7(a)-(d): Results of the pH modification experiments

In all of the experiments the sols with the modified pH were found to have a reasonably stable particle size for at least 90 days. Within the same time frame, the particle sizes in the original Low pH sols kept growing until aggregation and gelling occurred. Controllable particle size can then be achieved by using this technique of lowering the pH to promote particle growth and then raising the pH when the desired size is obtained.

7.3.3. Stage 3

The next phase of the research was to develop a method for creating 20 litres batches of colloidal silica for use in the silica scaling test rig. The experimental and analytical work performed during this stage was largely conducted by the author, with assistance from Pavlo Kokhanenko in making some of the sols and with measurement taking.

Figure 7.8: Experimental equipment used to produce 5 litre batches of sols

The experimental equipment used to produce the 5 litre batches of colloidal silica is shown in Figure 7.8 above. A 2-necked 10 litre spherical glass vessel was used, which sat in an Electrothermal MV2407 heating mantle. Stirring was achieved through the use of a plastic coated "magnetic flea" inside the spherical vessel with a custom-built stirring device. The base of this device is visible in Figure 7.8 and contains two magnets attached to a plate that is then connected to the output shaft of a small electric motor. A Hach HQ40d pH meter and PHC281 probe (with in-built thermocouple) was used to monitor the temperature and pH of the solution. The pH probe was calibrated using standard pH buffer solutions.

Based on the Stage 2 results, it was decided that increased reaction temperature and instant metasilicate addition would be used in these experiments. These modifications provided a greater storage pH and were more likely to be stable.

Only 5 litres could be reacted in the vessel at one time. The method for producing 20 litre batches was to consecutively create two sols at double concentration, dilute them both by half and then mix them together. It was found that sols could successfully be produced with a metasilicate concentration of 12g/litre and so a final concentration of 6g/litre could be achieved. The concentration of amorphous

silica in this case is about 1700ppm. The method for calculating concentration and the Standard Operating Procedure (SOP) for the whole production process is given in Appendix E.

Samples were taken during the full strength (FS), dilute (D) and mixing stages of these experiments. The particle sizes and pH of these samples were measured over time and the results are shown in Table 7.3 below.

Table 7.3: Measurement summary for Sols S29-S39

Sol No.	Initial Size (nm)	Initial pH	Average Growth Rate	
			Rate (nm/day)	*Measurement Period (days)*
S29-FS	21.2	8.98	0.36	49
S29-D	21.4	8.94	0.06	49
S30-FS	11.9	9.01	0.14	49
S30-D	12.6	8.92	0.06	49
S29+S30-D	17.8	8.95	0.15	49
S31-FS	13.2	9.00	0.28	42
S31-D	14.0	8.87	0.07	42
S32-FS	11.1	9.13	0.21	42
S32-D	10.2	9.03	0.10	42
S31+S32-D	12.6	8.82^{+}	0.05	17*
S33-FS	14.0	8.70	0.30	69
S33-D	14.4	8.61	0.01	69
S34-FS	11.8	8.93	0.19	69
S34-D	12.4	8.87	0.03	69
S33+S34-D	13.4	8.92	-	-
S36-FS	13.5	8.63	0.70	18^{++}
S36-D	14.2	8.59	0.16	52
S37-FS	17.3	-	2.70	17^{++}
S37-D	17.0	-	0.28	51
S36+S37-D	15.2**	8.81^{+}	0.03	51
S38-FS	19.1	-	0.38	19
S38-D	20.7	-	-0.09	19
S39-FS	17.1	-	1.62	19
S39-D	18.5	-	-0.01	19
S38+S39-D	18.8	-	-0.02	19

Notes	
+	pH first measured at 17 days (S31+S32-D) or 18 days (S36+S37-D) and was likely higher initially
++	Sol had large aggregates at end of measurement period, so previous measurement used
*	Size only measured up until 17 days
**	Initial size seemed erroneously high so Day 2 measurement used

Using the newly developed method, the initial particle size was within the approximate range of 10-20nm. This method consistently provides a relatively high initial pH, as was anticipated from Stage 2 of the research. The initial pH was found to lie within the range of pH8.6-9.1 and the variations observed are probably due to slight differences in reaction temperature and in the amount of acid and base used to adjust the pH.

Full strength and diluted samples yielded very similar initial particle size measurements. The maximum divergence in initial size was 1.6nm, which is likely to be within the accuracy of the Zetatrac. They also yield very similar initial pH measurements with the diluted sample always having a slightly lower level. This is to be expected because distilled water has negligible chemical buffering and hence diluting with distilled water will reduce the OH- concentration, therefore lowering the pH slightly.

The average growth rates are the most significant difference between the full strength and diluted samples. The full strength samples always have the higher growth rate and some of these rates are so large that aggregation is found to occur. The difference in growth rates is most likely due to the difference in concentration. The full strength samples have a metasilicate concentration of 12g/litre which is greater than the limit for the Hydrolysis method of 10g/litre, as suggested by George Starling.

When two sols were mixed together, the initial size was always found to lie between the initial sizes for the two original sols. The mixed solutions had similar growth rates to those of the diluted samples. The average growth rate for the mixed sols shown in Table 7.3 was about 0.05nm/day which corresponds to a growth of 1.5nm over a month. This is within the experimental uncertainty of the Zetatrac.

7.4. Conclusions

The results of Stage 3 of this investigation have shown that the modified Hydrolysis method is able to repeatedly produce sols of particle size 10-20nm that will negligibly change in size for at least one month. These sols can be used in the silica scaling test rig to perform the experiments planned in Chapter 5 that required a small particle size. Sols with larger particle sizes can be obtained by initially lowering the pH level, leaving the sol to grow to desired size and then raising the pH to a stable level.

There are some issues with the size measurement of these sols due to small particle sizes and low concentrations. To improve the accuracy of the measurements, bench vibration dampening and power supply quality should be investigated, and the cleanliness of measurement taking should be improved. The measurements should also be validated against other particle size measuring techniques.

Chapter 8. Experimentation and Preliminary Results

During the design and construction of the silica scaling test rig, a number of side experiments were performed to gain an understanding of whether or not deposition would occur in the laboratory. Once the rig had been commissioned, three preliminary experiments were performed. The results and analysis of all this experimentation is recorded in this chapter.

8.1. Side Experiments

8.1.1. Trial Rig

The trial rig was created to test whether deposition would occur at room temperature on steel pipe with constantly re-circulated fluid. The rig was constructed from a submersible water-fountain pump connected to polythene BSP threaded fittings and a short length of NB25 mild steel pipe. To keep from overheating, the entire rig was submerged in a tub and is shown in Figure 8.1(a) below.

(a) (b)

Figure 8.1: (a) The Trial Rig, (b) Scale that formed on the test section bottom during second experiment

Two experiments, using Sols L12 and L13, were performed in which the rig was left running constantly for a week. The first experiment yielded a green sludge on the bottom of the pipe. The pipe had corroded on the inside and on the outside during this experiment and it is likely that the presence of iron oxides caused the sol to gel.

For the second experiment, the outside surface of the pipe was painted and covered to prevent any corrosion. Also, when the rig was set up, more effort was made to bleed as much air as possible from the system. Figure 8.1(b) displays the scale that was found in the second experiment. This rippled morphology is what is typically seen in geothermal scales. However, unlike geothermal scales, this present scale was soft and could be easily scraped off. The fluid inside the rig had turned a cloudy, rusty colour and particle size measurements showed that significant aggregation had occurred. The

scale had settled and covered the bottom of the pipe across the whole length. Due to the settled nature of the deposit, it is likely that it consisted of large aggregated particles.

The conclusions of these early experiments were:

- Some forms of silica scaling will occur at room temperature from a re-circulated flow.
- Corrosion is likely to occur inside the pipe and it will likely cause aggregation.

8.1.2. Ferric Ion Experiments

Ferric chloride, $FeCl_3$, was used by Chan et al [37] to test the effects of ferric ions on silica deposition. They found that the addition of only a few ppm caused coagulation and deposition of colloidal silica particles. To test the influence of ferric ions on sol stability in this research, a series of tests using ferric chloride, $FeCl_3$, were performed. A prepared solution containing $FeCl_3$ was added to samples of sol S28-1 to obtain Fe^{3+} concentrations of 1, 3, 5, 10 and 100ppm. The particle sizes in the samples were then monitored for three days.

The S28-1 sol was found to be stable over the period of the experiment and it had a particle size of about 11nm. The particle size measurements of the 1ppm sample were similar to that of the original sol. However, for the 3, 5 and 10ppm solutions, significant aggregation of the particles was observed within one hour of the start of the experiment. For these measurements, the particle size for the largest peak in the Zetatrac output varied between 100-300nm. Repeatable measurements could not be obtained for these solutions, suggesting that random aggregation had occurred.

The 100ppm sample also had similar measurements initially. However, after two days it was found that yellow aggregates had settled on the bottom of the sample container. The fluid, which was once yellow in colour, had become clear and when the particle size in the clear fluid was measured, a similar result to the original sol was obtained. The ferric ions had likely initiated, and been incorporated into, the aggregates which had become so large that they were visible to naked eye and experienced gravitational settling. The settled, yellow deposits can be seen in Figure 8.2, which shows all of the samples photographed after four days.

Figure 8.2: Ferric Ion Experiments after four days

This experiment has shown that:

- ≥3ppm of Fe^{3+} will cause significant aggregation of these sols.
- 100pm of Fe^{3+} can cause aggregates large enough for gravitational settling to occur.

8.1.3. Stagnant Deposition Experiments

To investigate what deposition would occur under stagnant conditions, a series of experiments were conducted by placing small pieces of steel in a sol. Initially, small sections of the mild steel pipe used in the silica scaling test rig were placed in a container and just covered with sols of small (~10nm) and large (~100nm) particles.

After four days, the steel pieces in the solution with the large particles were almost completely covered with an orange deposit but the fluid remained clear. For the solution with small particles, less deposition was visible on the steel pieces and the fluid became a light rusty colour. After about one month, both solutions had become a dark rusty colour and it was recognised that the corrosion needed to be removed to obtain useful results.

The next set of experiments involved adding an oxygen scavenger to the sol, filling up the container completely and sealing it to prevent any further ingress of air. The two oxygen scavengers chosen to be investigated were sodium sulphide, Na_2S and sodium sulphite, Na_2SO_3. After over a month had passed, the fluid in both samples remained clear, suggesting that corrosion had been prevented. For the Na_2SO_3 sample, some greenish stains were left on the bottom of the container where the steel piece was in contact with the plastic. This was possibly a localised corrosion product.

The steel test piece in the fluid containing Na_2S became black during the experiment. This was likely due to some form of iron sulphide (pyrrhotite) being formed. Conversely, a white deposit formed on the upper surface of the test piece in the fluid containing Na_2SO_3, which can be seen in Figure 8.3(a) below. This deposit was analysed under a scanning electron microscope (SEM) to obtain the image shown in Figure 8.3(b).

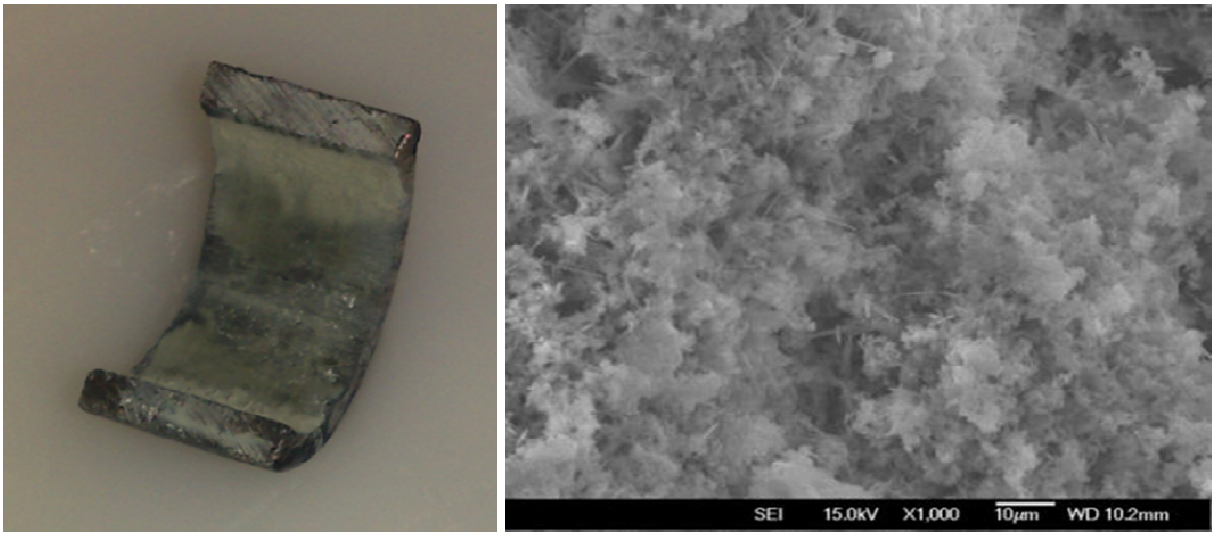

(a) (b)

Figure 8.3: Deposition formed in Na_2SO_3 stagnant experiment (a) test piece, (b) Close-up under SEM

The energy-dispersive X-ray spectroscopy (EDS) device attached to the SEM was used in the analysis of this sample and for later experiments. The reports for all of the EDS analyses described in this chapter are given in Appendix F. The EDS analyses were not run for sufficient lengths of time or repeated and averaged in such a way that accurate composition data could be obtained. The elements present in the reports will be accurate but the fraction of their occurrence will be qualitative rather than quantitative.

The deposit shown in Figure 8.3(b) was found to predominantly contain silicon and oxygen (Appendix F-1). It is likely that this deposit is a form of amorphous silica. Small amounts of iron, sulphur and sodium were also found to be present, all of which are present in the experiment.

On the basis of these results, sodium sulphite was selected as the oxygen scavenger to be used in the stagnant and silica scaling test rig experiments. Further stagnant experiments were then performed to test deposition from small and large particles onto different steel surfaces. Three steel surfaces were used: mild steel plate with mill scale still attached, mild steel plate with mill scale filed off and stainless steel plate.

Two sols, with particles sizes of about 15nm and 100nm, were brought up to pH 9 and then sodium sulphite was added. Three square samples of each of the three surfaces were then placed in the container with the sol and the container was sealed. The outcome of this experiment after 26 days is shown in Figures 8.4(a)-(b) below.

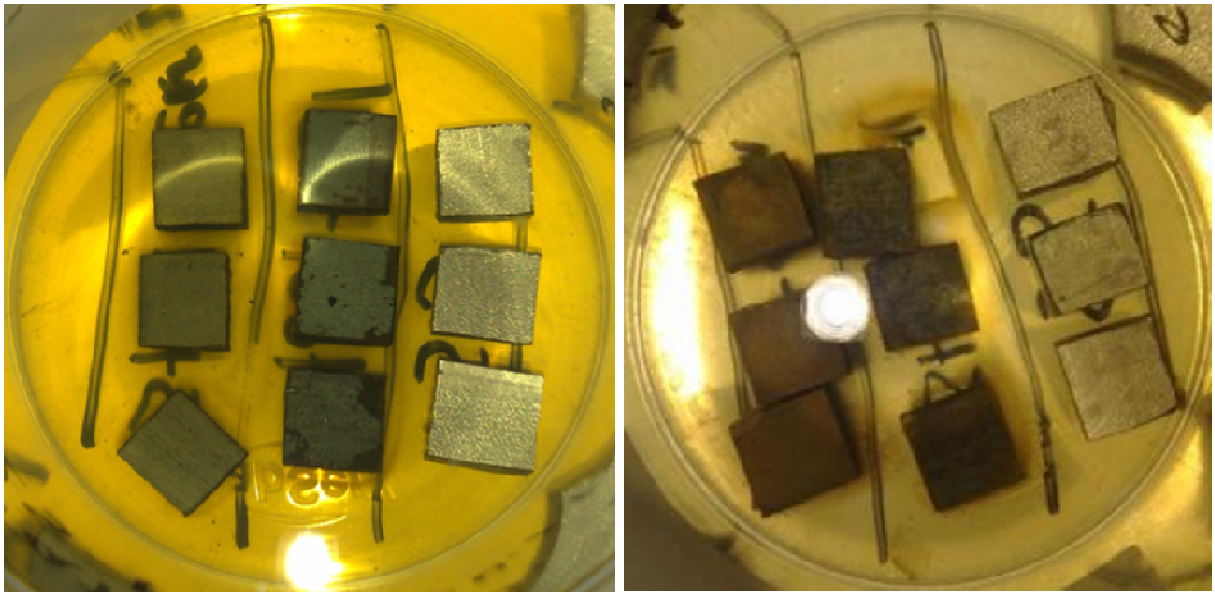

(a) (b)

Figure 8.4: Stagnant Experiments at 26 days. Left row: mild steel with mill scale removed. Middle row: mild steel with mill scale. Right row: stainless steel. (a) 15nm particle size. (b) 100nm particle size.

The yellowish background colour in Figures 8.4(a)-(b) is a combination of the light source used to take the photograph and the light rusty colour of the fluid. Despite using about five times the theoretically required amount of sodium sulphite to react with the dissolved oxygen in the fluid,

corrosion was still found to occur. The container was airtight but there was a small air space (~5mm) between the top of the fluid and lid. The oxygen present in this air space may have been greater than what was required to react with all of the sodium sulphite. Figure 8.4(b) shows a brown stain where one of the steel pieces was in contact with the plastic. Corrosion may have initiated here and be influenced by the contacting surfaces.

Figure 8.4(a) shows the experiment using a 15nm particle size. The only visible change in the square test pieces was some black areas that formed on the edges of the pieces of mild steel with mill scale. The cause for these black areas is unknown.

Figure 8.4(b) shows the different results obtained for the experiment using a 100nm particle size. For the pieces of mild steel with mill scale removed, the top surface was completely covered in a yellowish deposit. This deposit started as a small spot and grew to cover the whole surface over time. A yellowish deposit also formed on the pieces of mild steel with mill scale. It did not cover the whole top surface but was concentrated on the edges and corners. The deposits formed not only on the top surface but also on the side faces of the square samples. This occurred particularly on the mild steel samples but there were also some isolated deposits on the stainless steel samples as well. The composition of the deposit was not investigated but it is likely to contain silica, and the yellowish colour may come from ferric or sulphur ions.

The conclusions made for the stagnant experiments were:

- Using sodium sulphite in a sealed container can prevent corrosion and still allow silica deposition to occur.
- Under the same mass concentration, larger particles deposit more than smaller particles.
- Almost no visible deposition occurs on stainless steel.
- Deposition will occur on mild steel, particularly if the mill scale is removed.

Silica deposition rates under stagnant conditions will be useful for comparison with the results from the Silica Scaling Test Rig. To obtain comparable rates, the problems with corrosion must be eliminated and the deposition products must be identified.

8.2. Silica Scaling Test Rig Preliminary Experiments

8.2.1. Experiment #1a

The first experiment in the Silica Scaling Test Rig was chosen to be run at just above room temperature and at a relatively low pump setting to safely test the operation of the rig over an extended period of time. The experimental conditions are given in Table 8.1 and some photographs of the results are shown below. The rotameter was not yet installed and so the flow rate was estimated from pump manufacturer's chart for the average flow rate at the pump speed setting.

Table 8.1: Experimental Conditions for Experiment #1a

Sol	S29+S30-D (10 days old, ~20nm, 1700ppm)
Temperature	25.0°C
Flow Rate	5 litres/min (estimated)
Reynolds Number	7000
Duration	7 days
Notes	Mixing Tank open to air Test piece left to dry in air once removed from rig

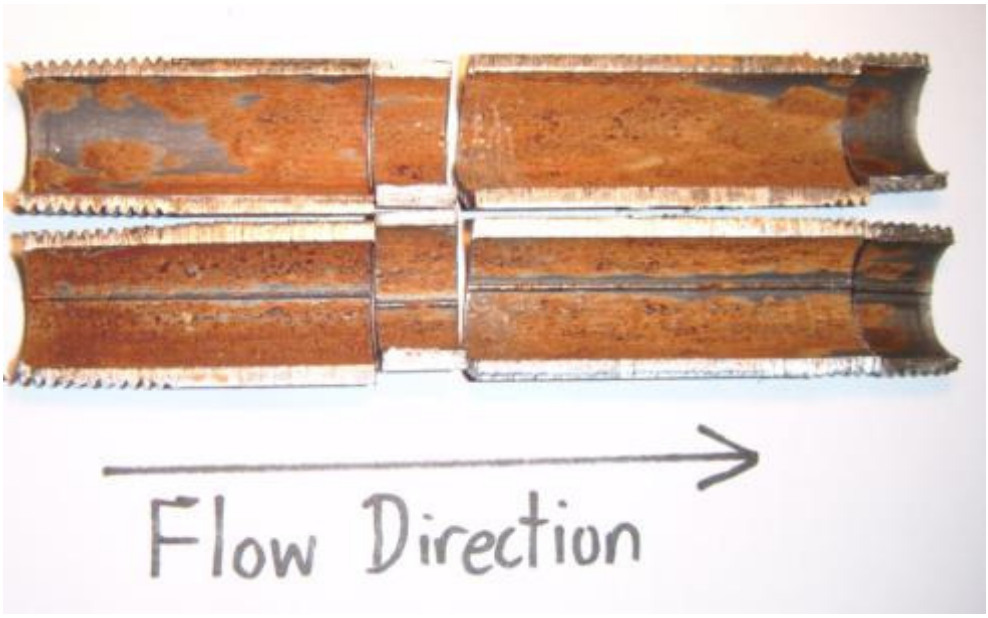

Figure 8.5: Test section from Experiment #1a

Figure 8.5 shows the test piece cut in half along its length. Corrosion has occurred on almost the entire inside surface of the pipe. There appears to be an absence of corrosion along the weld seam of the pipe and at the pipe exit.

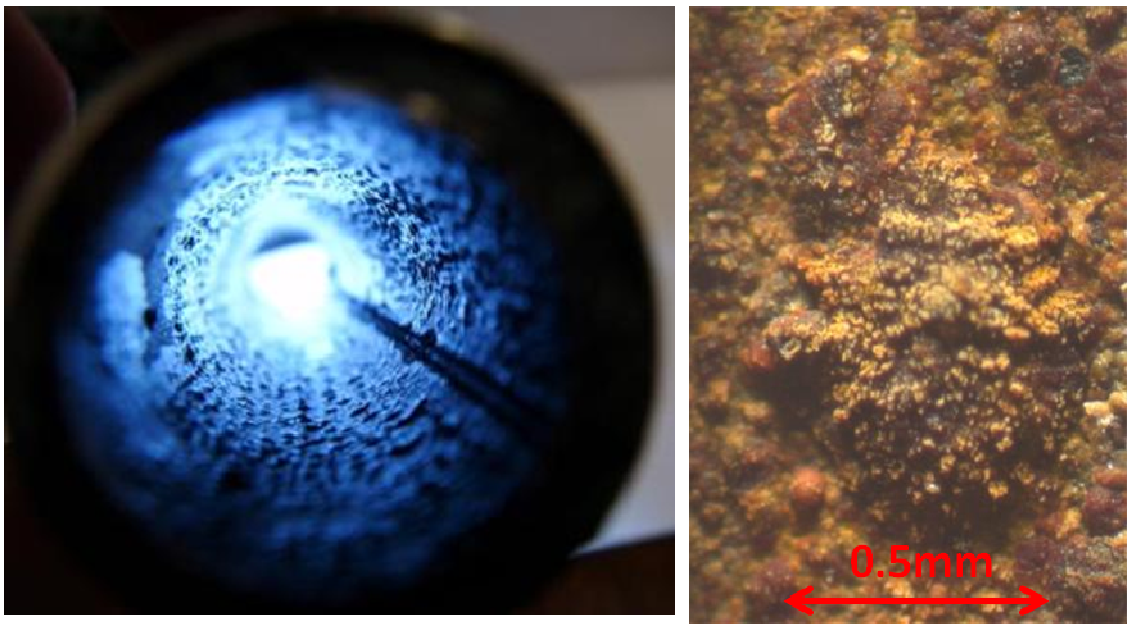

(a) (b)

Figure 8.6: (a) inside of Experiment #1a test section shortly after removal from rig, (b) close-up on protrusion

Figure 8.6(a) was taken shortly after the pipe was pulled from the rig and before the fluid had dried. Many protrusions were present and it was assumed that they were silica deposits. It appeared that the protrusions only occurred where corrosion had also occurred. The corrosion free areas that can be seen in Figure 8.5 were also free from these protrusions. Small sections of this pipe were investigated under an optical microscope with a digital camera attached. One of the protrusions was photographed and found to be about 0.5mm in size, as can be seen in Figure 8.6(b). The top of this protrusion appears to have smaller growths that protrude from it and consist of small particles.

8.2.2. Experiment #1b

To test the repeatability of the results from Experiment #1a, a new test piece was inserted into the rig and the experiment was continued using the same fluid and conditions as before. The Experiment #1a test piece was left to dry in air after it was removed from the rig and it is possible that some of the corrosion observed was due to this drying process. To remove this possibility in Experiment #1b, the test piece was removed from the rig, washed in ethanol and dried with a hot air blower.

Table 8.2: Experimental Conditions for Experiment #1b

Sol	S29+S30-D (17 days old, ~20nm, 1700ppm)
Temperature	25.0°C
Flow Rate	5 litres/min (estimated)
Reynolds Number	7000
Duration	7 days
Notes	Mixing Tank open to air Once removed from rig, test piece was washed in ethanol and dried with a hot air blower

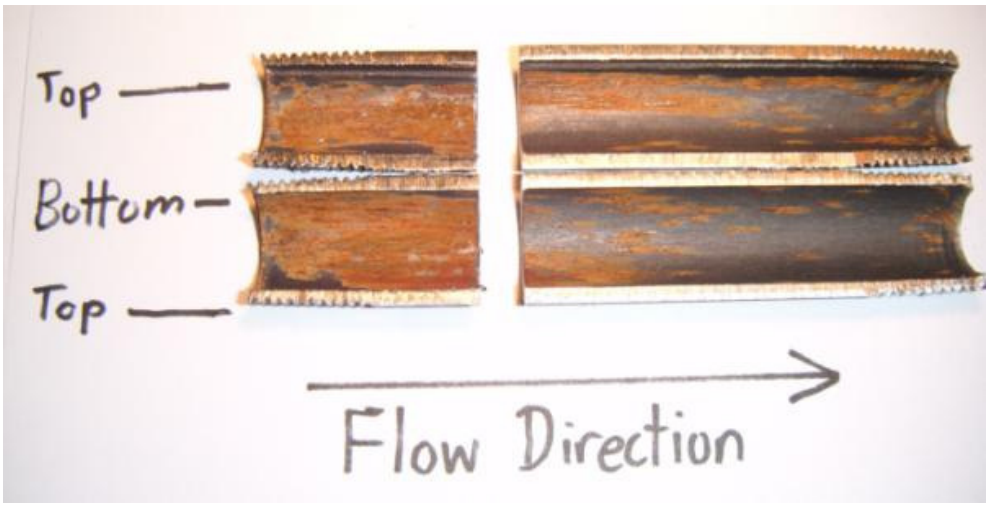

Figure 8.7: Test section from Experiment #1a

Figure 8.7 shows that corrosion was also experienced in Experiment #1b but not to the same extent as for Experiment #1a. The corrosion appears to be concentrated at the inlet end of the pipe. Similar protrusions to Experiment #1a were observed in this experiment. It also appears that the locations of corrosion and the protrusions coincide in this experiment as well. The weld seam is, again, free from corrosion and the protrusions.

8.2.3. Experiment #2

At the end of Experiment #1b, the DO level was measured to be about 6.9mg/litre (85% of saturation). After this experiment, the corrosion mitigation features were investigated for use on the rig. The first of them to be tested was the use of sodium sulphite but without the oxygen exclusion system, which had yet to be been constructed. Experiment #2 was begun with a new sol but with the same conditions as for Experiment #1. Sodium sulphite was added at the start of the experiment and the DO level was measured to be 0.24mg/litre (3% of saturation). The experiment was run for one day until the DO level was measured again and found to be 6.9mg/litre (85% of saturation). The experiment was then shut down and left stationary until the nitrogen blanket system had been constructed. With the new system in place, more sodium sulphite was added to the fluid and the rig was restarted with the same conditions as before. After three days the DO level had become about 2mg/litre (25% of saturation) and so the rig was stopped to once more add some sodium sulphite. This kept the DO level down to about 1% of saturation for the rest of the experiment.

Table 8.3: Experimental Conditions for Experiment #2

Sol	S31+S32-D (17 days old, ~12nm, 1700ppm)
Temperature	25.0°C
Flow Rate	5 litres/min (estimated)
Reynolds Number	7000
Duration	14 days
Notes	Day 1: 2g Na_2SO_3 added, rig started with Mixing Tank open to air Days 2-5: Rig turned off Days 6-14: 2g Na_2SO_3 added, rig started with oxygen exclusion system Day 8: Rig stopped, opened and 2g Na_2SO_3 added Day 14: Test piece washed in ethanol and dried with hot air blower

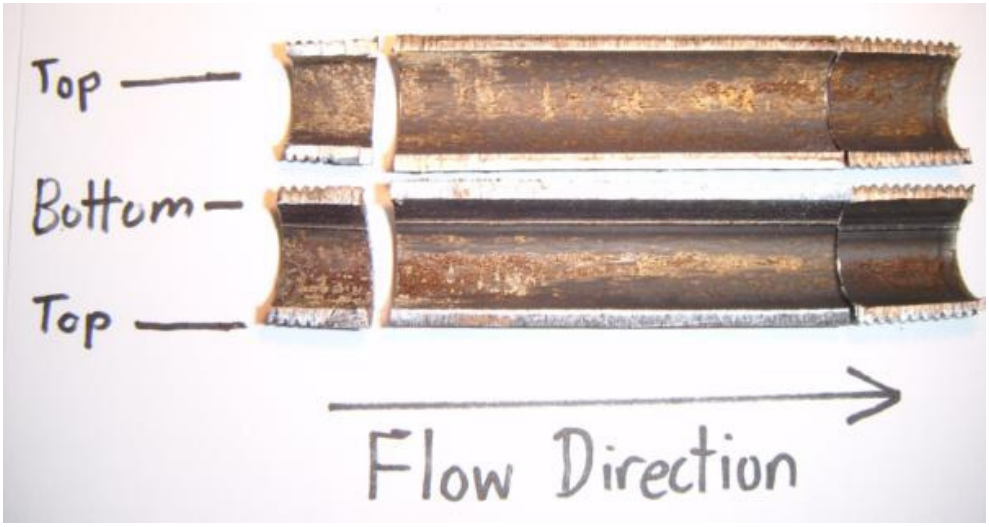

Figure 8.8: Test section from Experiment #2

Corrosion still occurred in Experiment #2 and can be seen in Figure 8.8 as the dark brown areas. However, substantially less corrosion occurred than during Experiment #1a despite the experiment duration being twice as long. It is likely that the corrosion occurred during the first day when the rig was running and during the next four days when the fluid was stationary because of the high DO level at this time. If this was the case then the corrosion prevention measures were successful.

The protrusions that were observed in Experiment #1 were not present in this experiment but a whitish deposit was found to coincide with most areas in which rust occurred. The whitish deposits were investigated with an optical microscope and SEM, in which Figures 8.9(a)-(b) were obtained.

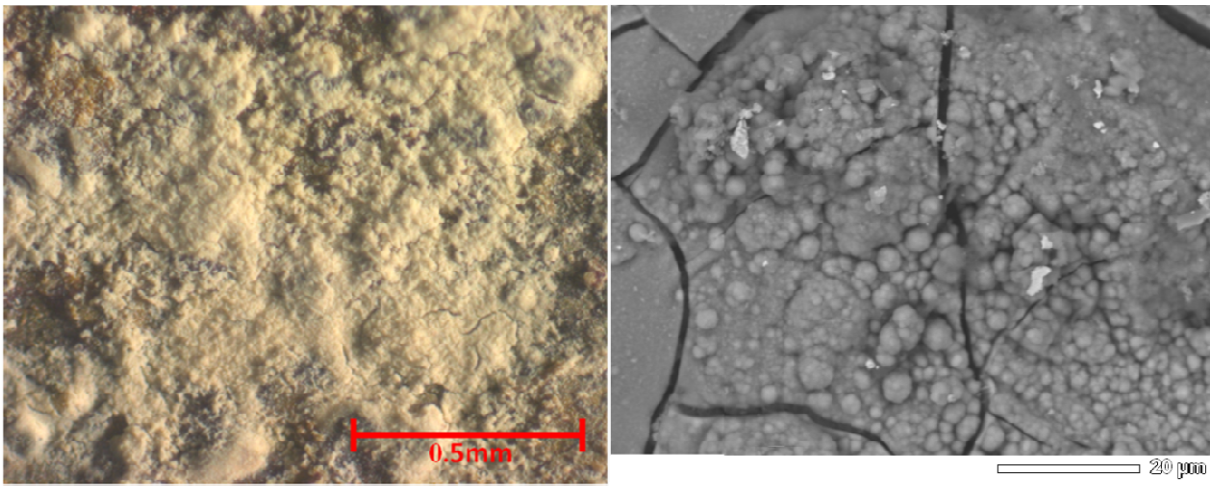

(a) (b)

Figure 8.9: Scale formed in Experiment #2 under: (a) microscope, (b) SEM

The whitish deposit appears grainy in Figure 8.9(a) and in places it covers the whole surface. Using a different part of the test piece, the SEM picture in Figure 8.9(b) shows a whitish deposit at even higher magnification. The grainy deposits appear to be made up of small globules that build up on top of each other. The globules have a size on the order of 1-5µm. The deposit appears to be built up on a flat

surface which has cracked into a number of plates. Some of the globules have been split in half along the cracks, which suggests that the cracks were formed after deposition had formed. Possibly this occurred when the test piece was cooled, washed in ethanol and dried.

EDS analysis was conducted on the area shown in Figure 8.9(b) (Appendix F-2, F-3). Particular locations of interest were the flat plates on the left edge of the image and the globules. In both locations, the elements found to be present, in order of decreasing magnitude, were oxygen, silicon, and iron with some traces of nickel and sodium. Given the large quantities of oxygen and silicon the deposit likely consisted of silica dioxide. The iron may be present in the deposit or it may be what lies below deposit and is picked up due to the penetrating nature of EDS. Sodium is present in large quantities in the solution and so it is not surprising to find it here. The nickel will have likely come from the stainless steel thread tape, which is impregnated with nickel.

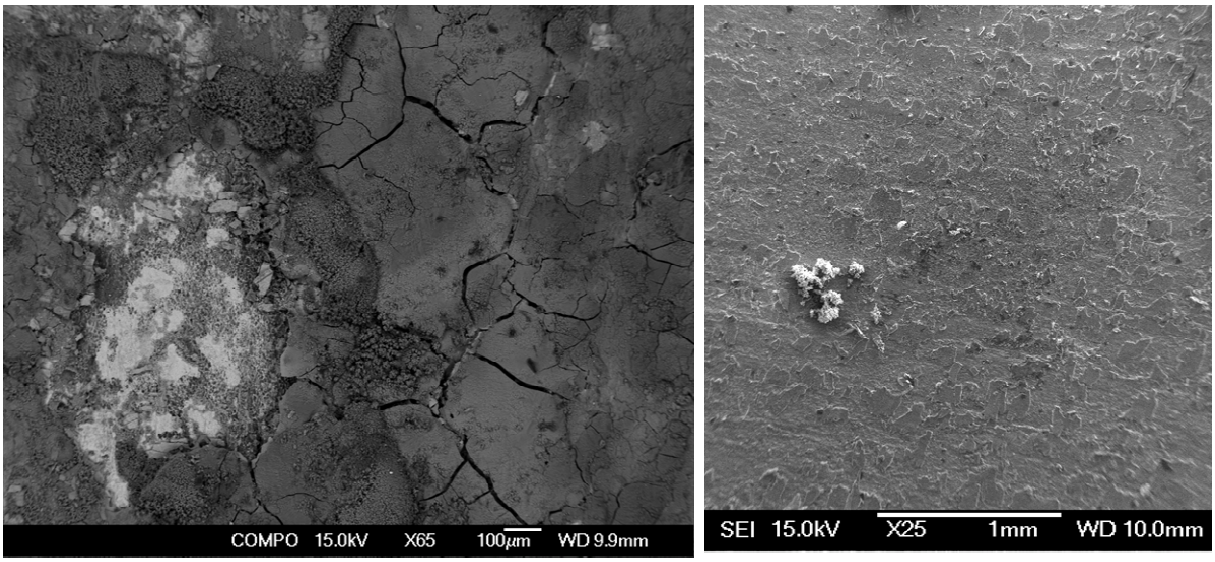

(a) (b)

Figure 8.10: (a) Scale formed in Experiment #2 under SEM showing the flat plate structure. (b) SEM image of clean pipe surface

The extent of the flat plate deposition is more clearly seen in Figure 8.10(a) where EDS has also confirmed that, to the EDS penetration depth, the plate-like structures consist mainly of silicon and oxygen with some iron (Appendix F-4). Figure 8.10(b) shows the surface of a clean, unused pipe for comparison. Clean pipe has a rough base surface with a number of islands protruding from the surface, of a size on the order of 100μm. The flat plate structure is substantially larger than these islands. The white deposit in Figure 8.10(b) is some type of contaminant introduced during sample preparation.

The large whitish area on the left of the image in Figure 8.10(a) was found to consist almost entirely of iron with no silicon and is possibly a corrosion pit (Appendix F-5). Some of the islands from the clean pipe surface can be seen in this area. The dark areas that surround this pit were found to consist mainly of silicon and oxygen and show the same globular deposition structure as in Figure 8.9(b) above but substantially more built up (Appendix F-6).

8.2.4. Experiment #3

The corrosion mitigation system was shown to work in Experiment #2, and was used from the start in Experiment #3. A longer experiment duration was chosen to obtain a greater amount of deposition than what was observed in Experiment #2.

Table 8.4: Experimental Conditions for Experiment #3

Sol	S36+S37-D (18 days old, ~14nm, 1700ppm)
Temperature	25.0°C
Flow Rate	5 litres/min
Reynolds Number	7000
Duration	21 days
Notes	Oxygen exclusion system used from the start Test piece washed in ethanol and dried with hot air blower

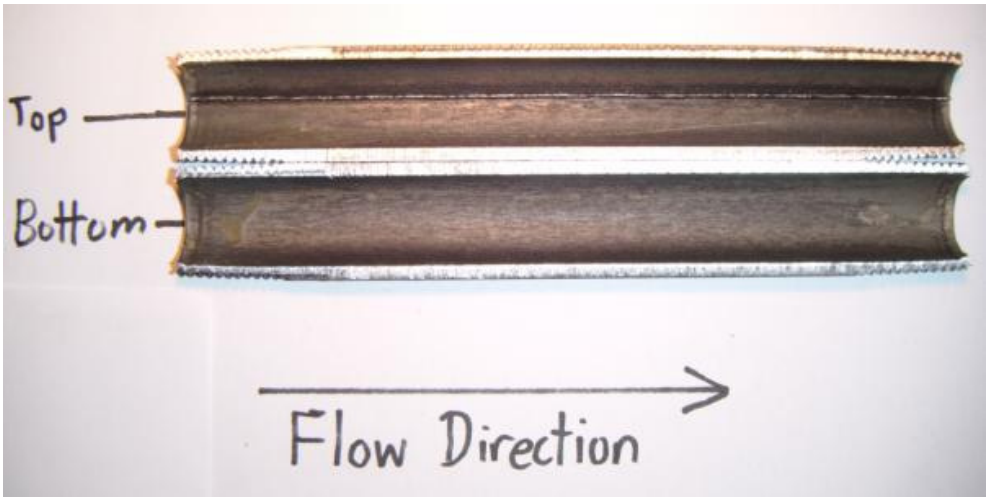

Figure 8.11: Test section from Experiment #3

Corrosion was completely avoided in Experiment #3, as can be seen in Figure 8.11 above. Visible deposition was almost completely absent. On the lower half of the pipe there are some small green patches at the inlet and outlet and on the upper half there is a faint green streak that spans almost the whole length. To investigate the presence of microscopic deposition across the whole length of the pipe, a section of unused pipe was first analysed under the SEM for comparison.

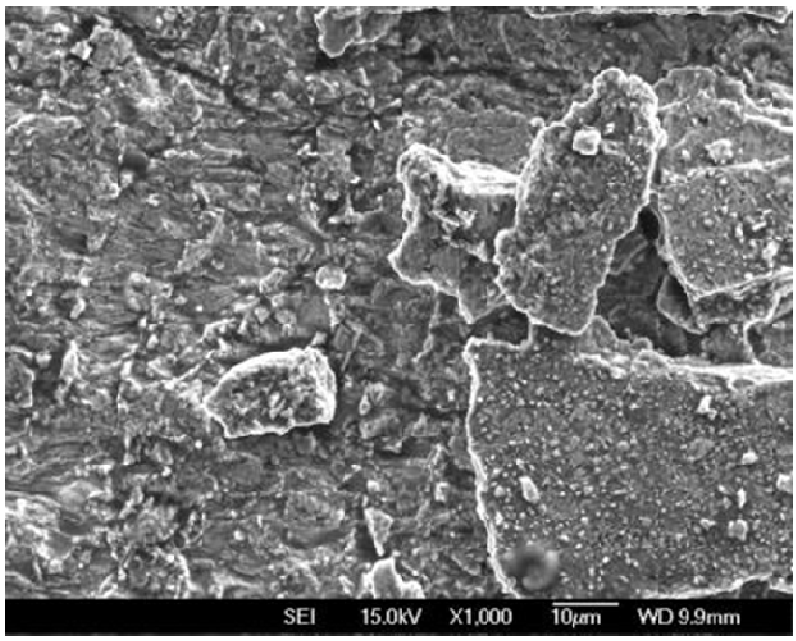

Figure 8.12: SEM image of clean pipe surface

Figure 8.12 displays a section of the clean pipe surface in Figure 8.10(b) at greater magnification, where the roughness elements can be seen. EDS analysis of this section of pipe showed that composition of the surface consisted of iron, oxygen and carbon (Appendix F-7). Carbon may not actually be present on the surface and the signal for it may have come in from the carbon-based products used in the SEM equipment. The presence of iron and oxygen suggests that this surface consists of iron oxides. No silicon was found in this analysis.

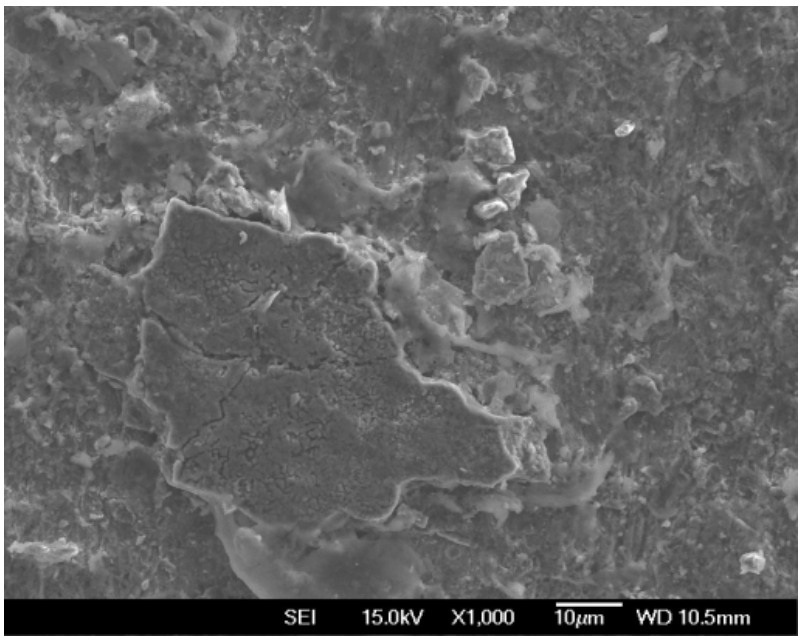

Figure 8.13: SEM image of Experiment #3 test section in area with no deposition visible to naked eye

Figure 8.13 is from a section of the Experiment #3 test piece that had no deposition visible to the naked eye. The base surface and the island surface look to be smoothed over when compared to Figure 8.12 above, which is for a clean piece of pipe but at the same magnification. EDS analysis has shown that there are small amounts (1-3% by weight) of silica present at all points investigated in Figure 8.13

(Appendix F-8, F-9, F-10). It could be that there is a thin layer of silica present over the whole surface. The depth to which the EDS technique measures may be greater than the thickness of this layer. Due to this, the composition obtained may predominantly reflect the iron oxide beneath the deposition.

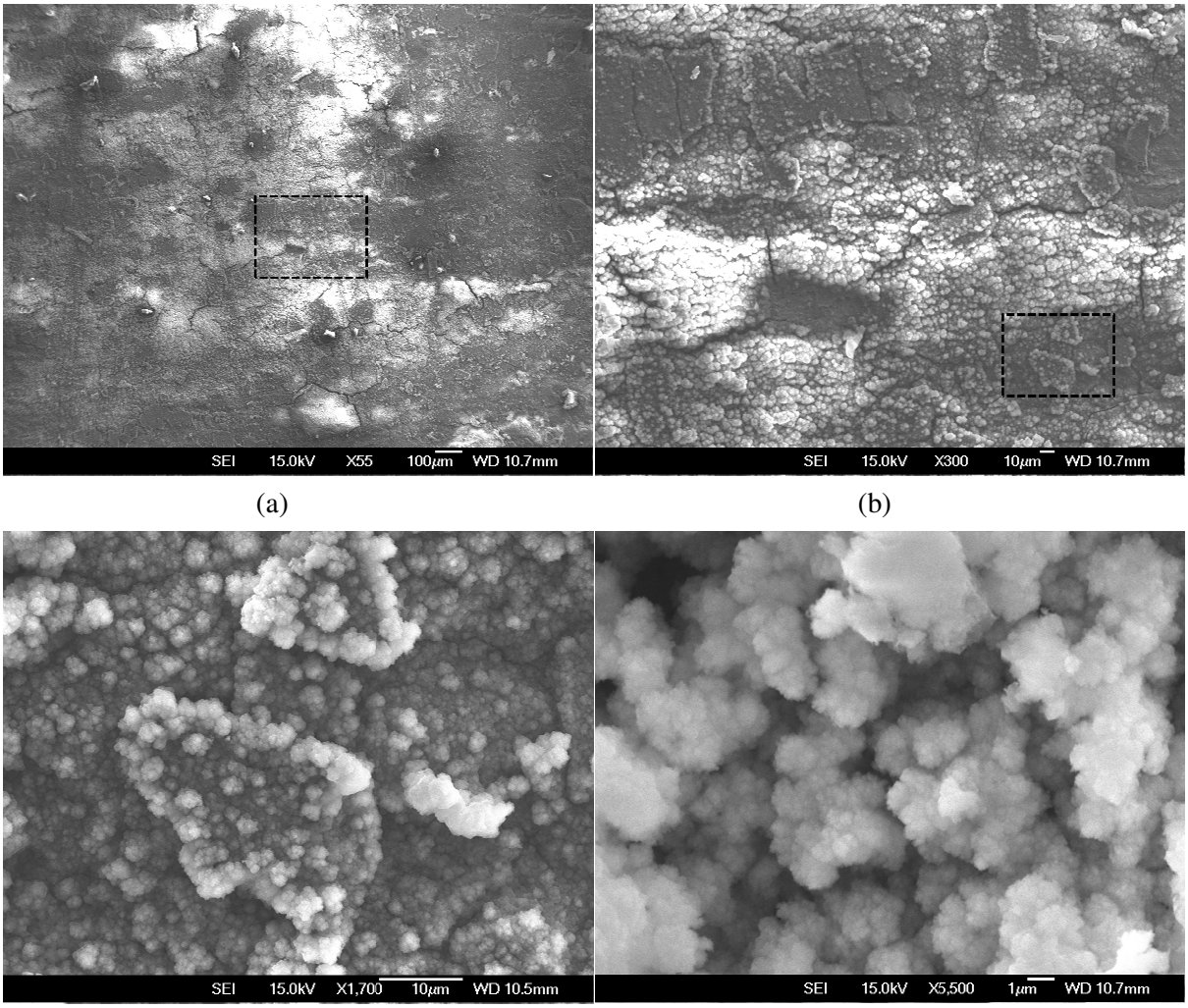

Figure 8.14: SEM images of Experiment #3 test section in area with visible deposition. (a)-(c) successive magnification of dotted area in preceding image, (d) Close-up in a different location

Figures 8.14(a)-(c) show the progressive magnification of a section of the Experiment #3 test piece that contained the greenish deposit. The dotted boxes show the area that the subsequent image was zoomed in to. The whitish regions in Figure 8.14(a) are the regions with the greatest density of the globular structures that can be seen at greater magnifications in Figures 8.14(b) and (c). From Figure 8.14(b), it appears that globular structures have covered the base surface of the pipe but with the islands still visible. Figure 8.14(c) shows two small islands with globular structures both surrounding them and also present on their surface. The globular deposits seem particularly concentrated on the edges of these islands.

Figure 8.14(d) was taken from a different section of the test piece that also had a greenish deposit. The same globular structure was observed and this image is taken at the greatest magnification with which a clear image could be obtained. The globular structures appear to be composed of even smaller

globules that are sub-micron in size. EDS analysis was conducted on the same patch of globular deposit from which Figure 8.14(d) was taken (Appendix F-11). The globular structures were found to be composed of, in order of decreasing magnitude, oxygen, silicon, carbon, iron and very small amounts of sodium. The globular structures are likely to be silica dioxide deposits. The carbon is likely to be contamination and the iron may be part of the deposit or what lies underneath the deposit.

8.2.5. Preliminary Experiment Measurements

The pH was measured regularly during experiments and all of the measurements made are shown in Figure 8.15 below.

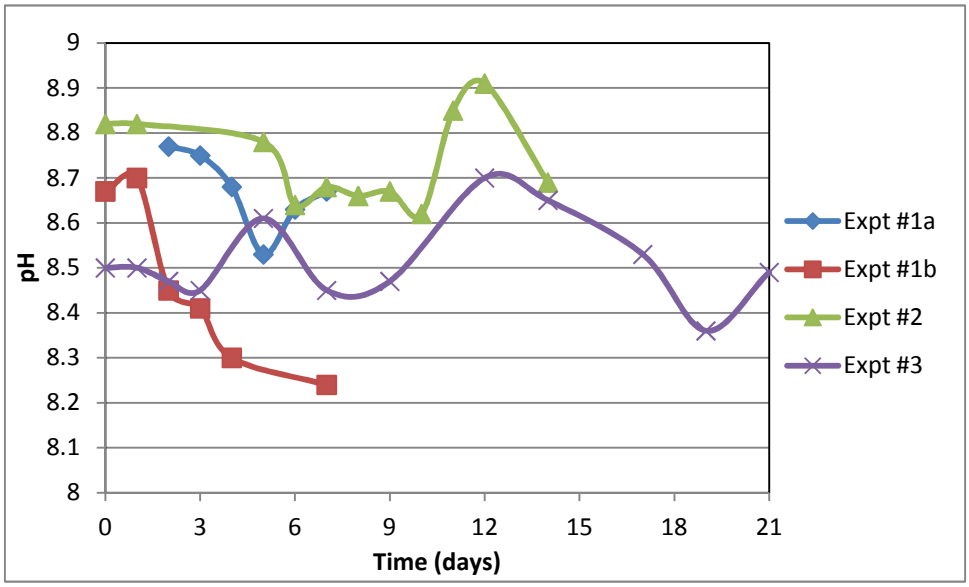

Figure 8.15: pH measurements made during preliminary experiments

For experiments #1a, #2, and #3, the pH varies by about 0.3 pH units over the duration of the experiment. No trend exists for the change in pH level and the variation may be due to the experimental uncertainty of pH probes used. The pH probes tended to become contaminated with silica over time and became hard to calibrate. The pH in experiment #1b varied by about 0.5 of a pH unit and appeared to decline over time. This may be entirely due to measurement uncertainties.

Due to the variability in the experimental conditions, the effect of pH level alone cannot be correlated to the deposition formed. Most of the measurements are between pH 8.5-8.9 which is a stable range for the sols used. This pH level is higher compared to the field experiments reviewed by Mroczek [17], where the range in pH for the geothermal brine was pH6.0-8.2.

In all experiments, the particle size distribution of the sol showed significant variability. Some of the sols initially showed similar measurements to those shown in Figure 7.1 but even they quickly became more variable once put in the rig. The average particle size distributions measured at different times over the duration of each experiment are shown in Figures 8.16(a)-(d) on the following page.

(a)

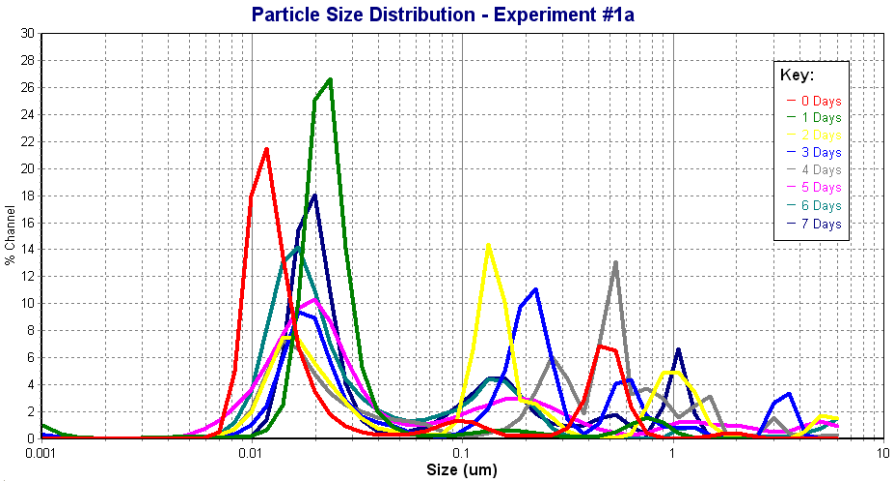

(b)

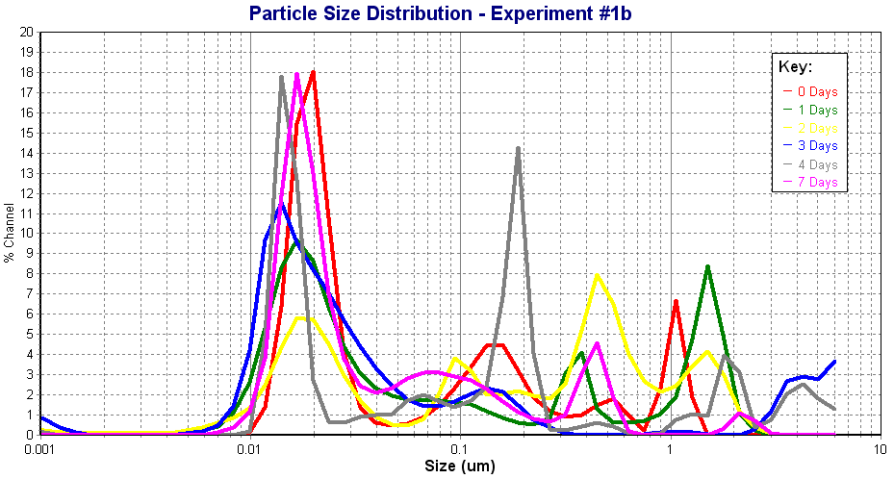

(c)

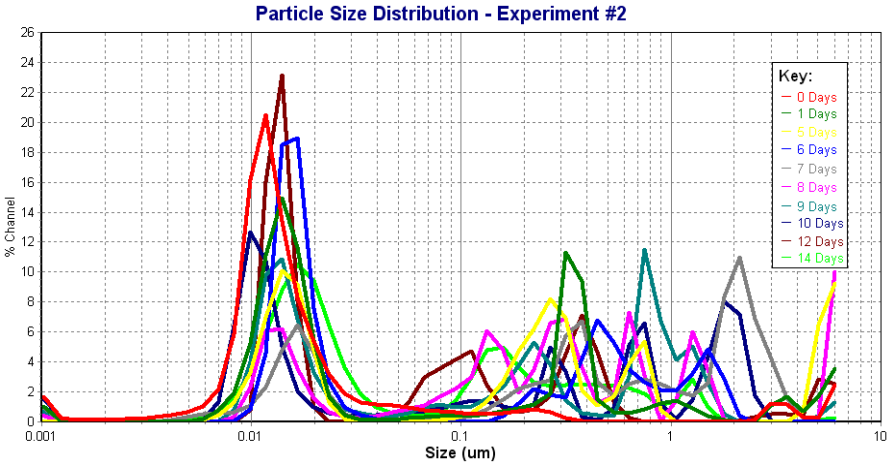

(d)

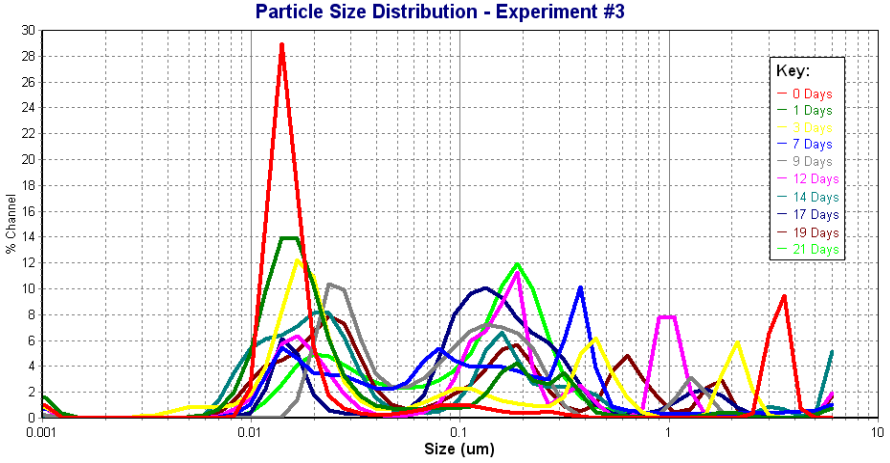

Figure 8.16: Average measurements of the particle size distribution during preliminary experiments

In all of the experiments, there is significant peak in the 10-20nm size range with no apparent trend with time. The other peaks for larger particle sizes are random and are not found repeatedly over several measurements. This suggests that the 10-20nm particles are the most common particle size present and the other peaks are noise. Due to the low particle concentrations in these measurements, a small number of large particles can significantly influence the measurements and this may be the cause for the results shown above. Possible causes for this noise include:

- Aggregates that remained from the previous experiment that were not cleaned away.
- The characteristics of the flow promoting aggregation.
- Low concentrations of Fe^{3+} dissolved into solution from steel pipe that initiate aggregation.
- Corrosion particles and other contamination being present in the fluid.
- The particle concentration decreases as silica deposits, making size measurements more susceptible to error.

The exception to the above discussion is Experiment #3. In Figure 8.16(d) it appears that there is a repeatable second peak in the 100-200nm size range. These results suggest that the particle size distribution in Experiment #3 was bi-modal.

8.3. Discussion

8.3.1. Deposition structure

Flat Plate Structure

The flat plate structure was observed mainly in Experiment #2. It was composed predominantly of silicon and oxygen and hence is likely to be silica dioxide, at least to the penetration depth of the EDS. Because of the flat nature of the deposit, it may have been formed in a film-like fashion from the direct deposition of monomeric silica. From Figure 8.10(a) it appeared to cover a relatively large area, on the order of square millimetres. This is substantially larger than the islands that were found on the clean pipe sample, which had a size on the order of 100μm. From Figure 8.10(a) it appears that the flat plate structure completely covers these islands. The globular silica deposition structure was found to form on top of these plates.

In Experiment #3, there appear to be cracks in the areas of greatest deposition in Figures 8.14(a) and (b). The deposition visible in these images is of the globular structure and it is built up to similar levels as for those dark patches in Figure 8.10(a). Possibly the globular deposition has formed on top of a flat plate structure to the extent that the plates are no longer visible. The cracks that are visible may then be in the flat plate structure that lies underneath.

Definitive conclusions about the nature of this structure cannot be drawn from the current results. Accurate identification of the deposited product and consecutive images of the deposition development over time may allow the mechanisms that drive this growth to be ascertained.

8.3.2. Globular Structure

The SEM photographs taken of the deposition in both Experiments #2 and #3 showed a structure consisting of small globules that built up on each other. EDS analysis showed that these structures were predominantly composed of silicon and oxygen and are likely to be amorphous silica deposits. Deposition from Experiment #2 is compared with silica deposition from other experiments in Figures 8.17(a)-(d) below.

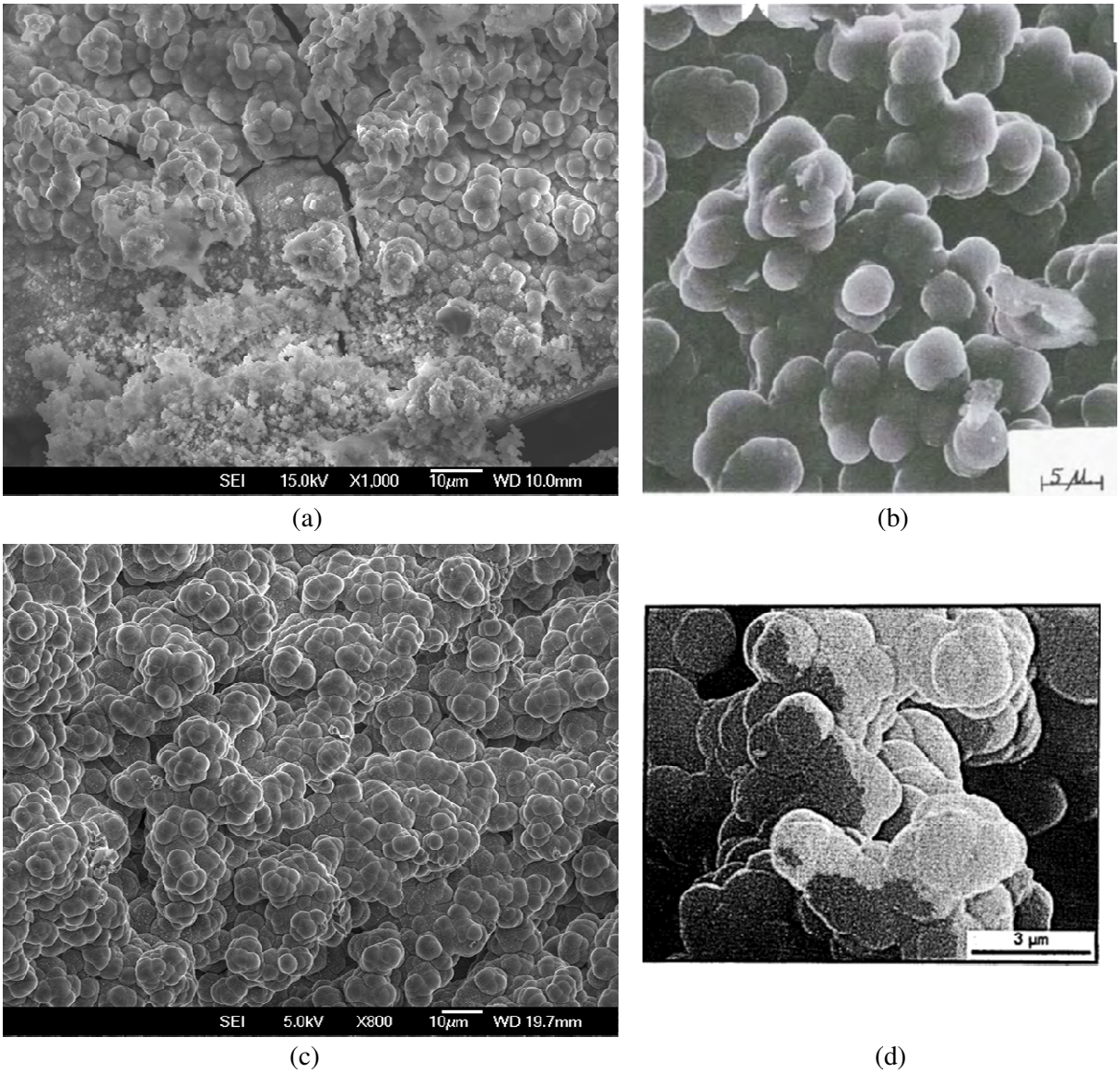

(a) (b)

(c) (d)

Figure 8.17: Globular silica deposition from (a) Experiment #2, (b) Experiment on the effect of aeration on silica scaling using geothermal brine - Source: [21] , (c) Silica scaling experiment at a New Zealand geothermal field, (d) Packed column experiment using synthetic brine - Source: [33]

Figure 8.17(b) is taken from Brown & McDowell's research on the effect of aeration on silica scaling using geothermal brine [21]. In all experiments they found nodules of silica deposition inside the pipelines and Figure 8.17(b) shows a close up on one. The experimental temperature for this sample is unknown but will be within the range of 52-115°C and the experiment ran for 48 days. The size and shape of this deposition is similar to that in Figure 8.17(a) for the current experimentation. Brown &

McDowell proposed, in agreement with Weres et al [34], that the growth mechanism of this structure was probably:

1. Nucleation of colloids in fluid.
2. Increase in particle size through direct growth and aggregation.
3. Deposition of colloidal particles onto pipe surface.
4. Cementation in place by direct deposition of monomeric silica.

A similar type of deposition structure is shown in Figure 8.17(c), which was from a pipe used in a silica scaling experiment performed at a geothermal power station. The experiment used geothermal brine at a temperature of about 130°C and the deposition was black and covered the whole inside surface of the pipe. The size and shape of this deposition at the micron scale is also very similar to that in Figure 8.17(a) despite a difference in appearance at a larger scale.

Bohlmann et al [33], also found a similar deposition structure, as can be seen in Figure 8.17(d). This deposition was formed on the Pyrex pipe that was used in their packed column experiments. The experiment was conducted under super-saturated conditions at pH 6 and 146°C. When a temperature of 56°C was used, the same structure was found but the globules were about 0.3µm in size. The measurements made during this set of experiments showed that there was little tendency for polymerised silica to deposit and they suggest Figure 8.17(d) was formed from monomeric deposition alone.

As mentioned previously, accurate identification of the deposited species is required to better understand the deposition mechanisms. The close similarities between Figure 8.17(a) and the other images in Figures 8.17(b)-(d) suggest that the same product, amorphous silica, has been deposited in this experiment. The amorphous silica may have deposited as monomeric silica or as a combination of polymerised and monomeric silica. The level of monomeric silica was not measured in the preliminary experiments but was likely to be at the saturation level for the temperature and pH. This would have been about 100ppm, whereas the polymerised silica concentration would have been about 1600ppm. The close-up picture of the globular deposits in Figure 8.14(d) showed that they were constructed of even smaller globules, sub-micron in size. These small particles could be from aggregations of the 20nm colloidal particles used in the experiments.

Figures 8.17(a)-(d) show that, despite great variation in the temperature, pH and brine composition of the experiment, a very similar silica deposition structure was obtained. The mechanisms involved with the development of these structures may be largely independent of these parameters. If this is the case, the results obtained on the Silica Scaling Test Rig may be able to be applied directly to geothermal applications despite using significantly different experimental conditions.

8.3.3. Factors influencing deposition

It was found that the presence of corrosion greatly increased the quantity of deposition formed. Experiment #1a showed the greatest amount of both deposition and corrosion. The least amount of deposition occurred in Experiment #3, where corrosion was completely removed. It was also observed that deposition and corrosion tended to form in the same place. Based on the results of the trial rig and ferric ion experiments, it is likely that the corrosion products promote aggregation. When the corrosion product lies on the pipe surface, this may promote localised aggregation and deposition. Once a silica deposit has formed, further deposition of silica may then form on top of it.

Less corrosion and deposition formed in Experiment #1b compared to #1a even though both were run under identical experimental conditions. The Mixing Tank was left open to the air in both experiments and so the dissolved oxygen levels were likely to have been the same and the same level of corrosion would be expected. The only significant difference for Experiment #1b was that the sol used had already been in the rig for a week and some of the silica had deposited. It may be that the formation of deposition on the pipe surface promotes further corrosion. With a lower particle concentration in Experiment #1b, this may have resulted in less deposition being formed and hence less corrosion.

In all experiments, no deposition or corrosion was found to occur on the weld seam of the pipe and the area near to it. This may be due to the hydrodynamic influence of the local turbulence in this area. Conversely, it may be due to chemical reasons as the steel has a slightly different chemical composition and grain structure in the heat affected zone of the weld.

8.3.4. Experimental Limitations

The preliminary experiments have shown that silica deposition can be made to occur in the Silica Scaling Test Rig. However, in Experiment #3 with the corrosion prevention measures in place, only a small amount of deposition was found after three weeks of operation. It is desirable to obtain a greater amount of deposition within such a time frame and different experimental conditions should be tested to try and speed it up. These may include temperature, flow rate, silica concentration, pH, and particle size. Modifications to the test section surface may also speed up the deposition process, such as pre-coating with amorphous silica, removing the mill scale and increasing the surface roughness.

An important factor to be tested in the planned experimentation is the particle size. The results from the preliminary experiments show that there is some uncertainty in what the actual particle size distribution is in the rig and it might be changing over time. The stability of the sols needs to be improved and the Zetatrac output needs to be validated.

8.4. Conclusions

Silica deposition was successfully produced during the preliminary experiments in the Silica Scaling Test Rig. Corrosion was initially a problem but the oxygen exclusion system was shown to be effective in preventing corrosion of the test section. The deposition rate is too slow to make qualitative measurements and different experimental conditions should be tested to find out if the rate can be increased. Improved sol stability and sols with larger particle sizes are also required to perform the planned experimentation.

Based on the results of the preliminary experiments, the following was concluded:

- The mild steel test section pipe corrodes with exposure to a sol with a dissolved oxygen level of about 6.9mg/litre. Protrusions, assumed to be silica deposits, form at the same locations as the corrosion, suggesting that one promotes the other.
- No deposition or corrosion forms on the weld seam or heat affected zone.
- When corrosion is prevented, very little deposition occurs after three weeks that is visible to the naked eye. However, a small amount of deposition does occur because silicon can be detected across the whole surface whereas none can be found on clean, unused pipe. This may be from monomeric deposition.
- The deposition visible to the naked eye is likely to be amorphous silica and consists of two deposition structures:
    - A flat plate-like structure that covers the pipe surface, possibly formed from monomeric deposition.
    - A globular structure that consists of 1-5µm diameter globules built up on each other. The globules appear to consist of sub-micron particles, possibly formed from aggregation of colloidal silica. The globular structure may form on top of the plate-like structure or on the pipe surface, preferentially on the edges of protrusions.

Chapter 9. Conclusions

The transport regime for colloidal silica particles in geothermal brines was found, theoretically, to be the Diffusion regime. This is in contradiction to the vertical cylinder experimental results of Brown, Dunstall and Zipfel, where inertial impaction was proposed to be the dominant transport mechanism. Possible explanations for the experimental results include: attachment forces favouring large particles over small, aggregation of small particles that then deposit, or some transport mechanism that hinders the transport of small particles.

An experimentation set has been developed that will be able to test the transport mechanisms of colloidal silica particles in cylindrical pipe flow. Three types of experiment were proposed:

1. Laminar flow – varying between a Reynolds number of about 750 and 1500, and a particle size of 10nm and 100nm.
2. Turbulent flow – constant Reynolds number of about 15,000 with viscous boundary layer varying between 0.06-0.38mm, and a particle size of 10nm and 100nm.
3. Turbulent flow – constant viscous boundary layer of about 0.27mm with Reynolds number varying between about 3000-23,000.

A Silica Scaling Test Rig has successfully been designed, built and commissioned that can perform this experimentation. The rig is currently set up with a temporary test section configuration to perform preliminary experiments to better understand the deposition characteristics in the experiments. There are still some issues with draining, flow measurement, and with the Flow Conditioner. Remedying these issues and constructing the full length test section configuration will enable the full set of experiments to be performed.

A method has been developed of producing amorphous silica sols with a particle size of 10-20nm which are stable for at least one month. Larger particle sizes can be obtained via the controlled growth of these sols at lower pH levels and then raising the pH when the desired size is achieved. Due to the small particle sizes and low concentrations in these sols, the particle size measurements are noisy and are susceptible to contamination. Efforts should be made to improve the accuracy and to validate the measurements against other particle size measuring techniques.

Three preliminary experiments have been conducted in the Silica Scaling Test Rig using these sols and silica deposition has successfully been obtained. The initial problems with corrosion were prevented after the implementation of an oxygen exclusion system. To perform the planned experimentation set, the rate of deposition needs to be increased and a number of experimental parameters that could be changed were suggested. A method of producing sols with larger particle sizes is also required and the sol stability during experiments needs to be investigated further and possibly improved.

The first preliminary experiment showed that significant corrosion occurs on the mild steel test section pipe when it is exposed to a sol with a dissolved oxygen level of about 6.9mg/litre. Protrusions were

found to form at the same locations as the corrosion and they were assumed to be silica deposits. The co-location of corrosion and deposition suggests that one process influences the other but it was not clear which was first to form. The weld seam and heat affected zone of the pipe was free of both deposition and corrosion.

The second experiment showed the success of the oxygen exclusion system but corrosion still occurred during the time before the system was implemented. Co-location of corrosion and deposition was also found to occur in this experiment. A whitish deposit was found and SEM-EDS analysis showed it to predominantly consist of oxygen and silicon, likely to be amorphous silica. Two types of deposition structure were found, a flat plate-like structure and a globular structure that grew on top. The plate-like structure covered square millimetres of surface area and was possibly formed from monomeric deposition. It appeared to form on top of the pipe surface and was substantially larger than the islands that exist on the clean pipe surface, which have a size on the order of 100µm. The other structure consisted of 1-5µm diameter globules that built up on each other. Each globule appeared to consist of submicron particles which may be aggregates of colloidal silica. The globular deposition structure found in these experiments was comparable to those from other field and laboratory experiments.

The third experiment utilised the oxygen exclusion system from the start and after three weeks no corrosion was found and very little deposition formed that was visible to the naked eye. SEM-EDS analysis of this experiment showed that silicon was present in small quantities across the surface. When a clean, unused section of pipe was investigated, no silicon was found. This suggests that deposition did occur everywhere in the third experiment, possibly due to monomeric deposition as no particulate deposition was observed. The deposition visible to the naked eye was of the same globular structure as in the second experiment but it was not clear whether the plate-like structure also had formed. The globular structures appeared to favour growth on the edges of protrusions on the pipe surface. However, no visible deposition occurred on the weld seam or heat affected zone.

Chapter 10. Future Work

The future work can be split into three areas: Silica Scaling Rig, Colloidal Silica Production, and Experimentation.

Silica Scaling Rig

- Test the Flow Conditioner to determine if plug flow exists at the outlet. If not, the contraction section should be re-designed so that the main body diameter is smoothly reduced to the test section diameter in one part, instead of two.
- Pressure sensor connection modified to reduce secondary flows affecting measurement.
- Commission and calibrate the Coriolis flow meter.
- Modify the rig to take the full length test sections.
- Improve the draining of the rig by adding more drains and sloping the pipework.
- Recheck HAZOP results and incorporate into maintenance and operational plans.

Colloidal Silica Production

- Develop method of rapidly producing sols with larger particle size. Investigate the use of the ion exchange method.
- Investigate the sol stability during experiments and, if necessary, find ways to improve it.
- Validate the Zetatrac measurements with other methods such as Transmission Electron Microscopy.
- Develop the synthetic sol to closer resemble geothermal brine.

Experimentation

- Investigate methods of increasing the rate of silica deposition.
    - Experimental Conditions: temperature, flow rate, silica concentration, pH, and particle size.
    - Test Section Modifications: pre-coating with amorphous silica, removing the mill scale and increasing the surface roughness.
- Perform the planned experimentation.
- Perform more stagnant experiments to determine deposition rates and compare to theoretical results.
- Further investigate the influence of turbulence on particle transport and deposition.
- Investigate the build up of scale over time by developing an insert that matches internal. surface of pipe that can easily be removed to monitor scale formation.
- Perform experiments using different concentrations of monomeric and polymeric silica to determine the deposited species.

References

[1] Mighty River Power. (2010, 02-12-2011). Geothermal Generation. Available: http://www.mightyriverpower.co.nz/Generation/PowerStations/Geothermal/

[2] Ministry of Economic Development. (2011, 04-01-2012). New Zealand Energy Data File. Available: http://www.med.govt.nz/sectors-industries/energy/energy-modelling/publications/energy-data-file/new-zealand-energy-data-file-2011

[3] D. Gallup and P. Hirtz, "Control of Silica Scaling in Geothermal Systems Using Silica Inhibitors, Chemical Treatment, and Process Engineering," in *The Science and Technology of Industrial Water Treatment*, ed: CRC Press, 2010, pp. 155-177.

[4] K. Brown, "Thermodynamics and kinetics of silica scaling," in *International Workshop on Mineral Scaling*, Manila, Philippines, 2011.

[5] R. K. Iler, *The chemistry of silica: solubility, polymerization, colloid and surface properties, and biochemistry*: Wiley, 1979.

[6] K. A. Rodgers*, et al.*, "Silica phases in sinters and residues from geothermal fields of New Zealand," *Earth-Science Reviews,* vol. 66, pp. 1-61, 2004.

[7] K. L. Brown and M. Dunstall, "Silica scaling under controlled hydrodynamic conditions," in *World Geothermal Congress*, Kyushu-Tohoku, Japan, 2000, pp. 3039-3044.

[8] N. Epstein, "Elements of particle deposition onto nonporous solid surfaces parallel to suspension flows," *Experimental Thermal and Fluid Science,* vol. 14, pp. 323-334, 1997.

[9] H. Zipfel, "Investigation of Hydrodynamic Influence on Silica Scaling on Circular Cylinders," Certificate of Proficiency, Geothermal Institute, University of Auckland, Auckland, 1998.

[10] M. C. Potter and D. C. Wiggert, *Mechanics of fluids*, 3rd ed. Pacific Grove, CA: Brooks Cole /Thompson Learning, 2002.

[11] J. F. McIlhenny, "Artificial Turbulent Bursts," Master of Science, Mechanical Engineering, Worcester Polytechnic Institute, 2002.

[12] T. K. Serghides, "Estimate friction factor accurately," *Chemical Engineering,* vol. 91, p. 63, 1984.

[13] M. V. Zagarola and A. J. Smits, "Mean-flow scaling of turbulent pipe flow," *Journal of Fluid Mechanics,* vol. 373, pp. 33-79, 1998.

[14] A. Klein, "Review - Turbulent developing pipe flow," *ASME, Transactions, Journal of Fluids Engineering,* vol. 103, pp. 243-249, 1981.

[15] J. Doherty*, et al.*, "The development of turbulent pipe flow," in *16th Australasian Fluid Mechanics Conference*, Gold Coast, Australia, 2007, p. 266.

[16] P. Gehrke*, et al.*, "A respirometer with controlled water quality and computerized data acquisition for experiments with swimming fish," *Fish Physiology and Biochemistry,* vol. 8, pp. 61-67, 1990.

[17] E. K. Mroczek, "Review of silica deposition rates at Ohaaki, Rotokawa, and Wairakei geothermal fields and comparison of observed rates with predicted deposition rates calculated using three different kinetic deposition models," Institute of Geological and Nuclear Sciences, 1994.

[18] E. K. Mroczek and G. McDowell, "Silica Scaling Field Experiments," in *10th New Zealand Geothermal Workshop*, 1988.

[19] E. K. Mroczek and R. R. Reeves, "The effect of colloidal silica on silica scaling from geothermal fluid," in *16th New Zealand Geothermal Workshop*, 1994.

[20] H. P. Rothbaum*, et al.*, "Effect of silica polymerisation and pH on geothermal scaling," *Geothermics,* vol. 8, pp. 1-20, 1979.

[21] K. L. Brown and G. McDowell, "The effect of aeration on silica scaling," in *4th New Zealand Geothermal Workshop*, 1982, pp. 127-130.

[22] T. Yanagase*, et al.*, "The properties of scales and methods to prevent them," *Geothermics,* vol. 2, Part 2, pp. 1619-1623, 1970.

[23] I. Gunnarsson*, et al.*, "Reducing silica deposition potential in waste waters from Nesjavellir and Hellisheidi power plants, Iceland," presented at the World Geothermal Congress, Bali, Indonesia, 2010.
[24] R. Itoi*, et al.*, "Experimental study on the silica deposition in a porous medium," *Geothermal Resources Council, Transactions,* vol. 8, pp. 301-304, 1984.
[25] Y. Kiyota*, et al.*, "Evaluation on geothermal injection treatment by pH modification," in *World Geothermal Congress*, Kyushu-Tohoku, Japan, 2000, pp. 3077-3082.
[26] E. K. Mroczek*, et al.*, "Deposition of amorphous silica in porous packed beds — predicting the lifetime of reinjection aquifers," *Geothermics,* vol. 29, pp. 737-757, 2000.
[27] K. L. Brown*, et al.*, "Pressure drops due to silica scaling," in *17th New Zealand Geothermal Workshop*, 1995, pp. 163-167.
[28] Z. Amjad and R. Zuhl, "Silica control in industrial water systems with a new polymeric dispersant - Lubrizol Carbosperse K-700," in *Association of Water Technologies Inc - Annual Convention & Exposition*, Hollywood, Florida, 2009.
[29] A. D. Baltazar*, et al.*, "Silica scale prevention technology using organic additive, Geogard SX," *Geotermia. Revista Mexicana de Geoenergía,* vol. 14, pp. 171-174, 1998.
[30] G. Darrell L, "Investigations of organic inhibitors for silica scale control in geothermal brines," *Geothermics,* vol. 31, pp. 415-430, 2002.
[31] O. Weres*, et al.*, "Kinetics of silica polymerization," *Journal of Colloid and Interface Science,* vol. 84, pp. 379-402, 1981.
[32] B. A. Fleming, "Kinetics of reaction between silicic acid and amorphous silica surfaces in NaCl solutions," *Journal of Colloid and Interface Science,* vol. 110, pp. 40-64, 1986.
[33] E. G. Bohlmann*, et al.*, "Kinetics of silica deposition from simulated geothermal brines," Oak Ridge National Laboratory, 1980.
[34] O. Weres and L. Tsao, "Chemistry of silica in Cerro Prieto brines," *Geothermics,* vol. 10, pp. 255-276, 1981.
[35] T. Sugama and K. Gawlik, "Anti-silica fouling coatings in geothermal environments," *Materials Letters,* vol. 57, pp. 666-673, 2002.
[36] S. H. Chan*, et al.*, "Silica Fouling of Heat Transfer Equipment---Experiments and Model," *Journal of Heat Transfer,* vol. 110, pp. 841-849, 1988.
[37] S. H. Chan*, et al.*, "Effect of Ferric Chloride on Silica Fouling," *Journal of Heat Transfer,* vol. 117, pp. 323-328, 1995.
[38] S. H. Chan*, et al.*, *Effects of sodium and potassium chlorides on silica fouling* vol. 115. New York, NY, ETATS-UNIS: American Society of Mechanical Engineers, 1993.
[39] F. Garibaldi and D. H. Freeston, "Effect of hydrodynamic flow conditions on silica deposition," in *3rd New Zealand Geothermal Workshop*, 1981, pp. 203-208.
[40] B. W. Mountain*, et al.*, "Experimental studies on New Zealand hot spring sinters: rates of growth and textural development," *Canadian Journal of Earth Sciences,* vol. 40, pp. 1643-1667, 2011/11/23, 2003.
[41] R. E. Jamieson, "Geothermal Silica Scaling," Masters, University of Auckland, Auckland, 1984.
[42] J. Pott*, et al.*, "Numerical simulation of silica scaling," in *18th New Zealand Geothermal Workshop*, 1996, pp. 41-46.
[43] E. Achenbach, "Distribution of local pressure and skin friction around a circular cylinder in cross-flow up to Re = 5 × 106," *Journal of Fluid Mechanics,* vol. 34, pp. 625-639, 1968.
[44] H. Schlichting and K. Gersten, *Boundary-layer theory*: Springer, 2000.
[45] X. Zheng and Z. Silber-Li, "The influence of Saffman lift force on nanoparticle concentration distribution near a wall," *Applied Physics Letters,* vol. 95, 2009.
[46] ISO5167-1:2003, "Measurement of fluid flow by means of pressure differential devices inserted in circular cross-section conduits running full - Part 1: General principles and requirements,"
[47] A. K. Coker, *Ludwig's Applied Process Design for Chemical and Petrochemical Plants (Fourth Edition)*. Burlington: Gulf Professional Publishing, 2007.
[48] K. Brown, "Personal Communication," 2010.

[49] BS IEC 61882:2001, "Hazard and Operability studies (HAZOP Studies) - Application Guide,"
[50] G. Starling, "Investigation into Colloidal Silica Production," Mechanical Engineering Department - University of Canterbury, 2011.

Appendix A - Calculations

Rig Heat Loss Calculations

The heat loss surfaces of the rig were simply modelled by three components:

1. Pipework, instruments and fittings: 8.5m of NB15 pipe (~20mm outside diameter)
   a. Surface area: $A_{pipe} = \pi DL = \pi(0.020m)(8.5m) = 0.53m^2$
2. Flow Conditioner: 0.4m of NB65 pipe (~75m outside diameter)
   a. Surface area: $A_{FC} = \pi DL = \pi(0.075m)(0.4m) = 0.09m^2$
3. Mixing Tank: 0.4m tall cylinder of 270mm outside diameter
   a. Surface area: $A_{MT} = \pi DL + 2\frac{\pi D^2}{4} = \pi(0.27m)(0.4m) + 2\frac{\pi(0.27m)^2}{4} = 0.45m^2$

Total heat loss surface area for rig: $A_{Total} = A_{pipe} + A_{FC} + A_{MT} = 1.07m^2$

The situation was modelled by considering only the heat transfer from the fluid to the surrounding air across A_{total}. All other heat losses were neglected. To obtain the highest heat loss values, the maximum experimental temperature, T_{fluid}, of 80°C was used. The following assumptions were made:

- Ambient temperature = T_a = 20°C
- As the pipe walls are made from steel and are relatively thin, they have infinite thermal conductivity => Temperature of outside surface is the same as for the fluid
- Insulation[1] has a thickness, t, of 19mm; a thermal conductivity, K, of 0.037 W/m-K; and an emissivity, ε, of 1
- Convection heat transfer coefficient, H, for free convection of air is[2] 25 W/m^2-K
- Stefan-Boltzmann Constant = σ = 5.67 x 10^{-8}

Case 1: Insulation is not used

Heat transfer from pipe surface to the surrounding air:

- Convection: $Q_{Conv} = A_{Total}H(T_{fluid} - T_a)$
- Radiation: $Q_{Rad} = A_{Total}\sigma\epsilon((T_{fluid} + 273)^4 - (T_a + 273)^4)$

Total heat loss from rig: $Q_{Loss,1} = Q_{Cond} + Q_{Rad}$

$$Q_{Loss,1} = [1.07 \times 25 \times (80 - 20)] + [1.07 \times 5.67 \times 10^{-8} \times 1 \times ((80 + 273)^4 - (20 + 273)^4)]$$

$$Q_{Loss,1} = 2100W$$

[1] From: "Armaflex FR Product Sheet" available on http://www.forman.co.nz/products.php?catid=24&proid=234 [Accessed 11-01-12]
[2] From: http://www.engineeringtoolbox.com/convective-heat-transfer-d_430.html [Accessed 11-01-12]

Case 2: Insulation is used

1. Heat transfer from fluid to outside surface of insulation, which is at temperature T_{ins}
   a. Conduction: $Q_{Cond} = A_{Total} K \frac{(T_{fluid} - T_{ins})}{t}$
2. Heat transfer from outside surface of insulation to the surrounding air
   a. Convection: $Q_{Conv} = A_{Total} H (T_{ins} - T_a)$
   b. Radiation: $Q_{Rad} = A_{Total} \sigma \epsilon ((T_{ins} + 273)^4 - (T_a + 273)^4$

Total heat loss from rig: $Q_{Loss,2} = Q_{Cond} + Q_{Rad} = Q_{Cond}$

To solve for $Q_{Loss,2}$, the insulation surface temperature, T_{ins}, is adjusted until $Q_{Conv} + Q_{Rad} = Q_{Cond}$

Using T_{ins} =23.5°C:

$$Q_{Cond} = 1.07 \times 0.037 \times \frac{(80 - 23.5)}{0.019} = 118W$$

$$Q_{Conv} + Q_{Rad} = [1.07 \times 25 \times (23.5 - 20)] + [1.07 \times 5.67 \times 10^{-8} \times 1 \times ((23.5 + 273)^4 - (20 + 273)^4)]$$

$Q_{Conv} + Q_{Rad}$ =115W

Therefore, $Q_{Loss,2} \cong 120W$

Heating Time Calculation

The following was assumed:

- Heating element power, P = 1000W
- Rig volume, V =20 litres = 0.020m^3. Rig is full of water with heat capacity, C_p = 4200 J/kg-K, and density, ρ = 1000 kg/m^3
- Water is uniformly heated from 20°C to 80°C with no heat losses

The heating time is then:

$$\text{Heating Time} = \frac{\rho V C_p (\Delta T)}{P} = \frac{1000 \times 0.020 \times 4200 \times 60}{1000} = 5040\text{s} = 84 \text{ minutes}$$

Pressure Loss Calculation

The pressure loss in the main loop of the rig, h_L, was assumed to be the sum of the pipe friction, h_p, and the total head loss through fittings, h_f. The whole of the main loop of the rig was assumed to consist of NB15 pipe. There would be some larger pipe sections but using the smallest diameter will give the largest friction losses. The fluid was assumed to be water and the following parameters were assumed and used in this model:

Parameter	**Symbol**	**Value**	**Unit**
Pipe inside diameter	D	17	mm
Total length of pipe	L	8.5	m
Roughness	e	0.0046[3]	mm
Gravitational acceleration	g	9.81	kgm/s^2
Temperature	T	30	°C
Kinematic Viscosity	ν	8.96E-07	m^2/s

The parameter that was varied in this study was the flow rate, Q [m^3/hr]. The flow rate is related to the average velocity, V [ms^{-1}], by:

$$V = \frac{Q}{3600\frac{\pi}{4}D^2}$$

The two types of pressure loss can then be calculated by[3]:

$$h_p = f\frac{L}{D}\frac{V^2}{2g} \qquad\qquad h_f = \sum K\frac{V^2}{2g}$$

where *f* is the Darcy Friction Factor and K is the loss coefficient for the fitting. The analysis was conducted during the Design stage of the project and the following was assumed to be all of the fittings to be used in the main line with respective loss coefficients[3]:

Fitting	**Quantity**	**K**
Standard Elbow	6	1.5
Tee	1	1.8
Re-entrant entrance	1	0.8
Pipe exit	1	1
Conical Expansion	1	0.2
Tube bundle	1	0.75[4]
Contraction	1	0.07
Coriolis Flow meter	1	3.5 (assumed)
Globe Valve - 1/4 open	0 or 1	57
Globe Valve - Fully open	0 or 1	8.2

[3] All values and equations are from: M. C. Potter and D. C. Wiggert, *Mechanics of fluids*, 3rd ed. Pacific Grove, CA: Brooks Cole /Thompson Learning, 2002.

[4] From: ISO5167-1:2003, "Measurement of fluid flow by means of pressure differential devices inserted in circular cross-section conduits running full - Part 1: General principles and requirements,"

To create the pressure loss versus flow rate curve in Figure 5.9, the following calculation procedure was followed:

1. The flow rate value was set and the corresponding average velocity was calculated
2. The Reynolds number was calculated from Eq. (2.6)
3. The Darcy Friction Factor was determined from Eqs. (2.11) – (2.14)
4. The K value for the Globe Valve was set to either the Fully open or ¼ open value
5. h_p and h_f can be calculated => h_L
6. Steps 1-5 were repeated for all flow rate values chosen

Net Positive Suction Head Calculation

The Net Positive Suction Head (NPSH) available in the rig was determined under the worst case condition of being at the cut-off fluid temperature of 90°C. The fluid was assumed to be water at atmospheric pressure and the fluid properties under these conditions were determined using a fluid property calculator. The following parameters were assumed and used in this model:

Parameter	**Symbol**	**Value**	**Unit**
Atmospheric Pressure	P	101,000	Pa
Saturation Pressure	P_s	69,783	Pa
Density	ρ	965	kg/m^3
Kinematic Viscosity	ν	3.26E-07	m^2/s
Gravitational acceleration	g	9.81	kgm/s^2

The NPSH can be determined from[5]:

$$NPSH = \frac{P - P_s}{\rho g} + \Delta z - h_p$$

where Δz is the height of the fluid free surface above the pump impeller and h_p is pipe friction loss that occurs between the reservoir and the pump impeller. The following parameters were assumed for this analysis:

Parameter	**Symbol**	**Value**	**Unit**
NB25 Pipe Inside Diameter	D	25	mm
Roughness	e	0.046	mm
Length of pipe between Mixing Tank and pump	L	0.5	m
Height of Mixing Tank fluid level above pump inlet	Δz	0.3	m

[5] From: M. C. Potter and D. C. Wiggert, *Mechanics of fluids*, 3rd ed. Pacific Grove, CA: Brooks Cole /Thompson Learning, 2002.

To create the NPSH available versus flow rate curve in Figure 5.10, the following calculation procedure was followed:

1. The flow rate value was set and the corresponding average velocity was calculated
2. The pipe friction loss was calculated in the same way as in the previous section except using the current values
3. The NPSH available can be calculated
4. Steps 1-3 were repeated for all flow rate values chosen

Planned Experimentation Parameter Calculations

To create Tables 5.5 to 5.7 for the planned experimentation parameters, a number of assumptions were made:

- The fluid behaves as water at 30°C and at atmospheric pressure
    - Kinematic Viscosity, ν = 8.03E-07 m^2/s
    - Fluid Density, ρ = 995.7 kg/m^3
- A uniform velocity profile exists at the pipe entrance and a fully developed velocity profile is achieved after 80 pipe diameters in length
- The viscous boundary layer thickness, Y, is given by $\frac{u_\tau Y}{\nu} = 5$, according to Figure 2.3. This thickness is assumed to be larger than the roughness elements on the pipe surface
- The pipe roughness, e = 0.045mm, a typical value for wrought iron[6].

The following procedures were used to obtain experimental conditions:

Laminar experiments - Table 5.5

1. The flow rate value and test section inside diameter were set
2. The average velocity was determined by:

$$V = \frac{Q}{3600\frac{\pi}{4}D^2}$$

3. The Reynolds number and required test section length were calculated from Eq. (2.6) and Eq. (2.7) respectively

Turbulent experiments with constant Re - Table 5.6

[6] From: M. C. Potter and D. C. Wiggert, *Mechanics of fluids*, 3rd ed. Pacific Grove, CA: Brooks Cole /Thompson Learning, 2002.

1. The flow rate value and test section inside diameter were set
2. The average velocity and Reynolds number were calculated
3. Steps 1-2 are repeated, modifying the flow rate value, until a Reynolds number of about 15,000 is achieved
4. The Darcy Friction Factor was determined from Eqs. (2.11) – (2.14)
5. The shear stress is calculated from Eq. (2.9)
6. The shear velocity is calculated from Eq. (2.8)
7. The viscous boundary layer thickness is determined from: $Y = \frac{5\nu}{u_\tau}$
8. The required test section length is 80 times the pipe inside diameter

Turbulent experiments with constant Boundary Layer Thickness - Table 5.7

1. The flow rate value and test section inside diameter were set
2. The average velocity and Reynolds number were calculated
3. The Darcy Friction Factor was determined from Eqs. (2.11) – (2.14)
4. The shear stress is calculated from Eq. (2.9)
5. The shear velocity is calculated from Eq. (2.8)
6. The viscous boundary layer thickness is determined from: $Y = \frac{5\nu}{u_\tau}$
7. Steps 1-6 are repeated, modifying the flow rate value, until a viscous boundary layer thickness of about 0.27mm is achieved
8. The required test section length is 80 times the pipe inside diameter

Appendix B – Example HAZOP worksheet

As an example of the HAZOP process that was performed, the following excerpt has been taken from the analysis for the first part in the rig. Two guide words are applied to the element "Heating"

Part No.:	1	**Part Name:**	Mixing Tank
Inputs:	Silica sol, Acid/Base, Water, Other Chemicals		
Activity:	Homogenise fluid concentration and temperature, heat fluid to desired temperature, keep fluid level above set height, Add fluid/chemicals		
Source:	Throttling Valve	**Destination:**	Test Section
Elements:	Heating, Homogenisation, Fluid Level, Added fluid/chemicals, Temperature, Pressure, Flow,		

Hazard No.	1	2	3	4	5	6
Guide Word	NO	NO	NO	NO	NO	NO
Deviation	No heating occurs in Mixing Tank	No heating occurs in Mixing Tank	No heating occurs in Mixing Tank	No heating occurs in Mixing Tank	No heating occurs in Mixing Tank	No heating occurs in Mixing Tank
Operation Stage	A,B	A,B	A,B	A,B	A,B	A,B
Possible causes	Element wiring is broken	Element is damaged	Element is not plugged in	Relay is broken	Powercut	Probe is giving faulty reading
Possible Consequences	Element sits there doing nothing	Live wires exposed => electrocution	No heating occurs but fluid is still pumped around the rig	Permanently switched OFF. No heating		Probe gives too high a reading and so controller sends no ON signal and nothing happens
Frequency	Constantly (5)	Constantly (5)	Constantly (5)	Constantly (5)	Constantly (5)	Constantly (5)
Likelihood	Rare (1)	Rare (1)	Possible (3)	Rare (1)	Rare (1)	Unlikely (2)
Severity	Minor (1)	Major (4)	Minor (1)	Minor (1)	Minor (1)	Minor (1)
Risk Level	Low (5)	Medium (20)	Medium (15)	Low (5)	Low (5)	Low (10)
Experimental Risk	Significant	Significant	Significant	Significant	Devastating	Significant
Safeguards & Mitigation	Easily noticed during startup or daily inspection that temperature is not rising. Replace the element	Generic Electrocution Mitigation. + will be visibly obvious due to some sort of impaction. Mitigate by inspecting heating element before switching on power.	Easily noticed during startup or daily inspection that temperature is not rising.			Calibrate probe on regular occasions
New Frequency		Constantly (5)				
New Likelihood		Rare (1)				
New Severity		Minor (1)				
New Risk Level		Low (5)				
Comments		Danger is in exposed live wires – isolate and minimise this	No mitigation required as there is no risk of injury or damage from this	Easily found by troubleshooting, no risk of harm	Can't do anything about it	If probe is faulty by giving too high a reading (hence gives no signal to heat) does not put anything at risk except experiment
Actions required		Add to Start-up Checklist				Add to Maintenance Checklist

Hazard No.	7	8	9	10	11	13
Guide Word	MORE	MORE	MORE	MORE	MORE	MORE
Deviation	More heating occurs in MT than designed for - raise in system temperature	More heating occurs in MT than designed for - raise in system temperature	More heating occurs in MT than designed for - raise in system temperature	More heating occurs in MT than designed for - raise in system temperature	More heating occurs in MT than designed for - raise in system temperature	Heating still on during shutdown and draining
Operation Stage	A,B	A,B	A,B	A,B	A,B	C
Possible causes	Controller setpoint is set too high	Relay is broken => permanently switched on	Probe is giving faulty reading	Controller is broken => permanently or too frequently signals ON	Heating element too large for system	Power still on during Stage C
Possible Consequences	System heated to high temperature, if set higher than equipment limits or to boiling => burn/skin irritation risk.	System overheats, possible serious burn metal parts of tank or escaping steam	Probe gives too low a reading so controller too frequently signals ON. System overheats and boils => serious burn risk	System overheats and serious burn risk	System heats too quickly for controller to respond to, will regularly overheat by a few degrees. Burn risk	Risk of severe burn while draining system
Frequency	Constantly (5)	Constantly (5)	Constantly (5)	Constantly (5)	Constantly (5)	Monthly (2)
Likelihood	Possible (3)	Rare (1)	Unlikely (2)	Rare (1)	Unlikely (2)	Possible (3)
Severity	Catastrophic (5)	Major (4)	Major (4)	Major (4)	Severe (3)	Severe (3)
Risk Level	High (75)	Medium (20)	Medium (40)	Medium (20)	Medium (30)	Medium (18)
Experimental Risk		Significant	Significant	Significant	Noticeable	Negligible
Safeguards & Mitigation	Generic Overtemperature & Splash/Leak & Electrocution Mitigation + investigate having temperature controlled switch in tank	Generic Overtemperature Mitigation	Generic Overtemperature Mitigation + calibrate the temperature probe regularly and replace if problem observed	Generic Overtemperature Mitigation + Check regularly that Controller behaves as expected and replace if necessary	When selecting heating element size in design process, ensure that time taken for fluid volume to be heated is determined and choose appropriate size	Ensure that the power is turned off and system left for a period to cool before draining
New Frequency	Constantly (5)	Constantly (5)	Constantly (5)	Constantly (5)	Constantly (5)	Monthly (2)
New Likelihood	Possible (3)	Rare (1)	Unlikely (2)	Rare (1)	Rare (1)	Unlikely (2)
New Severity	Minor (1)	Moderate (2)	Moderate (2)	Moderate (2)	Moderate (2)	Moderate (2)
New Risk Level	Medium (15)	Low (10)	Medium (20)	Low (10)	Low (10)	Low (8)
Comments	There is still a reasonable likelihood that this could happen. The mitigation will remove the harmful consequences and so is acceptable		Even with regular calibration checks, probe failure could be abrupt. However, burn risk is minimised and so is acceptable			
Actions required	Investigate temperature controlled switch	Add to Operational Checklist. Look at backup for relay failure	Add to Maintenance Checklist		Ensure this is done in Design Process	Add to Shutdown Checklist

HAZOP SUMMARY: Silica Scaling Rig

Preliminary Study Report - 31/03/11

Study Information

Design Stage:	Pre-Detailed Design
Date performed:	18/02/11 to 31/03/11
Performed by:	Luke Sinclair
	Paul Siratovich (initial pre-earthquake assistance)
Summary Prepared by:	Luke Sinclair

Study Results

Equipment & Procedures to add to Design

Generic Mitigations Procedures: Procedures were developed for mitigating against the potential problems of: Electrocution, Fire, Overtemperature & Splash/Leak and are attached as Appendix A at end of this report.

Checklists: Checklists were created for Rig Shakedown, Startup, Operational, Shutdown and Maintenance stages and are attached as Appendix B at end of this report.

Temperature Controlled Switch: As an added safety measure, insert a temperature controlled switch (set at about 90°C) into the Mixing Tank. Have at same height or lower than the heating element. This will provide protection against a range of problems with heating system that cause too much heating to be applied

Emergency Shut-off Switch: Have an easily accessible switch that completely shuts down power to the rig

Pressure Relief Valve: Add a pressure relief valve between pump outlet and the Bypass Tee joint which is set to just below the maximum pump head (~19m). This provides protection against overpressure if:

- System becomes closed and temperature increases
- Complete blockage occurs downstream of pump

Multiple Draining Points: Have a number of drains around the loop rather than just the single one on the Mixing Tank.

Design Considerations

Heating System:

- Calculate time required to heat fluid and potential heat loss rate => size heating element appropriately (not too fast, not too slow)
- Calculate fluid mass loss rate to evaporation.
- Ensure Relay for power supply to heating element is normally OFF
- Always have temperature set point above room temperature

Mixing Tank:

- Ensure that the Mixing Tank can hold entire volume of fluid in the rig without spillage
- Inlet pipes must be higher than outlet pipes
- Have the speed control for Mixer situated so that operator is clear from Mixing Tank openings when it is used
- Ensure impeller is designed and built to spin in same direction as motor
- Choose appropriate gearbox to get adequate mixing
- Ensure that there is no chance of collision between equipment in Mixing Tank and the Shaft & Impellor. Especially look at case of flexing shaft

- Ensure level switch location is above the inlet pipes and switching level is well above heating element. Insert at the level where the fluid is anticipated to fill up to and switch float is horizontal
- Ensure that when the Level switch provides no signal, power is normally OFF

Rig:
- Ensure design allows all fluid to fully drain from rig
- Bypass is to be always partly open during experiments in case main line blocks up

Work still to complete/Ideas to pursue

- Complete wiring design and perform HAZOP on it. Particularly on how to mitigate against relay failure
- Look into a level controlled, distilled water feed system into Mixing Tank for when leaks/evaporation occurs
- Calculate expected deposition rate of monomeric silica at design concentration
- Investigate use of torque controlled clutch for Mixer motor if it got jammed
- Find out whether Temperature Controller still operates with no signal input. Find range for set point value and find if this can be limited somehow
- Investigate use of surge arrestors in rig and if required
- Determine condition for when rig gets shutdown because of suspected blockage by observing daily decrease in flow rate
- Calculate the conditions for cavitation in the pump occurring. Investigate installing a permanent orifice plate that provides enough resistance that cavitation won't occur
- Specify the straightness, concentricity and smoothness of test section and its connections
- Determine if a cooling system is required for pressure transducer usage. Ensure that overpressure limit for transducer is greater than that for the pressure relief valve
- Determine thermal expansion of system and whether any problems will arise

Appendix A – Generic Mitigation Procedures

Generic Electrocution Mitigation:
- Have all electrical equipment (pump, Mixer motor, Heating system) independently earthed and mounted on materials that electrically isolate it from other parts of the rig where possible.
- If any problem is suspected with electrical equipment turn power off before inspecting.
- Regular electrical safety checks for all equipment.
- Have RCDs or ciruit breakers on all equipment.
- Earth piping system and make all pipework electrically connected

Generic Fire Risk Mitigation:
- Have fire alarm and sprinkler system => inspect building's system to find if sufficient
- Ensure rig is mounted on non-flammable surface (ie concrete),
- Ensure components that can potentially burn out (pump, Mixer motor, Heating element) are not mounted on or near flammable materials.

Generic Overtemperature Mitigation:
- Have signs warning to keep away from rig and have rig shielded off from bystanders
- Insulate or cover all exposed metal where possible – pipework, Flow Conditioner, Mixing Tank
- Always stand back when opening Mixing Tank to avoid potential steam buildup

Generic Splash/Leak Mitigation:
- Have signs warning to keep away from rig and have rig shielded off from bystanders
- Have rig sitting in tray(s) that catch any spillage and prevents from spreading.
- Always stand back when opening Mixing Tank to keep away from splash.

- Wear gloves and safety glasses when inspecting irregular behaviour or leaks, particularly around the Mixing Tank

HAZOP SUMMARY: Silica Scaling Rig

Revision #1 Study Report - 26/04/11

Study Information

Design Stage: Post-Detailed Design, Pre-construction
Date completed: 26/04/11
Performed by: Luke Sinclair
Summary Prepared by: Luke Sinclair

Study Results

Changes to Rig since HAZOP Rev. 0 study

The following changes were made to the rig design and were analysed in this study. The incorporation of Rev. 0 outcomes in the design are given in Appendix A.

- Pressure Relief Valve is no longer required. A dangerous pressure increase situation is implausible due to the 19m Head limit of pump and the Mixing Tank riser keeping system open. The pump has an in-built over-temperature switch which will shut pump down when max pressure situations will occur (due to blocked/closed valves etc) making a relief valve redundant.
- The check valve on Bypass Line can be removed with no significant consequences. The only possibility of flow travelling in reverse direction is when pump is turned off and some leak occurs in system. In this case the fluid would still travel out the main line anyway.
- When the flow rate drops below a certain value, the flow meter will send a Low Flow trip signal to pump which will shut the pump off. This provides protection for the pump during: scenarios where an obtrusion is significantly choking flow and leak and evaporation scenarios where the pump might end up running on air.
- The flow meter has been moved to be before the Flow Conditioner with no significant consequences. It was moved for the convenience of mounting the heavier equipment down one end and to allow the display to be closer to the operator when adjusting the flow rate.
- A sampling point with valve has been added. This doubles up as an extra draining point which was one of the action points from the Rev. 0 study.
- The temperature controller probe has been moved to a thermowell at the Mixing Tank Outlet. This will ensure that the output temperature is controlled to the desired value. The only potential risk from this move is if the outlet were to become completely blocked by a scale deposit or foreign body. The fluid being measured would not in contact with the fluid being heated which could cause overheating. This risk is mitigated by having the Capillary Thermostat shutting down system if overheating were to occur.

New changes to be made from the HAZOP Rev. 1 study

- The Generic mitigations have been modified slightly and are given as Appendix B at the end of this report
- Test the failure mechanisms (over-temperature, low level and low flow) during Shakedown and on regular occasions as part of Maintenance procedures
- During Shakedown determine the calibration of the Capillary Thermostat

- Physically limit the Capillary Thermostat dial to not be set higher than 90°C. Have dial inside an electrical box where it cannot be bumped or changed by a passerby.
- Put temperature controller inside a box where it cannot accidentally be bumped
- Containers large enough to hold entire rig volume are to be placed under all drains
- Add a covering to gearbox to prevent hair/clothing etc getting caught in it

Appendix A - Revision #0 Incorporation in Design

Equipment & Procedures to add to Design

Description	Incorporated		Comments
	Yes	No	
Generic Mitigations Procedures	•		Modified in Rev 1 study and being incorporated into design
Checklists	•		Modified in Rev 1 study and will be used
Temperature Controlled Switch	•		Capillary Thermostat Switch added
Emergency Shut-off Switch	•		
Pressure Relief Valve		•	See reasons above
Multiple Draining Points	•		Drains are on Mixing Tank, Flow Conditioner and at end of test section

Design Considerations

Description	Incorporated			Comments
	Yes	No	Not Yet	
Heating System				
Heating element size calculations	•			1kW element was selected. It will heat system from room temperature to 80°C in 80 minutes
Fluid mass loss to evaporation			•	Simple calculations performed but it is hard to determine. Trial and error will be best way to determine this
Relay for power supply to heating element is normally OFF	•			
Temperature set point above room temperature	•			Added to the SOP
Mixing Tank				
MT can hold entire volume of fluid in the rig	•			MT currently can hold 23 litres (3 more than required)
Inlet pipes higher than outlet pipes	•			About 150mm higher
Mixer Speed Controller location			•	Will find an appropriate place for it when constructing rig
Impellor to spin in same			•	Will ensure this once motor is received and

direction as motor				direction determined
Gearbox size	•			25:1 is typically used. With a frequency converter even lower speeds can be obtained
Shaft & Impellor obstruction in Mixing Tank	•			Mixing Tank designed so there should be no chance of obstruction
Level Switch location	•			Level switch located below the anticipated fluid level to allow up to 3 litres of fluid to be leaked before switching. Location is above inlet pipes and heating element
Level Switch controlled relay normally OFF	•			
Rig				
Design allows all fluid to fully drain from rig	•			A slight slope will be included on the long lengths of pipe to improve flow to drain
Bypass is to be always partly open during experiments	•			Added to the SOP

Work still to complete/Ideas to pursue

Description	**Incorporated**			**Comments**
	Yes	**No**	**Not Yet**	
Complete wiring design and perform HAZOP on it	•			Wiring Design completed and HAZOP analysis was effectively performed on it during general analysis
Distilled water feed system for Mixing Tank			•	May look into if the need is found
Expected deposition rate of monomeric silica			•	May look into in future
Torque controlled clutch for Mixer motor		•		Unnecessary
Temperature Controller operation	•			By using a normally OFF relay, even if no signal comes from temp controller it will be safe. Controlled temperature range is range that probe can measure
Surge arrestors		•		No need as there is an RCD in the power socket
Condition shutting down rig due to suspected blockage			•	Will determine this by trial and error
Conditions for cavitation in the pump occurring	•			At cut-out temperature (90°C) and max flowrate (2m^3/hr) there is still 0.9m of head above the NPSH => there should be no risk of cavitation when the pump operates under the manufacturers pump curve
Permanent orifice plate to increase resistance			•	Still to determine. It may not be required
Straightness, concentricity and smoothness of test section and its	•			See engineering drawings

connections				
Cooling system is required for pressure transducer			•	Probably required
Overpressure limit for pressure transducer	•			Limit is greater than 19m head therefore it will be fine
Thermal expansion of system			•	Likely to be negligible as system is reasonably symmetric

Appendix B – Modified Generic Mitigation Procedures

Generic Electrocution Mitigation:

- Have all electrical equipment (pump, Mixer motor, Heating system) independently earthed and mounted on materials that electrically isolate it from other parts of the rig where possible.
- Earth piping system and make the Mixing Tank and all pipework electrically connected
- Regular electrical safety checks for all equipment.
- Power supply has an in-built RCD. All major electrical components to have fuses
- SOP additions: If any problem is suspected with electrical equipment turn power off before inspecting.

Generic Fire Risk Mitigation:

- Have fire alarm and sprinkler system => inspect building's system to find if sufficient
- Ensure rig is mounted on non-flammable surface (ie concrete),
- Ensure components that can potentially burn out (pump, Mixer motor, Heating element) are not mounted on, near or below flammable materials.

Generic Overtemperature Mitigation:

- Insulate or cover all exposed metal where possible – pipework, Flow Conditioner, Mixing Tank
- Ensure that Mixing Tank sits on insulating pad rather than on bare metal framework
- Have signs warning to keep away from rig. Put rig in back corner of room
- Mixing Tank design is to provide riser that channels steam build-up away from operator when working near tank. All other openings in Mixing Tank are to be sealed
- Pump has Overtemperature protection which will shut it down when system is blocked and may potentially increase in temperature
- Capillary thermostat switch should shut down system when it reaches 90°C before it boils
- SOP additions: Before injecting fluid through riser check to see if steam is coming out of it

Generic Splash/Leak Mitigation:

- Have signs warning to keep away from rig. Put rig in back corner of room
- Have rig sitting in trays that catch any spillage and prevents from spreading. Have buckets large enough to contain all fluid in rig underneath each of the drains
- Mixing Tank design is to eliminate the risk of splash. All openings in Mixing Tank except for riser are to be sealed
- Mixing Tank lid is to have a viewing glass so that fluid agitation and surface level can be observed
- SOP additions: Wear gloves and safety glasses when inspecting irregular behaviour or leaks, particularly around the Mixing Tank

Appendix B – Checklists

Rig Shakedown Checklist

Installation

- Ensure pump and check valve(s) are installed in correct direction
- Ensure no foreign bodies (such as thread tape) end up in rig

Shakedown

- Fill system with cold water and check entire system for leaks
- Start pump and check entire system for leaks again
- Check the switching circuits (temperature and level) operate as designed

Startup Checklist

Colloidal Sol Production

- Make extra amount of Sol to take into account any spillage or leakage.
- Only take the required amount of fluid to fill rig from the Chemistry lab to the Rig Room so overfilling can't occur
- Be pedantic with cleanliness
- Ensure containers used are clear and well labelled

Before Filling Rig

- Visually inspect fluid to make sure it looks as expected
- Ensure Drains are closed
- Check entire system to see that every piece of equipment: is properly in place, sealed, plugged in etc. Especially:
    - Heating Element – plugged in, not colliding with Impellor or Mixing Tank wall, properly screwed in place
    - Temperature Probe - plugged in, properly screwed in place
    - Level Switch – check it is free to move, straight up and down, plugged in, properly screwed in place

Before Starting Pump

- Check entire system for leaks => if found, drain rig and fix

While Running and going towards Steady State

- Continuously monitor temperature
- Continuously monitor flow rate and adjust pump speed, throttling valve and bypass valve to obtain design flow rate
- Check entire system for leaks again => if found, shutdown, drain and fix

Notes: Minimise time with test section being wet and exposed to air. Try keep test section dry before installing in rig.

Operational Checklist

During Daily Checkup

- Inspect Heating system and that it appears to operate normally
    - If problem observed, use clip-on ammeter to determine that leads and relays are working and shutdown if necessary
- Monitor temperature and adjust set point if necessary
- Check that Mixer is operating normally and that fluid level is sufficient and not too choppy **NB: use appropriate safety gear and open Mixing Tank lid cautiously**
- Check system for leaks and fix where possible
- When adding chemicals be pedantic with cleanliness of measuring equipment etc
- Take small sample of fluid from drain and measure the particle size and pH
- Check flow rate and adjust pump speed, throttling valve and bypass valve to obtain design flow rate. Be on the lookout for anything malfunctioning

<u>Shutdown Checklist</u>

Before Starting disassembly

- Ensure that power to rig is completely turned off before proceeding at all
- Set buckets of sufficient size underneath all drains. Open all drains fully and leave open
- Leave rig for an empirically determined length of time to cool before disassembling

During Test Section disassembly (performed after every experiment)

- Check, where possible, for scale deposits and foreign bodies in pipes and fittings. Remove and clean if found
- Inspect and clean Mixing Tank and its connections from inside

During Complete disassembly (frequency to be determined)

- Inspect all pipes, valves and tanks for scale deposits and foreign bodies. Remove and clean if found
- Test all valves are operational

Notes:

- Care must be taken with disassembly as there may be fluid still trapped in rig => use gloves when first disassembling
- Minimise time with test section being wet and exposed to air - try dry as soon as possible. If test section is to be re-used in 2nd experiment ensure it is washed down well and rust removed
- Extra care must be taken while disassembling Flow Conditioner which will likely still have some fluid still in it
-

<u>Maintenance Checklist</u>

NB: Frequencies at which to perform maintenance still needs to be determined

- Regularly calibrate: Temperature probes, pressure transducer and flowmeter
- Regularly inspect flow meter for scale build-up and clean
- Regularly service: Pump, Mixer motor and Heating System
- Check gearbox operates normally and that connection to motor and shaft is adequate
- Test Level Switch for functionality regularly

Appendix D – Zetatrac Settings

The following parameters were used in the "Measurement SOP Options" for the Zetatrac to perform the particle size distribution measurements.

Timing Tab

Run time:	60s
Number of Runs:	3

Analysis Tab – Particle Information

Particle Refractive Index:	1.46
Transparency:	Transparent
Shape:	Spherical
Density:	1.1 g/cc

Analysis Tab – Fluid Information

Fluid Refractive Index:	1.333
High Temperature:	30°C
High Temperature Viscosity:	0.797 mPa.s
Low Temperature:	20°C
Low Temperature Viscosity:	1.002 mPa.s

Analysis Tab – Analysis Options

Filter:Resolution:	High:High
Sensitivity:	High

Perspective Tab

Progression:	Standard
Distribution:	Intensity
Size Range:	0.0008-6.54 μm

Appendix E – Colloidal Silica Production Method

Standard Operating Procedure:

1. Add 15mL of 18M Sulphuric acid to 5 litres of distilled water
2. Add solution to spherical vessel in heating mantle and bring the temperature up to 70-75°C
3. Measure 60g of sodium metasilicate and add to vessel in two parts, allowing the first to fully dissolve before adding the next
4. Measure the pH of the solution and adjust to pH 8.0 by adding small amounts of 1M sulphuric acid or 1M sodium hydroxide as required. Start timer
5. Monitor and record the temperature and pH of the solution regularly. Adjust the heating mantle as required to keep the temperature between 70-75°C. The pH should slowly increase over one hour from pH 8.0 to about pH 8.3; if the pH becomes outside of this range then adjust with small amounts of 1M sulphuric acid or 1M sodium hydroxide as required
6. After 60 minutes has elapsed on the timer remove the fluid from the vessel and leave to cool before storing in a bucket
7. After solution has cooled, add distilled water until the volume is 10 litres
8. Repeat steps 1 to 7 and add the two solutions together to form a 20 litre batch

Amorphous Silica Concentration Calculation

The following parameters were used in this calculation:

Parameter	**Symbol**	**Value**	**Unit**
Total Volume	V	20	litres
Total $Na_2SiO_3.5H_2O$ added	m	120	g
Molecular mass of $Na_2SiO_3.5H_2O$	M_m	212.1	g/mol
Molecular mass of SiO_2	M_s	60.1	g/mol
Density of water	ρ	1000	g/litre

Molar concentration of silica dioxide in solution:

$$C = \frac{m}{M_m} M_s \frac{1}{\rho V} = \frac{120g}{\left(212.1 \frac{g}{mol}\right)} \left(60.1 \frac{g}{mol}\right) \frac{1}{(20\ litre)\left(1000 \frac{g}{litre}\right)}$$

$$= 1.70 \times 10^{-3} \frac{g}{g}\ (3\text{ s.f.}) = 1700\text{ppm (3 s.f.)}$$

Appendix F – Energy-dispersive X-ray spectroscopy reports

F-1

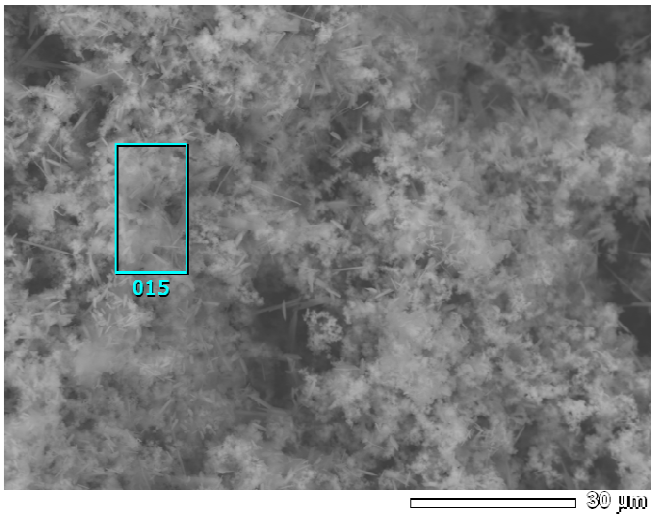

ZAF Method Standardless Quantitative Analysis

Fitting Coefficient : 0.1766

Element	(keV)	mass%	Error%	At%
C K	0.277	4.8	0.2	9.1
O K	0.525	35.1	0.1	50.6
Na K	1.041	4.8	0.2	4.8
Si K	1.739	28.7	0.1	23.5
S K	2.307	2.9	0.1	2.1
Fe K	6.398	23.7	0.8	9.8
Total		100.0		100.0

F-2

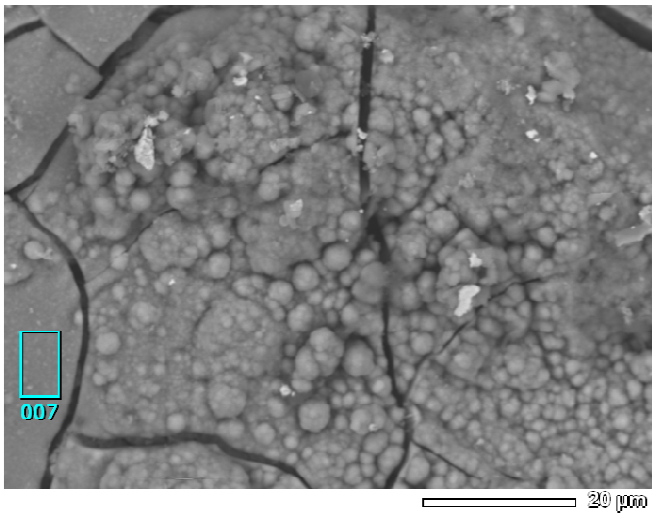

ZAF Method Standardless Quantitative Analysis

Fitting Coefficient : 0.2342

Element	(keV)	mass%	Error%	At%
O K	0.525	30.7	0.1	52.4
Na K*	1.041	1.3	0.2	1.6
Si K	1.739	26.7	0.2	25.9
Fe K	6.398	37.3	0.8	18.2
Ni K	7.471	4.0	1.4	1.9
Total		100.0		100.0

F-3

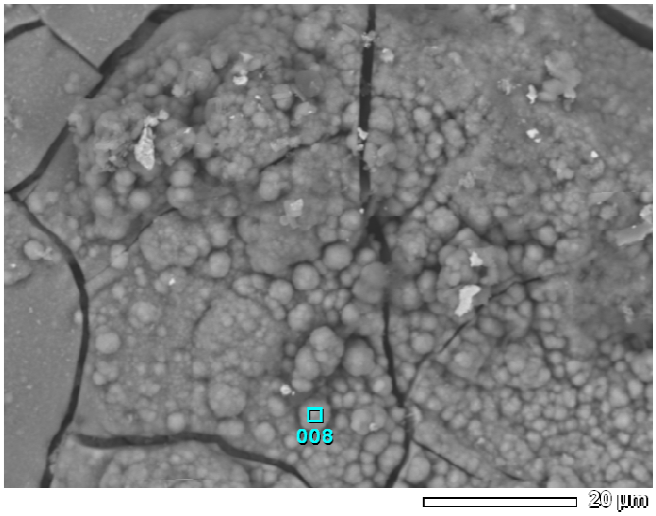

ZAF Method Standardless Quantitative Analysis

Fitting Coefficient : 0.2313

Element	(keV)	mass%	Error%	At%
O K	0.525	21.2	0.1	41.1
Si K	1.739	27.5	0.1	30.5
Fe K	6.398	46.8	0.6	26.0
Ni K	7.471	4.5	1.1	2.4
Total		100.0		100.0

F-4

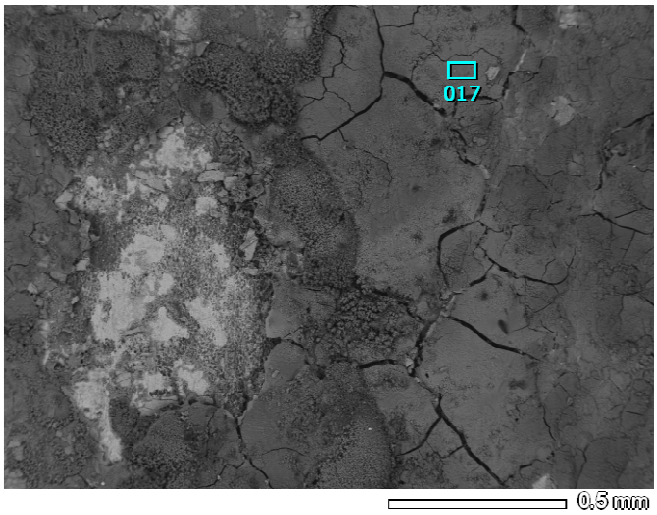

ZAF Method Standardless Quantitative Analysis

Fitting Coefficient : 0.2324

Element	(keV)	mass%	Error%	At%
O K	0.525	43.0	0.2	64.3
Na K	1.041	1.1	0.3	1.1
Si K	1.739	25.5	0.2	21.7
Fe K	6.390	27.7	1.1	11.9
Ni K	7.471	2.7	2.0	1.1
Total		100.0		100.0

F-5

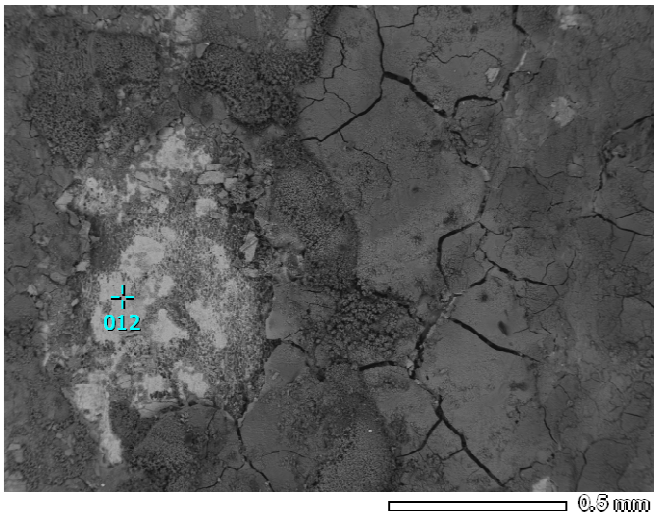

ZAF Method Standardless Quantitative Analysis

Fitting Coefficient : 0.1901

Element	(keV)	mass%	Error%	At%
O K	0.525	1.0	0.0	3.3
Si K	1.739	0.1	0.1	0.2
S K*	2.307	0.3	0.1	0.5
Fe K	6.398	98.4	0.3	95.8
Ni K*	7.471	0.3	0.5	0.2
Total		100.0		100.0

F-6

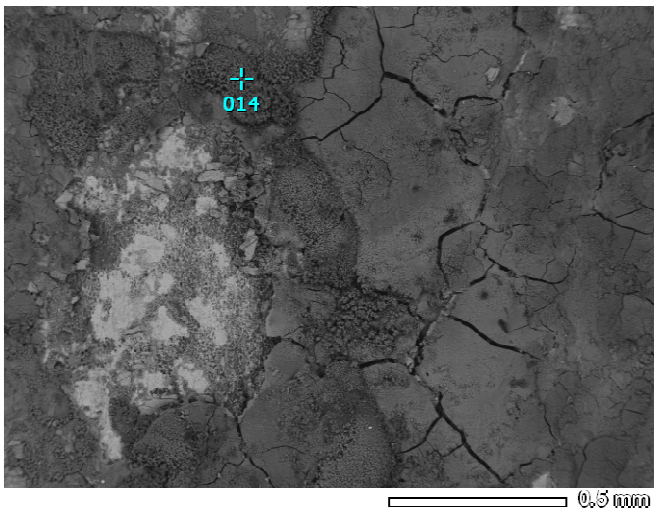

ZAF Method Standardless Quantitative Analysis

Fitting Coefficient : 0.2285

Element	(keV)	mass%	Error%	At%
O K	0.525	38.1	0.2	57.3
Na K	1.041	1.7	0.2	1.7
Si K	1.739	35.1	0.2	30.1
Fe K	6.398	23.0	1.0	9.9
Ni K	7.471	2.1	1.8	0.9
Total		100.0		100.0

F-7

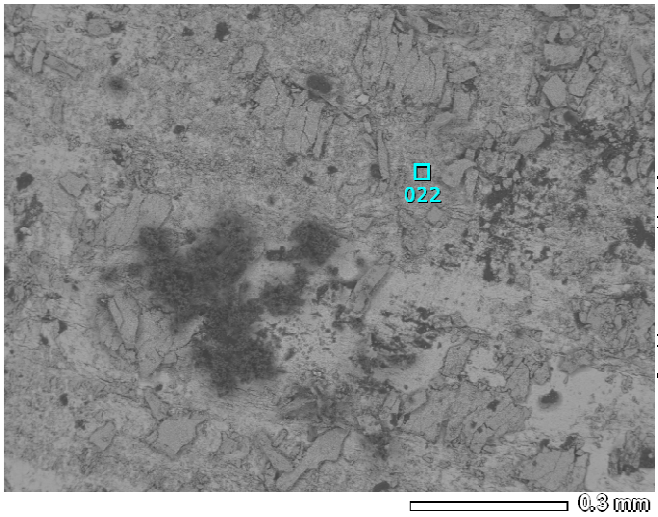

ZAF Method Standardless Quantitative Analysis

Fitting Coefficient : 0.2254

Element	(keV)	mass%	Error%	At%
C K	0.277	18.4	0.0	43.9
O K	0.525	11.1	0.1	20.0
Fe K	6.398	70.5	0.4	36.2
Total		100.0		100.0

F-8

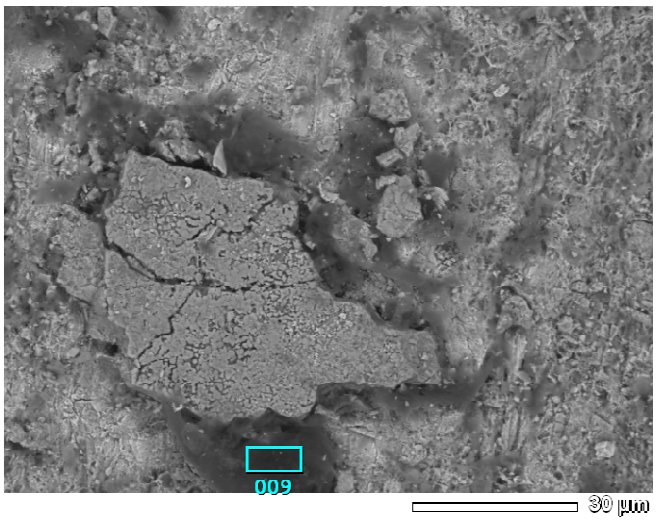

ZAF Method Standardless Quantitative Analysis

Fitting Coefficient : 0.2916

Element	(keV)	mass%	Error%	At%
C K	0.277	36.2	0.1	58.7
O K	0.525	10.1	0.2	22.0
Na K	1.041	2.0	0.2	1.7
Al K	1.486	0.8	0.1	0.6
Si K	1.739	5.3	0.1	3.7
S K	2.307	1.1	0.1	0.6
Fe K	6.398	36.5	0.0	12.7
Total		100.0		100.0

F-9

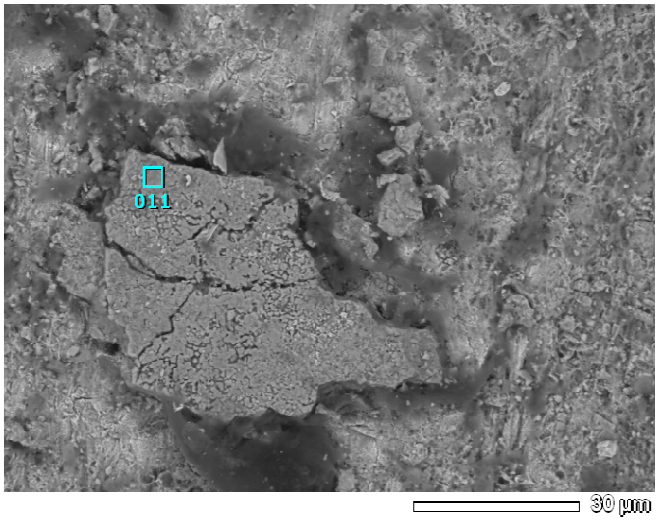

ZAF Method Standardless Quantitative Analysis

Fitting Coefficient : 0.2181

Element	(keV)	mass%	Error%	At%
C K	0.277	5.0	0.0	16.7
O K	0.525	15.6	0.1	33.7
Si K	1.739	1.5	0.1	1.9
Fe K	6.398	75.0	0.4	46.6
Cu K	8.040	2.1	1.1	1.2
Total		100.0		100.0

F-10

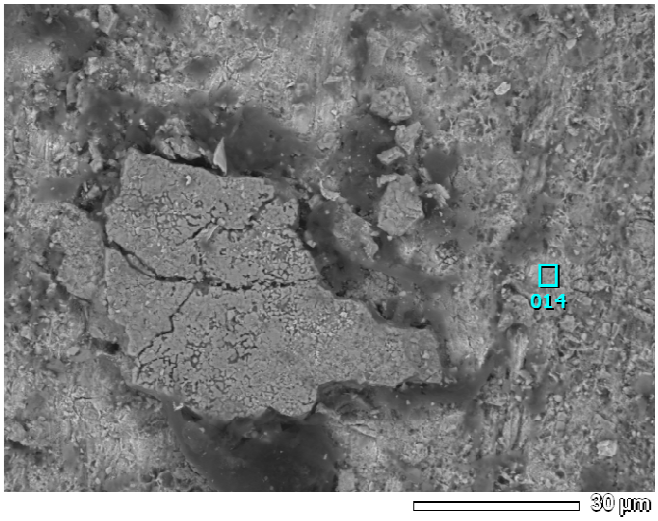

ZAF Method Standardless Quantitative Analysis

Fitting Coefficient : 0.1666

Element	(keV)	mass%	Error%	At%
C K	0.277	8.2	0.0	25.4
O K	0.525	6.1	0.0	14.2
F K	0.677	1.7	0.0	3.4
Si K	1.739	1.4	0.1	1.9
S K	2.307	1.2	0.0	1.3
Fe K	6.398	79.3	0.2	52.6
Cu K	8.040	2.0	0.6	1.2
Total		100.0		100.0

F-11

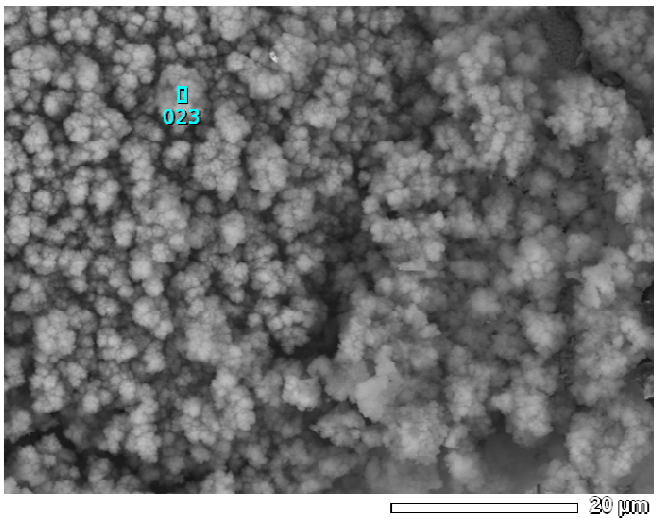

ZAF Method Standardless Quantitative Analysis

Fitting Coefficient : 0.1818

Element	(keV)	mass%	Error%	At%
C K	0.277	5.8	0.2	10.9
O K	0.525	37.4	0.1	52.6
Na K	1.041	1.6	0.2	1.6
Si K	1.739	31.6	0.1	25.4
Fe K	6.398	23.5	0.8	9.5
Total		100.0		100.0